UNIVERSIDADE FEDERAL DE ENGENHARIA MECÂNICA

PROGRAMA DE PÓS GRADUAÇÃO EM ENGENHARIA MECÂNICA

METHODOLOGIES TO MITIGATE ATTENUATING EFFECTS IN FLARE GAS FLOW MEASUREMENT BY ULTRASONIC TECHNOLOGY AT LOW PRESSURE AND HIGH CARBON DIOXIDE CONCENTRATION

LIGIA GAIGHER FRANCO

VITÓRIA

2020

LIGIA GAIGHER FRANCO

METHODOLOGIES TO MITIGATE ATTENUATING EFFECTS IN FLARE GAS FLOW MEASUREMENT BY ULTRASONIC TECHNOLOGY AT LOW PRESSURE AND HIGH CARBON DIOXIDE CONCENTRATION

A dissertation submitted in partial fulfilment of the requirements for the degree of Master of Science in Mechanical Engineering.

Supervisor: DSc. Rogério Ramos

Vitória

2020

LIGIA GAIGHER FRANCO

METHODOLOGIES TO MITIGATE ATTENUATING EFFECTS IN FLARE GAS FLOW MEASUREMENT BY ULTRASONIC TECHNOLOGY AT LOW PRESSURE AND HIGH CARBON DIOXIDE CONCENTRATION

A dissertation submitted in partial fulfilment of the requirements for the degree of Master of Science in Mechanical Engineering.

Approved in May 29th, 2020.

Rogério Ramos
Supervisor
Universidade Federal do Espírito Santo (UFES)

Márcio Ferreira Martins
Committee President
Universidade Federal do Espírito Santo (UFES)

Márcio Coelho de Mattos
External Committee Member
Universidade Federal do Espírito Santo (UFES)

Oscar Maurício Hernandez Rodriguez
External Committee Member
Universidade de São Paulo (USP)

ACKNOWLEDGEMENTS

Finishing the master's degree is the realization of a dream. I dedicate this work to everyone who supported and helped me.

First, I thank God for the blessings and opportunities along my life.

I thank my parents, Juscélio and Estélida, and my sister, Luisa. Family doesn't choose, so I am a lucky person. I am eternally grateful you for all the love, affection and education you have given me. You are my examples of honesty and persistence. I also thank my uncles, aunts, cousins, grandparents and longtime friends.

I thank my supervisor Professor Rogério Ramos by the opportunity, besides to the confidence placed in me over the years. You inspire me to be the best engineer I can. I am thankful to Professor Márcio Martins for lending important equipment to this work and to Professor Márcio Coelho for the relevant discussions throughout the project.

I thank Gabriel Fontoura, for the endless support in Labview. To my co-workers Marcelo Aiolfi and Thiago Hülle, thank you for the tips and interesting discussions on our daily coffee times. I thank my friend Matheus Damacena, who was essential for the velocity profile results, I learned a lot with you.

I appreciate the support of 2Sovle team, especially Maurício Calheiros, in the assembly and execution of experiments.

I express my gratitude to CAPES, for the scholarship granted, and to PPGEM, for the master's degree offered.

My acknowledgement to Petrobras and ANP for financing the project that originated this work.

ABSTRACT

Worldwide, hydrocarbon flow measurement is governed by regulations. It is well known in literature that CO_2 strongly attenuates wave generated by ultrasonic flow meters, which is the technology most used in flare gas application. In this context, this work proposes and tests methodologies to mitigate ultrasonic flow measurement failures due to signal attenuation in low pressure gas with high CO_2 concentration. First, the flow meter is examined in zero-flow condition in order to isolate gas composition effect, establishing a reference state for further analysis. Although the meter didn't fail, it is noticeable loss of signal power. Then, flow metering performance is evaluated in wind tunnel at several flow levels. For this purpose, a closed-circuit wind tunnel is projected. Due to hydrodynamic similarity, wind tunnel results can be extended to offshore flare gas flow, considering the same Reynolds number. The velocity profile in test section is validated using laser doppler velocimetry technique. Failure criteria are applied to detect and account failure in ultrasonic flow metering readings. With transducers in reference position, flow measurement fault begins in 70% of CO_2 at Q_{min} = 2,500 Nm³/h and in 45% of CO_2 at Q_{max} = 9,300 Nm³/h. Two methods are tested in order to mitigate CO_2 attenuation: i) transducers approximation and ii) recovery angle. With transducers approximation, there are no permanent failures up to 100% of CO_2. Recovery angle strategy increased CO_2 limit without failure to 84% at Q_{min} = 2,500 Nm³/h and 54% at Q_{max} = 9,300 Nm³/h.

Keywords: Ultrasonic Flow Meter, Flare Gas, Flow Measurement, Attenuation, Carbon Dioxide.

LIST OF FIGURES

LIST OF TABLES

LIST OF SYMBOLS

Abbreviations

ANP	Agência Nacional do Petróleo, Gás Natural e Biocombustíveis
CO_2	Carbon dioxide gas
INMETRO	Instituto Nacional de Metrologia, Qualidade e Tecnologia
NEMOG	Núcleo de Estudos em Escoamentos de Óleo e Gás
USFM	Ultrasonic flow meter

Latin Symbols

A	Cross section area
A_0	Uncorrected amplitude
$A(z)$	Corrected amplitude
B_1	Linear coefficient from linear regression
B_2	Angular coefficient from linear regression
c	Sound speed
C_1, C_2	Auxiliary constants
c_p	Specific heat at constant pressure
D	Pipe internal diameter
e	Pipe roughness
f	Transducer nominal frequency or friction factor
F_{index}	Failure index
f_{rtm}	Maximum attenuation by thermal relaxation frequency
K	Wave number
k	Profile factor
k_{AGA10}	Empirical profile factor
k_{CL}	Coverage factor
L	Path length
Ma	Mach number
M_{mol}	Molecular weight
n	Exponent for Nikuradse turbulent fully developed velocity profile

n_A, n_B, n_C	Total of failure events by criteria A, B and C
p	Acoustic pressure or gas pressure
p_0	Acoustic pressure at emitter
P_D	Differential pressure
P_{ref}	Reference pressure according to ANP
Q	Flow rate
Q_{Pitot}	Pitot tube flow rate
Q_{std}	Flow rate in standard conditions
Q_{USFM}	Ultrasonic flow meter flow rate
R	Universal gas constant
R_c	Reflection coefficient
Re	Reynolds number
S	Sutherland constant
S_A	Normalized position
SoS_{ref}	Reference sound speed
SoS_{USFM}	Speed of sound measured by ultrasonic flow meter
t_{AB}, t_{BA}	Transit times
T	Temperature
T_0	Reference temperature
T_c	Transmission coefficient
TI	Turbulent intensity
T_{ref}	Reference temperature according to ANP
T_{RT}	Environmental temperature
T_{TIT}	Gas temperature
u_c	Combined uncertainty
u_t	Friction velocity
u_+	Dimensionless velocity
U	Expanded uncertainty
V	Flow velocity
v_{max}	Maximum velocity
v_{USFM}	Flow velocity along acoustic path
x_i	Molar fraction
X	Axial length
y_+	Dimensionless position

$y(r)$	Radial position
y_c	Corrected flow rate by linear regression
z	Separation between emitter and receiver
Z	Acoustic impedance

Greek Symbols

α	Attenuation coefficient or discharge coefficient
α_c	Classical attenuation coefficient
α_{rtm}	Thermal relaxation attenuation coefficient
$\alpha\lambda$	Attenuation per wavelength δQ
γ	Beam drift or isentropic coefficient
δQ	Flow rate relative variation
ΔQ	Flow rate variability
ΔSoS	Speed of sound relative variation
ε	Compressibility factor
θ	Transducer acute angle
θ_1	Incidence angle
θ_2	Refraction angle
κ	Thermal conductivity
λ	Wavelength
μ	Kinematic viscosity
μ_0	Reference viscosity
ρ	Gas density
σ	Flow rate standard deviation
ω	Angular frequency

CONTENTS

1 INTRODUCTION

1.1 MOTIVATION

In oil production, flare gas systems are applied to vent and burn off hydrocarbon gases under routine gas purge and emergency conditions, for example in unexpected compressor shutdown or blow up events. Ultrasonic flowmeters are often a viable technology choice, due to the typical characteristics of the flow in offshore gas flare tubing, such as: low pressure (approximately 1 atm), wet gas, variable molecular composition, wide flow rate rangeability (which can reach 2000:1), presence of impurities in gas stream, technical recommendation for no-obstructive flow measurement process.

Flare gas processes are also characterized by high velocity gradient. Typically, almost 90% of gas is flared in 5% of operational time, whereas only 10% of gas is flared in 95% of time [1].

In this way, ultrasonic flow meters (USFM) show advantages over other technologies such as:

i) Operation in a wide flow range (typically more than 100:1);
ii) Tolerance to wet gas;
iii) No moving parts;
iv) Nonintrusive installation.

Transit time ultrasonic flow meters represents the technology most used for flare gas measurement, counting thousands of units installed worldwide in offshore applications, process plants and refineries [2].

Due to the strategic role of natural gas production, flow measurement performance is governed by environmental and legal laws. In Brazil, Resolução Conjunta ANP / INMETRO No. 1 (2013) [3] governs the measurement of hydrocarbon flow. It establishes conditions and procedures for operational and fiscal measurement under which flow measurement systems should be installed, in addition to defining the calibration frequency and uncertainty class. Due to the high capital values, taxes involved and environmental issues in these processes, the demand for technological research for improvements in such measurement systems has increased, for example in flare gas application.

On the other hand, carbon dioxide gas (CO_2) is the natural gas component which most affects the USFM performance. This occurs due signal attenuation promoted by CO_2 on transducer's operational frequency, which causes ultrasonic signal attenuation [4], [5]. Consequently, flare gas flow measurement systems may fail in such condition. CO_2 concentration in flare gas systems may reach about 95% [2] in pre-salt production province.

Such ultrasonic attenuating effect is predicted in AGA Report No. 9 [6]. So, the technological challenge is to define the performance of ultrasonic flow meters, in typical flare flow rates operating at high CO_2 content.

In such way, ray rescue angle technique, also known as recovery angle, is a proposal in high flow rate applications of transit time USFM [1]. As a mechanical wave, ultrasonic signal blows away by high velocity flows, resulting in missing the “perfectly aligned” target receiving transducer [7]. In this context, recovery angle can be implemented offset the beam drift effect in ultrasonic pulse packets in both upstream and downstream transducers [7].

Several studies propose alternatives to mitigate effects of attenuating media on ultrasonic flow measurement. Barros [8] examines the path length reduction by transducer approximation to reduce failure in flow rate measurement during operation in high CO_2. Barros & Ramos [9] establish a methodology based in criteria for fault flow reading identification. These criteria can be applied to develop a methodology to real-time data diagnoses and processing of operational flow rate measured, identifying faults and providing to the operator a less noisy flow rate information, without interfering in accumulated gas volume information.

High variation in flow velocity, typical of gas flaring operations, also alters ultrasonic signal performance [2]. However, before assessing the velocity profile and CO_2 absorption on the performance of the flare gas ultrasonic flow meter, it is essential to establish a reference state for further analysis. This reference state, mounted in a so-called dry calibration arrangement, is applied in inert gas at zero-flow condition.

In dry calibration, the attenuation of ultrasonic pulse due to chemical composition of the gas is evaluated in flare gas operating flow meters.

1.2 OBJECTIVES

The general objective of this study is to propose methodologies to evaluate flare gas ultrasonic flow meter performance in wind tunnel operating in high flow rate levels and high carbon dioxide concentration.

To achieve the main goal, the following specific objectives are defined:

- To establish a reference state, in order to evaluate the flow meter performance at zero-flow condition and high CO_2 concentration in atmospheric air.
- Validation of a closed loop wind tunnel, from evaluation of experimental velocity profile.
- Evaluation of ultrasonic flow measurement performance in several flow rate levels and several CO_2 levels in atmospheric air.
- Proposal of methodologies to mitigate CO_2 attenuation effects in flow readings and failure reduction in flow rate measurement.

2 ULTRASONIC WAVES: BASIC CONCEPTS

Waves are present in several areas of science, for example, in acoustics, optics and electromagnetics. Wave formation depends on the physical properties of the propagation medium, as well as the geometry of the wave's source. This chapter presents the basic concepts involving wave propagation in gases. The aim of this chapter is to present basic acoustical phenomena which modify the wave during its propagation. This issue represents a challenge on gas ultrasonic flow measurement.

2.1 WHAT IS ULTRASOUND?

Mechanical waves oscillating above human hearing limit is named ultrasound. Although such limit varies with age and from person to person, it is established that ultrasonic range lies above 20 kHz.

The same acoustical laws of sound are valid for ultrasonic waves. However, the acoustic phenomenon is frequency dependent. Thus, various acoustic phenomena, that influence wave propagation, are shifted as frequency increases. For example, diffraction effects are not significant in audible frequency. Sound attenuation is often neglected in the audible range, but become expressible at ultrasonic frequency [10].

2.2 PROPAGATION OF ULTRASOUND IN GASES

By analogy, an ultrasonic wave may be considered to consist of an infinite number of small oscillating masses, connected by elastic springs [10]. The oscillating masses form a system with the surrounding medium, in which the particles are bound together by elastic bonds [11]. Each element is affected by the motion of its nearest neighbor. If a disturbance is induced in an element, the first element transfers energy to the next one in line. The second element influences the third similarly and so on. Thus, the acoustic energy propagates in the medium from element to element, until it is dissipated by internal losses (thermal, mechanical or chemical).

The wave motion is characterized by propagation and transmission of energy, without mass transfer.

The wave processes are characterized by a velocity of propagation c [m/s], a wavelength λ [m], a frequency of oscillation f [Hz] and an angular frequency ω [rad]. These parameters are related as:

$$\begin{cases} c = \lambda f \\ \omega = 2\pi f \end{cases} \tag{2.1}$$

In terms of flow measurement by ultrasonic technology, where ultrasonic waves are induced in a fluid medium, it worth to observe that frequency is defined by the resonance frequency of piezoelectric transducers and sound speed is a

thermodynamic property of the medium. Thus, it remains to estimate the wavelength by Equation (2.1).

Considering that bulk fluids are homogeneous, isotropic and compressible with equilibrium of pressure and density, the bulk wave motion is characterized by compression and expansion regions [12]. The plane wave assumption is the simplest model to characterize a bulk wave model [13].

The general equation to describe the acoustical wave motion is given by:

$$\nabla^2 \vec{v} = \frac{1}{c^2} \frac{\partial^2 \vec{v}}{\partial t^2} \tag{2.2}$$

Where ∇^2 is the Laplacian operator, $\vec{v}(x,y,z)$ is the three-dimensional velocity profile and c is the sound speed.

The radiation of sound takes place when an incident sound wave makes the surface vibrate. Part of the power, which the vibrating surface produces with the exciting acoustic pressure, is radiated as effective power to infinity; this gives rise to the radiation loss of the surface [14].

The simplest case of radiation of an ultrasonic wave is considering as a point source is a small plate where all points oscillate with the same amplitude and phase. By Huygens' principle, the radiation of ultrasound from source is isotropic which gives rises to a spherical wave [11].

The acoustical field generated by a transducer is characterized by two distinct regions: the near field and the far field. The near field is closer to the emitting surface, characterized by a series of constructive and destructive interference. It's a complex region, because the maximum amplitude of acoustical pressure sometimes occurs out of the acoustic axis [15]. In far field region, the acoustical field is regular, forming principal lobule at the acoustic axis. Near field and far field regions are illustrated in Figure 1.

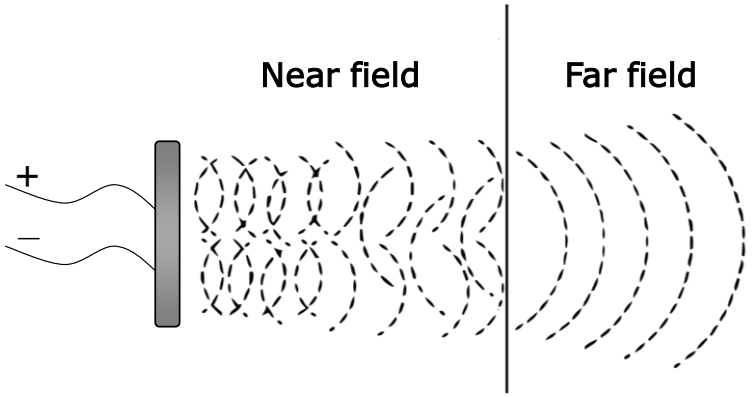

Figure 1 - Near field and far field regions

2.3 SOUND SPEED

A disturbance propagates through a medium at its respective sound speed, also called as “velocity of sound” or “speed of sound”. The sound speed depends upon the type of wave, the elastic properties of the medium, the density of the medium and the modes of vibration associated [10]. In high frequency cases, the wave frequency and amplitude also interfere on sound speed of real gases [11].

In gaseous media, only compression waves are transmitted. The expression to sound speed in gases is derived from equations of state. Generally, the propagation of ultrasonic energy in gases is adiabatic because the variations in pressure and volume is so fast that there are no significant heat loss in this process [10].

The sound speed c [m/s] in gases is estimated by Newton-Laplace Law:

$$c^2 = \gamma \left(\frac{\partial p}{\partial \rho} \right)_s \tag{2.3}$$

Where:

- γ [dimensionless] is the isentropic coefficient;
- p [Pa] is the gas pressure;
- ρ [kg/m³] is the gas density.

Hence, assuming perfect gas model, the sound speed is calculated as:

$$c^2 = \frac{\gamma R T}{M_{mol}} \tag{2.4}$$

Where:

- R [J/mol.K] is the universal gas constant;
- T [K] is the temperature;
- M_{mol} [g/mol] is the fluid molecular weight.

Sound speed is not pressure dependent in pressure variation range of 0.5 atm [16]. The change in sound speed is about 0.1% per MPa [11].

Increasing humidity, sound speed varies approximately linearly. At 50% of relative humidity in air, sound speed increases 1% and at the level of relative humidity of 100% it increases 2% [11].

In real gases, especially polyatomic ones, sound speed is frequency dependent [11]. This is explained by acoustic dispersion that are influenced by several factors, such as internal friction, relaxation and resonance phenomena.

2.4 REFLECTION AND TRANSMISSION OF AN ULTRASONIC WAVE

Waves that propagate from one medium to another with different properties transmit and reflect mechanical energy. This phenomenon is related to acoustic impedance.

Acoustic impedance is a concept highly used in ultrasonics. It can be understood as wave resistance. When a wave travels from medium 1 to medium 2, the energy portion which is transmitted is a function of the acoustic impedance of each medium. The acoustic impedance is analogously to impedance in electrical circuits [13]: maximum power transfer between two circuits is in case when impedances are matched.

Specific acoustic impedance z is a characteristic property of the medium and depends on the type of wave is being propagated. It is useful in calculations involving the transmission of acoustic waves from one medium to another. Correspond to the ratio between acoustic pressure p to the associate particle speed u in a medium.

$$z = \frac{p}{u} \tag{2.5}$$

For standing plane waves or diverging waves, specific acoustic impedance z is represented by complex number:

$$z = r + jx \tag{2.6}$$

Where r is the specific acoustic resistance and x is the specific acoustic reactance of the medium for the wave being considered.

Under assumption of plane wave, the acoustic impedance Z [kg.m/s^2] of an acoustic wave is:

$$Z = \rho c \tag{2.7}$$

Where ρ [kg/s] is fluid density and c [m/s] is speed of sound.

Any operation with ultrasonic waves means transmitting acoustic energy from one medium to another [13]. In this context, it is important to understand the reflection and transmission process of an infinite ultrasonic wave, as shown in Figure 2.

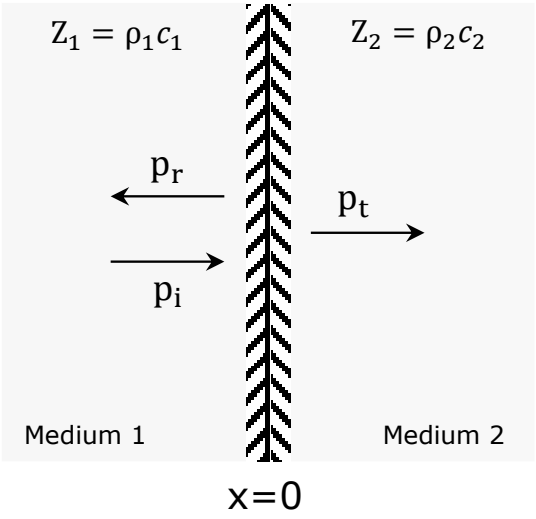

Figure 2 - Perpendicular incidence of an ultrasound wave on the interface of two media

However, wave propagation is influenced by any boundary surface. At the boundary of two media, part of the wave is reflected and part is transmitted. Besides, in case of oblique incidence the wave is also refracted.

Considering perpendicular incidence and fluid-fluid interface, the ratio of the intensity of the reflected wave to the incident wave, considering is called reflection coefficient R_c. The reflection coefficient is calculated using wave resistance Z.

$$R_c = \frac{Z_2 - Z_1}{Z_2 + Z_1} \tag{2.8}$$

Where Z_1 and Z_2 are the acoustic impedances of medium 1 and 2, respectively.

The intensity of acoustic energy which is emitted from medium 1 and penetrates into medium 2 is called transmitted coefficient T_c as Equation (2.9).

$$T_c = 1 - R_c \tag{2.9}$$

Transmission and reflection intensity are the square of their respective coefficients. Since cross-section areas of all the beams are equal, the power coefficients are equal to the intensity coefficients.

In special case that both wave resistances are the same, the wave passes undisturbed from one medium to another. All divergence in wave resistance culminates in transmission losses.

The main question faced emitting ultrasonic energy in a gas medium is poor matching between high impedance of transducer and low acoustic impedance typical of gaseous media. For example, air acoustic impedance is 5 orders lower than acoustic impedance of nearly all piezoelectric ceramics [16].

Table 1 shows the comparison between acoustic impedance of air, CO_2 and water, using Equations (2.7) to (2.9). The transmission and reception coefficient in these media are also calculated, considering a titanium transducer with acoustic impedance of $Z = 2.7x10^6$.

Table 1 - Acoustic impedance of air, carbon dioxide and water at 25ºC and 101.325 kPa

Medium	**ρ [kg/m³]**	**c [m/s]**	**Z [kg/m²s]**	**R_c [%]**	**T_c [%]**
Air	1.18	346.7	410.6	99.97	0.03
CO_2	1.79	368.7	661.6	99.95	0.05
Water	997.8	1497	$1.4x10^5$	29.77	70.23

Hence, the generation of high intensity ultrasound field in gas media, like air, is greatly limited because of impedance differences between medium and transducer, requiring large amplitudes of vibration. In practice, there are limits in transducer power and maximum amplitudes of vibration [17] for operation in hazardous areas, for reasons of intrinsic safety operation and harmonic distortion.

2.5 REFRACTION OF ULTRASONIC WAVE

Refraction is direction changing of travel of a wave front due to differences in propagation velocity. The refraction of ultrasonic waves is analog to the refraction in geometric optics. Figure 3 illustrates the propagation of a wave in the interface of two media.

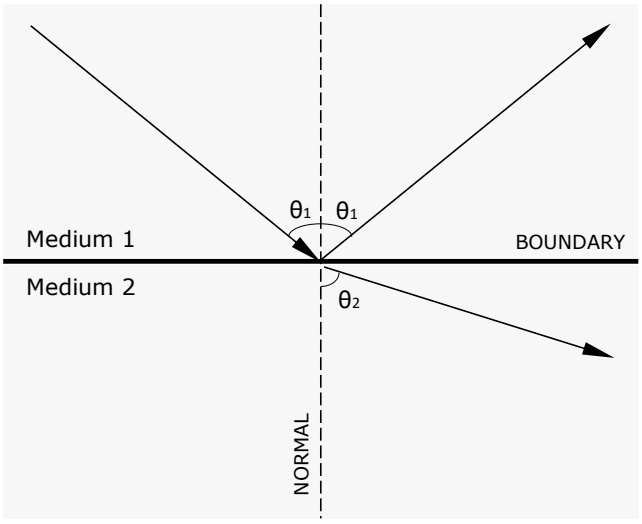

Figure 3 - Refraction of a longitudinal wave at the interface of two stationary media

Snell law of refraction holds true [11]:

$$\frac{\sin\theta_1}{\sin\theta_2} = \frac{c_1}{c_2} \tag{2.10}$$

Where:

- c_1 and c_2 are the sound velocity in medium 1 and medium 2;
- θ_1 is the incidence angle and θ_2 is the refraction angle.

The ratio of sound speed has the same meaning as the reflective index does for light [11].

Any properties change of the ultrasonic wave propagation medium results in refraction phenomena, for example thermal gradient [11]. The variation of velocity profile also affects the wave propagation due to refraction effects [18].

To understand the velocity profile effect, Figure 4 illustrates the transmission of a plane wave thought two semi-infinite media with relative motion from medium 1 to medium 2. Each medium travel at its on velocity v_1 and v_2. At the interface between two media at T point, the evolution of sound field must be the same. According to Bruneau [19]:

$$\frac{c_1}{\cos\theta_1} + v_1 = \frac{c_2}{\cos\theta_2} + v_2 \tag{2.11}$$

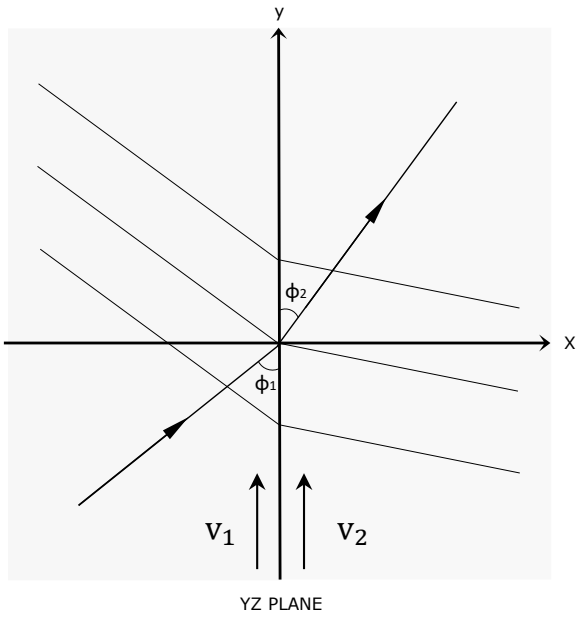

Figure 4 - Interface between two media in relative motion

2.6 ATTENUATION OF ULTRASONIC WAVES

In many situations, the wave equation may be derived under the assumption that all acoustic energy losses can be neglected. In fact, the acoustic energy is converted into random thermal energy. This dissipation sources presents two general categories [12]: i) Those intrinsic to the medium and ii) those associated with the medium's boundaries.

Losses in the medium characterizes the absorption of an ultrasonic wave, that leads to attenuation of ultrasonic signal. Attenuation of acoustic pressure results from energy transfer mechanisms of the acoustic wave into other forms of energy. It can be understood as ultrasonic wave weakening caused by absorption and diffusion processes.

Due to wave propagation, the harmonic acoustic pressure *p* decreases proportionally to the distance *L*, from the emitter to receptor, according to an exponential relation [20] as Equation (2.12).

$$\frac{p}{p_0} \sim e^{-\alpha L} \tag{2.12}$$

Where:

- p_0 [Pa] is the amplitude of the acoustic pressure at the emitter;
- α [m^{-1}] is the attenuation coefficient.

Medium's losses present three basic types: i) losses from viscous process, ii) heat conduction losses and iii) losses associated with internal molecular process. In fact, any acoustic loss in fluids can be described as a phase lag between acoustic pressure and medium response [13].

In absence of any external perturbation, the internal degrees of freedom are in equilibrium, and the attenuation is only due to classical effects (viscosity, heat conduction, diffusion). Energy exchanges between external energy and the rotational-translational energy of molecules by means of thermal equilibrium adjustment is related to ultrasonic wave frequency [21], a phenomenon known as thermal relaxation. In such case, an external perturbation, such as emission of an ultrasonic wave, thermal relaxation losses arise from the incomplete establishment of thermal equilibrium in a system [22].

The attenuation coefficient is calculated by:

$$\alpha = \alpha_c + \alpha_m \tag{2.13}$$

Where:

- α_c [1/m] is the classic attenuation coefficient that arises from transport phenomena (viscosity, heat conduction and diffusion);
- α_m [1/m] is the thermal relaxation attenuation coefficient due to molecular internal degrees of freedom, also known as relaxation process.

Acoustic attenuation in gases is challenging to measure and predict [4]. Studies in this subject, either experimental and theoretical [20], have been done since 1900's century.

2.6.1 The classical absorption

The propagation of acoustic waves is characterized by regions of molecules compression and expansion. Thus, the fluid is not homogeneous, presenting density and temperature changing in space and time. Classical acoustic attenuation results from irreversible losses of acoustic energy due to viscosity and thermal conductivity related to the rarefaction and compression of the acoustical wave [4].

The loss of acoustic energy by viscosity is caused by the relative movement between adjacent portions of the medium. As a result of the viscosity, the movement of the particles undergoes friction and energy is lost [23]. The viscous processes require time to reach equilibrium of temperature and particle density. This time delay for both thermal and molecular equilibrium promotes the conversion of acoustic energy into thermal energy.

In a fluid subjected to an acoustic process, compressed regions reach higher temperatures than rarefied regions. As all medium presents finite and not null thermal conductivity, heat is transported from the hot regions (compression) to the cooler regions (rarefaction), created by the sound wave [13]. As explained for viscous effects, the temperature gradient will lag the applied ultrasonic pressure, leading to additional attenuation.

The classic attenuation coefficient is calculated according to Stokes-Kirchoff equation, as the sum of the viscous and thermal absorption coefficients [22].

$$\alpha_c = \frac{\omega^2}{2\rho c^3}\left[\frac{4}{3}\mu + (\gamma - 1)\frac{k}{c_p}\right] \tag{2.14}$$

Where:

- ω [rad/s] is the angular frequency;
- ρ [kg/m³] is the gas density;
- c [m/s] is the sound speed;
- μ [Pa.s] is the kinematic viscosity;
- γ [dimensionless] is the isentropic coefficient;
- k [W/m².K] is the thermal conductivity;
- c_p [J/kg.K] is the specific heat at constant pressure.

According to Equation (2.14), the attenuation coefficient is proportional to the quadratic frequency of the transducers. So, higher operating frequency of a transducer leads to higher absorption of acoustic energy.

According to Kinsler et al. [12], observed experimental data presents good agreement for monoatomic gases, such as argon and helium. However, classical attenuation coefficient is very different from experimental results for polyatomic gases.

2.6.2 Molecular thermal relaxation

In the beginning of 20th century, more accurate experimental methods for attenuation measurement were reached. Such results indicated that classical absorption theory may be inadequate for some class of fluids. Consequently, it became necessary to develop additional absorption mechanisms, in order to consider binding energies within and between molecules [12]. These mechanisms are referred as molecular or relaxation sound absorption. In this process, a certain time is necessary to the acoustic wave reaches equilibrium [11].

Monoatomic and inert gases presents only translational degrees of freedom (translation in x, y and z direction), so that the relaxation time is very short and there is no excess of attenuation above the “classical” value [13]. However, in polyatomic gases in addition to the three degrees of translational freedom each molecule possesses, they also present internal degrees of freedom associated to rotation and vibration levels [12]. The possibilities of molecular motion are sketched in Figure 5, for a two-atomic molecule.

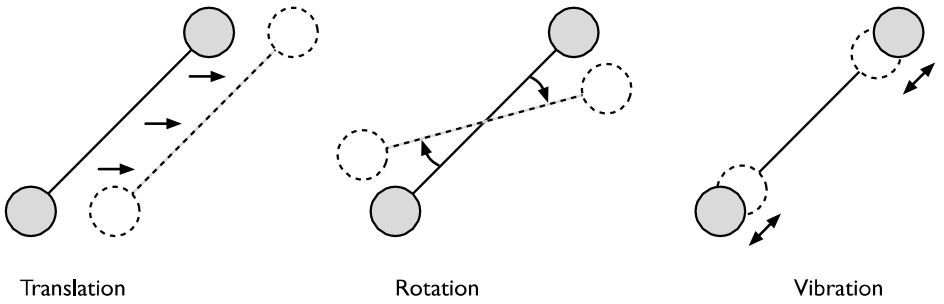

Figure 5 - Possibilities of motion for a polyatomic molecule

The rotation and vibration levels require a finite time to take up the energy exceeded. Molecular thermal relaxation results from retarded energy exchange between translational and intramolecular vibrational degrees of freedom [24].

The compression and rarefaction associated to the wave motion cause perturbations in the local translational energy. The energy is transmitted from translational to internal degrees of freedom during the compression phase of the wave and returned during the rarefaction phase [25]. Translational modes achieve equilibrium very quickly, while vibrational modes require much longer time. These nonequilibrium effects generate damping of the acoustical wave.

Through collision of molecules, the translational energy is redistributed to the rotational and vibrational degrees of freedom.

A classic example of attenuation due to molecular relaxation is the case of carbon dioxide. A relaxation peak is centered about 30 kHz and the attenuation magnitude is about to 1200 times higher than the classic attenuation coefficient at this frequency [12].

A representative way to emphasize relaxation effects on acoustic attenuation is by representing the normalized attenuation $\alpha\lambda$, where λ [m] is the wavelength. The thermal relaxation attenuation coefficient α_m is estimated by empirical model [23]:

$$\alpha_m = 2\left[\alpha\lambda_{\max}\right]\frac{f/f_m}{1+\left(f/f_m\right)^2} \tag{2.15}$$

Whereby:

- f [Hz] is the transducer nominal operational frequency;
- f_m [Hz] the maximum thermal relaxation frequency of attenuation;
- $\alpha\lambda_{\max}$ is the maximum attenuation coefficient per wavelength.

The molecular relaxation processes can lead to a complex mechanism of vibrational-translational and vibrational–vibrational energy transfer between different molecular energy levels [24]. These mechanisms produce several effective relaxation frequencies depending on the vibrational modes involved in the relaxation process.

Dain and Lueptow [24] investigated the attenuation due to relaxation process of ternary mixtures of nitrogen, methane and water vapor. This model was compared to experimental evaluation [4]. Other techniques can also be used for attenuation prediction, for example:

- Direct simulation Monte Carlo [26];
- Combining the parallel and series relaxation theory [27];
- Decoupling multimode vibration relaxation [28].

The absorption of acoustical wave is generally evaluated over a wide frequency range, which is illustrated by the acoustic absorption spectra or attenuation spectra.

The experimental difficulty on attenuation measuring is caused by the sensitivity of the observed relaxation frequencies to the presence of minimal traces of impurity molecules [22]. Besides, the effect of the attenuation measured is often combined with those of diffraction (inhomogeneities in ultrasound field) and those of scattering (inhomogeneities in the medium of propagation) [29].

2.6.3 Air attenuation

The knowledge of acoustical attenuation in atmospheric air is important in many industrial applications. The methodology for air attenuation prediction has been extensively studied in literature [30], including standards [31]. The basically assumption on these models is simplifying air composition, i.e., nitrogen, oxygen, carbon dioxide and water vapor.

The attenuation of sound in air shows a pronounced dependence on humidity. Figure 6 shows the absorption spectra of air with humidity.

Above a frequency of 1 kHz, the absorption of sound in air increases in the presence of humidity [17], [30]. Above 500 kHz, the effects of humidity becomes insignificant, and it can be neglected [32]. In a frequency range between 60 kHz and 500 kHz, the higher is the humidity the higher is the attenuation coefficient.

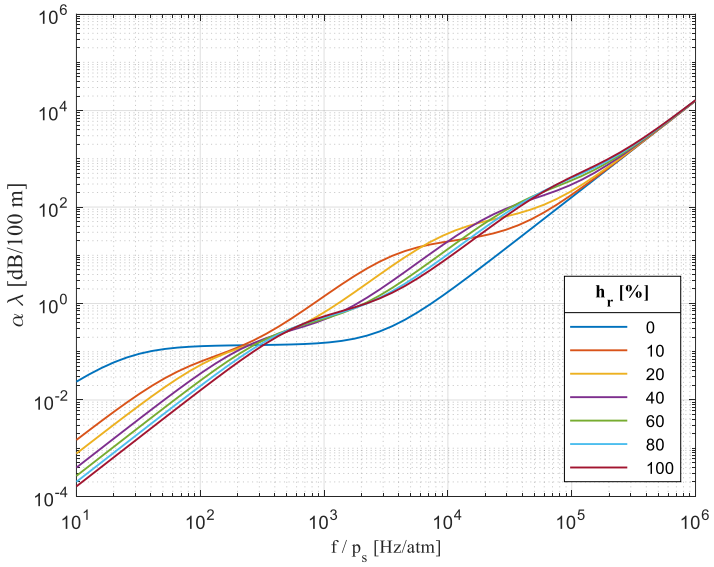

Figure 6 - Attenuation coefficient per atmosphere for air at 20°C according to relative humidity “h_r” [33]

2.6.4 Carbon dioxide attenuation

In terms of CO_2 attenuation, thermal relaxation absorption dominates in kHz range, and this explains the difficult of USFM operations in gases with high CO_2 concentration. Classical absorption contributes significantly above 1 MHz.

Figure 7 compares the frequency effect on the attenuation of dry air and CO_2 using Equation (2.14) and Equation (2.15).

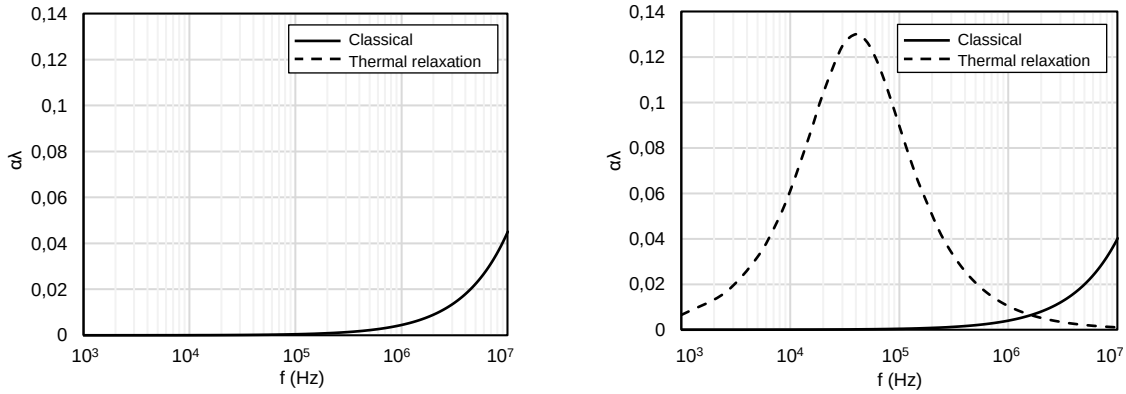

a) Dry air b) Carbon dioxide

Figure 7 - Comparison between attenuation coefficient of air and CO_2

The absorption of acoustic signal in ultrasonic frequency by CO_2 has been studied since last century. Abello [34] measured the intensity of acoustic pressure it exerted against a torsion vane and found that there was a nearly logarithmic decrease in the intensity with an increase in CO_2 concentration. Curtis [35] applied a similar experiment to measure absorption coefficients in ultrasonic frequency range in air and carbon dioxide mixtures and found an absorption coefficient not described by classical absorption theory. Kittel [22] made a literature review in absorption modeling in gases with thermal relaxation effects.

Dain and Lueptow [24] described a model that predicts the attenuation from vibrational relaxation in gas mixtures based on Euler gas equations. In order to validate this model, Ejakov et al. [4] measured the attenuation coefficient using a pulse technique for several gases, including CO_2. CH_4 and N_2. The technique consider that pure CO_2 has so strong attenuation that the received signals levels do not reach detection threshold limit.

In order to illustrate the influence of CO_2, a comparison between the attenuation spectrum of mixtures of methane in nitrogen and carbon dioxide in nitrogen is shown in Figure 8. Data points are experimental values [4] and solid curves are theoretical calculation [24]. The attenuation magnitude is substantially higher in mixtures with CO_2 than in CH_4. Maximum peak in 100% Methane is 0.035 [4] while in pure CO_2 is 0.130 [28]. So, a difference about 3,600% approximately.

In same way, addition of water vapor in CO_2 strongly affects the absorption coefficient. Water vapor acts as catalysts, reducing the average number of collisions for the transfer of energy into ant out of carbon dioxide vibrational states. Kinsler et al. [12] exemplifies that in a case of 1% of water vapor in carbon dioxide. In this situation, the relaxation frequency changes from 30 kHz to around 2 MHz.

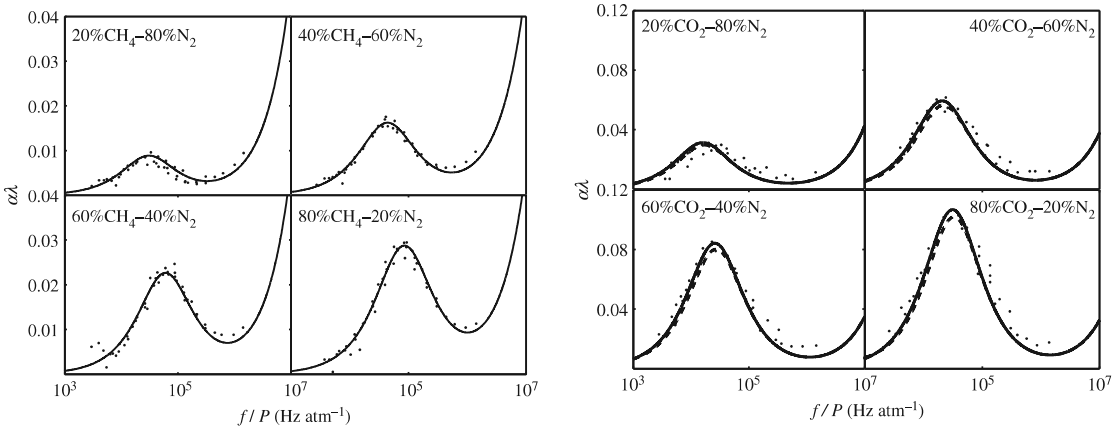

a) Mixtures of CH_4 and N_2 b) Mixtures of CO_2 and N_2

Figure 8 - Attenuation spectra in mixtures of methane and carbon dioxide with nitrogen [4]

Despite industrial requirement and relevance, there are just few studies about CO_2 attenuating effects applied to current engineering challenges, for example in

ultrasonic flow measurement applications. Helden et al. [5] and Vermeulen et al. [23] evaluated some transducers frequencies to the absorption promoted by carbon dioxide, inside a pressure vessel, in mixtures of N_2 + CO_2. Barros and Ramos [9] examined a 100 kHz transducer in wind tunnel and atmospheric air experiments and proposed a methodology to detect CO_2 attenuation effects, based on a fault counter technique.

The authors concluded that transducers approximation improve USFM readings, since increase signal strength. So, it is an alternative to high CO_2 applications. Considering current diagnose capabilities provided by nowadays development in microelectronics and high processing capabilities, turns the USFM technology usable in rich CO2 applications [5].

2.6.5 Experimental methods for attenuation evaluation

Since the attenuation coefficient is a function of the ratio between frequency and pressure *"f/p"*, either frequency or pressure can be varied. Most researchers work with pressurized chambers, since transducers presents one main resonance frequency, as done in several studies [4], [23], [36], [37].

The attenuation measurement is performed directly determining the impulse response of the medium in the time domain. However, accurate measurement of the wave attenuation isolated, that can be called as intrinsic attenuation [38], is difficult to obtain because, in addition to intrinsic damping, factors such as geometric spreading, reflection and scattering may strongly affect wave propagation. So, it is useful to refer to measured attenuation as "apparent attenuation" [38].

The principle is based in the fact that voltage produced in the receiving transducer is proportional to the acoustic pressure [4]. Thus, the attenuation can be found by the logarithmic slope of the voltage amplitude as function of the separation length between emitter and receiver, as described by some authors [4], [38]. In addition, it is necessary to correct diffraction effects of the sound wave with an appropriate model [39].

Ejakov et al. [4] evaluated three different methods to measure the amplitude of the received signal: maximum of the signal, minimum of the signal and the RMS value. They found that the experimental attenuation coefficient was similar for all three techniques.

Petculescu et al. [37] proposes an acoustical gas sensor based on attenuation, combining experimental sound speed and attenuation measurement. Although it is a very complex task, this study concluded that it is a potential application.

Helden et al. [5] examined the attenuation of mixtures of CO_2. CH_4 and N_2 in a high-pressure chamber using transducers with different frequencies (80 kHz, 135 kHz and 208 kHz). Vermeulen et al. [23] tested the absorption of CO_2 in a pressure vessel,

varying pressure, path length, gas composition (mixtures of N_2 and CO_2) and frequency of transducers.

2.7 DIFFRACTION OF ULTRASONIC WAVE

Acoustic waves emitted by a source are not confined to a region defined by the transducer surface and are not normal to the emitting surface, as well. This occur because a transmitted signal does not propagate as a plane wave, due to diffraction effects, as exemplified in Figure 9.

According to Huygens' principle, every vibrating point at a wave is regarded as the center of a new disturbance. The new disturbances act as point sources, each emitting a spherical wave, which is assumed to produce effect only along its wave front [10].

Transducers have a finite size and the acoustical beams spread out into a diffraction field. The diffraction phenomenon can introduce errors in attenuation and velocity measurements, especially in low frequencies and small transducers [40]. To diffraction modeling, transducers are assumed to be a piston source in an infinite rigid baffle radiating into a semi-infinite medium [40].

To explain the diffraction occurrence, consider two transducers, one transmitter and one receiver of ultrasonic waves, with parallel faces. The integral of the acoustical field at the receiver presents an average acoustical pressure with amplitude smaller than a plane wave presented by the emitter. Thus, there is a reception loss known as diffraction. Diffraction prevents full utilization of a wave [10].

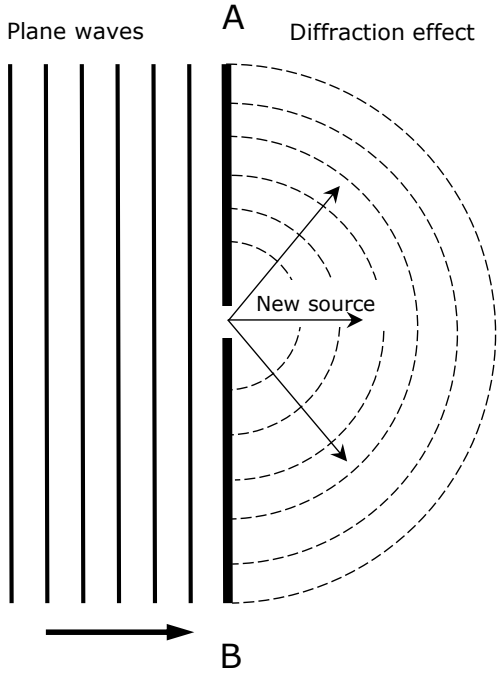

Figure 9 - Plane waves incident on a small hole sets up spherical wave fronts on the other side due to diffraction of sound

In far field region, the sound amplitude decreases as the distance from emitter increases due to spreading and diffraction. These effects and attenuation phenomenon are independent process.

It is necessary to correct the diffraction effect. Pinkerton correction, in Equation (2.16), calculates the corrected amplitude on the far field zone from a circular source. This correction is validated in far field region [4], [37].

$$A(z) = A_0 e^{-\alpha z}\left\{\sin\left[\frac{1}{2}K\left(\left\{z^2 + R^2\right\}^{1/2} - z\right)\right]\right\} \tag{2.16}$$

Where:

- $A(z)$ is the corrected amplitude;
- K [1/m] is the wave number $\left(K = 2\pi/\lambda\right)$;
- z [m] is the separation between emitter and receiver;
- R [m] is transducers radius.

The application of diffraction correction is done by dividing each measured intensity by the calculated correction at that distance between emitter and received [4].

Buiochi [15] presents a methodology for correcting the signal amplitude. The corrected amplitude is equivalent the case that the received acoustic field is a plane wave. Firstly, it is necessary to calculate the normalized position S_A:

$$S_A = \frac{zc}{R^2 f} \tag{2.17}$$

Then, consider for the value of S_A in the curve at Figure 10.

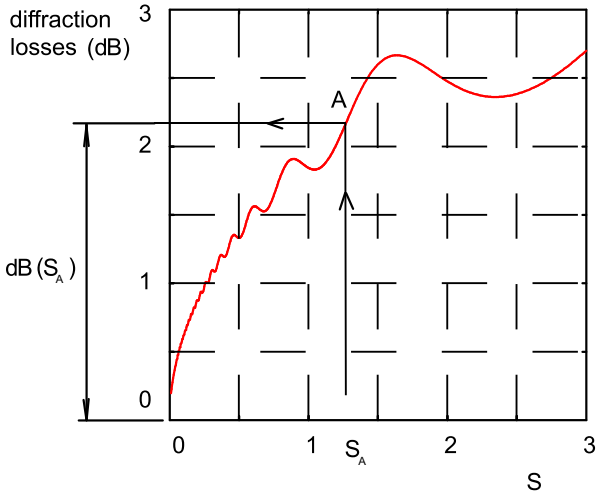

Figure 10 - Curve for diffraction correction [15]

The value $dB(S_A)$ corresponds to the diffraction loss. Finally, the corrected amplitude $\tilde{A}$ can be calculated through Equation (2.18).

$$dB(S_A) = 20.\log\left(\frac{\tilde{A}}{A}\right) \tag{2.18}$$

Correcting the diffraction effects of experimental data, the physical radius of the piezoelectric element is a subject to most potential uncertainty [41]. This radius is not a measure of the physical radius of transducer element but is rather a measure of the effective radius of the radiating (and receiving) apertures.

3 PRINCIPLES OF ULTRASONIC TRANSIT TIME FLOW MEASUREMENT

3.1 INTRODUCTION

Ultrasonic principle is applied in various fields, as medical devices, sonar and industrial applications. One important application of ultrasonic technology is on flow measurement of hydrocarbon in oil and gas industry. This chapter is concerned with introducing the operational fundamentals of flare gas flow measurement using ultrasonic time of flight technique.

3.2 FLARE GAS FLOW MEASUREMENT

Flaring is deemed the safest technique applied to remove unwanted gas or evacuate excess of gases quickly. The flare often takes the form of a flame burning at the tip of a stack [42]. Flaring gas process is typical from petrochemical facilities, such as offshore oil rigs, onshore production and refineries.

Flaring gas installations are installed for safety purposes, avoiding blow-outs and enabling free passage of high flow rate of hydrocarbon gas, such as during unexpected compressor shutdown. Under routine gas purge, an amount of gas is aligned to the flare to keep the pilot flame and to maintain back pressure. This procedure is very important, since it avoids blow-back of external air down the flare stack, which could bring about explosion and detonation of the plant [42].

Flaring process is a major source of greenhouse emissions and airborne pollutants [43]. The emissions estimation is based on the volume reported to a regulation agency [44]. Thus, the regulations of flaring gas process became stricter due to environmental, social, economic and tax motivations.

In this context, flaring gas flow measurement is governed by regulations worldwide, thus being a legal metrology issue. In Brazil, Portaria ANP/INMETRO nº1 (2013) [3] establishes conditions and proceedings for operational and fiscal metering that flow measurement systems must present. This ordinance imposes that the uncertainty of flaring gas flow measurement must be under 5%.

Typical flow in gas flare tubing are characterized by large diameters (up to 40 inches), low pressure (around atmospheric), wet gas with variable molecular composition, wide flow rate rangeability (can reach 2000:1), presence of impurities in gas stream and indication for no-obstructive flow measurement process. Flaring gas molecular composition is characterized by high content of organic hydrocarbons, such as methane, ethane, propane and carbon dioxide [23], [45].

Since 1990's, ultrasonic flow meters have been established as preferred flow meter for flaring gas applications. At current applications, for instance in pre-sault oil reservoirs in Brazil, flare gas presents high concentration of carbon dioxide (CO_2).

3.3 TRANSIT TIME ULTRASONIC FLOWMETER

The first registered application of ultrasonic transit time for flow measurement is dated from Rütten's patent in 1928 [1], [46], in applications for water and steam flow measurement in large canals. In 1980's, transit time ultrasonic technique resurged due to the improvement of electronics and challenges of flow measurement in industrial applications. Ultrasonic flow meter is especially attractive for the following reasons:

i. *Nonobstructive* – Ultrasonic transducers can be or not intrusive, as well as in some applications it's necessary to position transducer facing the inner wall of the tube. However, transducers do not obstruct flow velocity profile [1]. Thus, USFM introduce minimal pressure drop, which is a mandatory requirement in high flaring events.
ii. *No moving parts* – USFM have no moving parts other than vibrating ceramic crystals.
iii. *High rangeability* – USFM can cater for metering problems with high turnout ratio [1]. The high rangeability is based on suitable signal processing to overcome noise and orientation of transducers to guarantee mutual transmission and reception.
iv. *Bidirectional* – USFM can identify flow direction, since flow rate estimation is a function of measured transit times.
v. *Self-diagnoses* – USFM provides information about medium, such as sound speed measured, molecular weight estimation and density estimation [47]. They also have alarms, reporting failures. The variability of flow rate measured also gives a self-diagnosing capability, since noise level can be correlated to flow rate standard deviation and each meter has references values [48].
vi. *Accuracy* – USFM achieve accuracy, despite uncertainty in velocity profile [47].
vii. *Low maintenance* – Since USFM has no moving parts, the maintenance is reduced [2], [49].

Ultrasonic flow meters also present disadvantages, such as:

i. *High acquisition cost* – USFM are expensive flow meters, when comparing to pressure differential devices.
ii. *Calibration* – There are a few institutions around the world able to perform flow calibration in USFM.
iii. *Wet gas flow* – The performance of USFM is compromised in wet gas flow, because transducers' operational frequency to propagate ultrasonic waves in gases and liquids are different.
iv. *Gas with high carbon dioxide* content – In gases with high CO_2 concentration, USFM may fail due to signal attenuation [9].

Ultrasonic transducers are classified according to principles which allows radiation of sound. In modern ultrasonic flow meters applications, piezoelectric transducers are of main interest [50] because of the advantages of new production technologies . Transducer's operating frequency is particular to each application. Noise spectrum and impedance often represents limitations of minimal operating frequency.

3.3.1 Principle of measurement

Flow measurement process by transit time ultrasonic technology is based on time measurement of ultrasonic pulse packets, which are transmitted and received by transducers, made by piezoelectric materials. The piezoelectric component is a ceramic or crystal. It is encapsulated within the transducer and is responsible for the operation capacity as both emitter and receiver of ultrasonic waves.

The ultrasonic transit time technique requires at least one pair of ultrasonic transducers (one acoustic path). In the arrangement in focus here, the center lines between transducers are inclined with respect to the flow pipe axis. These transducers operate as both emitter and receiver of ultrasonic waves.

The pulse packet emitted from upstream transducer will reach the downstream transducer faster than the pulse packet emitter from downstream transducer and received by downstream transducer. This is because the pulse packet in flow direction is accelerated by velocity profile, while the reception of ultrasonic pulses, which propagate against the flow, is delayed. The difference of transit times is proportional to flow velocity [1]. Figure 11 shows a single path USFM installation sketch.

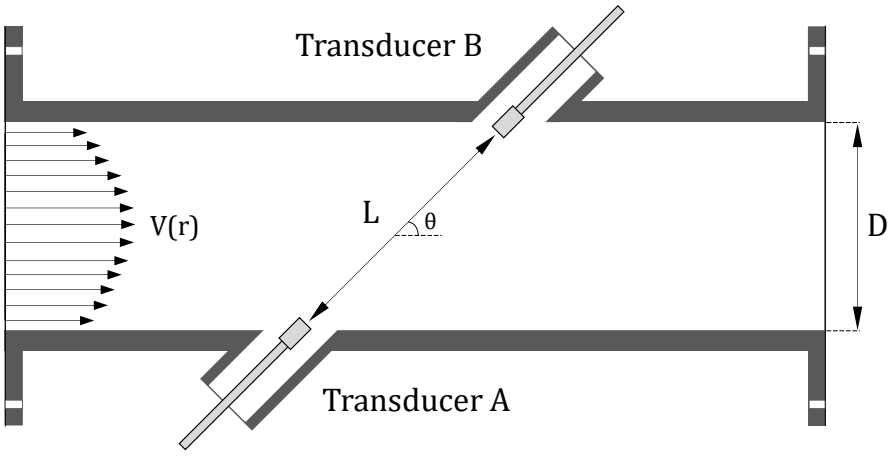

Figure 11 - Schematic illustration of a single path ultrasonic flow meter

Transit time ultrasonic flow meters measure line average velocity of ultrasonic pulses, along acoustic path length between two transducers. However, ultrasonic signal propagates at uniform velocity on acoustic path only in case of uniform velocity profile, which is an ideal case. In fact, velocity profile may cause a deviation of the acoustical path from straight lines. Considering a turbulent fully developed velocity profile, flow rate is always overestimated by uniform velocity assumption [51].

So, velocity profile impact ultrasonic propagation. Velocity gradient refracts acoustical pressure propagation [18]. Therefore, acoustical path is not uniform and nor a straight line, since it is distorted by carry-along effect by velocity profile [1]. Velocity profile is function of various flow parameters and, besides many efforts [52], it is very difficult to predict it, except in case of axisymmetric turbulent fully developed velocity profile. In transit time USFM applications, it is widely considered that acoustical path length is a straight line, which length is distance between transducers. This assumption is quite adequate for Mach numbers bellow 0.1 [53].

Considering the exposed conditions, the mathematical expression involving the parameters of interest for ultrasonic flow meter technology by transit time, results in a linear algebraic system composed by two equations, as Equation (3.1), and two unknown variables: c and v_{USFM}, that considers pipe geometric parameters (D and θ) and the measured transit time of ultrasonic pulses (t_{AB} and t_{BA}).

Considering average flow velocity projection on acoustic path:

$$\begin{cases} c + v_{USFM} \cos\theta = \dfrac{L}{t_{AB}} \\ c - v_{USFM} \cos\theta = \dfrac{L}{t_{BA}} \end{cases} \tag{3.1}$$

Where:

- c [m/s] is sound speed;
- v_{USFM} [m/s] is flow velocity along acoustic path;
- L [m] is the acoustic path length;
- θ [°] is the acute angle between the ultrasonic path and the axis of pipe section;
- t_{AB} [s] and t_{BA} [s] are, respectively, downstream (flow direction) and upstream (against flow direction) transit time.

Pipe internal diameter D and transducers acute angle θ are geometric parameters that are generally well known or can be measured by dimensional tools. Thus, the following trigonometric relations are valid, leading to acoustic path length L and axial length x:

$$\sin\theta = \frac{D}{L} \tag{3.2}$$

$$\cos\theta = \frac{x}{L} \tag{3.3}$$

Concerning to acute angle, θ is typically 45°. According to Ramos [54], the 45° angle provides less uncertainty for flow rate calculation.

The analytical solution of Equation (3.1) system leads to two important expressions on ultrasonic flow metering: measured sound speed c in Equation (3.4), and velocity of ultrasonic propagation on the acoustic path v_{USFM}, as Equation (3.5).

$$c = \frac{D}{2\sin\theta}\left(\frac{1}{t_{AB}} + \frac{1}{t_{BA}}\right) \tag{3.4}$$

$$v_{USFM} = \frac{D}{\sin(2\theta)}\left(\frac{1}{t_{AB}} - \frac{1}{t_{BA}}\right) \tag{3.5}$$

It is important to point out that velocity measured is a function only of transit time of ultrasonic pulses and piping geometrical parameters. So, the measurement of fluid velocity by ultrasonic flow meter is independent of temperature, pressure and molecular composition.

The accuracy of ultrasonic flow measurement performance depends on several factors. The major factor is the accuracy in transit time measurement. For each path length, the systematic contribution to measured transit times are [55]:

- Time delay due to electromagnetic wave propagation in electronics and cables;
- Time delay due to elastic wave propagation in the piezoelectric transducers;
- Time delay due to sound propagation in the two transducer port cavities;
- Time delay due to diffraction effects at transducers;
- Difference between measured upstream and downstream transit times at zero flow;
- Deposits at transducer front (oil, liquid, grease, etc.);
- Systematic effects in signal processing;
- Sound refraction due to flow profile effects.

On the other hand, sound speed is a thermodynamic property. So, it depends on temperature, pressure and chemical composition and independent of flow velocity measurement. For this reason, speed of sound readings by USFM may be monitored in USFM applications and used as a diagnostic performance parameter of USFM, when compared to estimated thermodynamic sound speed. Such flow meter operation performance is reliable since the measured speed depends on the same parameters of flow velocity.

Sound speed is the must use diagnostic tool of an ultrasonic flow meter. It is used in the dry calibration procedure and is monitored in industrial facilities. For multipath ultrasonic flow meters, the sound speeds of each paths are compared to the average sound speed calculated by the meter.

Temperature and pressure from the medium can be installed in USFM electronics for evaluation of flow in standard conditions (20°C, 1.01325 MPa).

3.3.2 The profile factor

The velocity of ultrasonic propagation on acoustic path can be related to the flow velocity considering the relation of velocity component variation on acoustic path and the average velocity along pipe's cross section.

The flow pattern effect on USFM is predicted by American Gas Association's Report No. 9 [6]. Several technical studies on this subjected have been done since the utilization of USFM in 1990's. The specialized bibliography [6] usually refers such ratio as profile factor – *k*. The *k* factor is expressed as:

$$k = \frac{\bar{v}}{v_{USFM}} \tag{3.6}$$

Jung & Seong [56] presents a methodology for estimation of profile factor in diametral USFM.

Other denominations of profile factor are: hydrodynamic factor [57], k factor [1], [6], [58], flow profile correction factor [56], [59] and hydraulic profile factor [51], [60], [61].

Once velocity profile is known, the profile factor is obtained as Equation (3.7)

$$k = \frac{\frac{1}{A}\int_A v(r)\cdot dA}{\frac{1}{L}\int_L v(r)\cdot dA} \tag{3.7}$$

Where:

- A is the area of cross section;
- $v(r)$ is the velocity profile and L is the acoustic path length.

Thus, flow rate can be calculated as Equation (3.8)

$$Q = k.v_{USFM}.A \tag{3.8}$$

A profile factor of one (k = 1) means that the velocity profile measured along acoustic path is equates exactly to the actual mean velocity. Such hypothesis considers: steady, unidirectional and uniform flow. In most industrial applications, flow pattern is turbulent and is not fully developed due to installation effects. That's why the knowledge of velocity profile is so important in USFM applications.

Considering velocity distribution as symmetric and fully developed, the flow pattern depends on Reynolds number. Consequently, the profile factor also changes. For high Reynolds number, the velocity profile tends to be closer to uniform behavior, because of turbulent mixing. For example, for Reynolds number range between $1x10^5$ and $4.5x10^6$, the profile factor changes 0.15% [61].

Since real time information of velocity field is impracticable, commercial USFM assumes turbulent and fully developed velocity profile [62], [63]. AGA 9 [6] proposes to consider turbulent and fully developed flow and suggest using the semi empirical velocity profile proposed by Nikuradse [64]. The mathematical function associated to such profile is semi-empirical power law function, based on experimental methods for smooth pipes, calculated as (3.9):

$$v(r) = v_{\max}\left(\frac{r}{R}\right)^{1/n} \tag{3.9}$$

The constant *"n"* represents an empirical exponent, derived from experimental data. It is calculated as Equation (3.10).

$$n = 2 \cdot \log\left(\frac{\mathrm{Re}}{n}\right) + 0.8 \tag{3.10}$$

Considering k factor definition as Equation (3.7), and Nikuradse's power law as Equation (3.9), the analytical form of AGA9's k factor become:

$$k_{AGA9} = \frac{2n}{2n+1} \tag{3.11}$$

The changes of profile factor due to path trajectory deviation from straight line may be estimated by [60]:

$$\frac{\Delta k}{k} = -Ma^2 \tag{3.12}$$

Where Ma is Mach number - $Ma = v / c$.

Concluding this section, measured flow rate is affected by profile factors. Thus, in practical applications is essential to understand the installation effects on asymmetrical velocity profiles, considering piping characteristics upstream to the measured section. Thereby, profile correction factors may be estimated considering such effects.

3.3.3 Installation effects

As described in last sections, the knowledge of turbulent fully developed flow over a wide range of Reynolds number is well defined. However, for short straight tubes length the velocity profile behavior deviates from the ideal form, due to induced asymmetry, cross flows and swirl. In such case, disturbed flow analysis plays a very particular issue to each installation configuration. Figure 12 exemplifies flow disturbance downstream to elbows in flare gas conditions.

Manufactures of ultrasonic flow meters mostly recommend installation of the meter at least 20 straight diameters (20D) upstream and 10 straight diameters (10D) downstream [63], [65] to the metering section. In the other hand, industrial applications represent a challenge, if enough dimensions of straight tubing are not available.

Ultrasonic flow meters are very sensitive to flow patterns, since market models available assumes operation under a turbulent and fully developed velocity profile. However, this condition is seldom achieved in oil and gas industry due to presence of curves, valves and elbows. A proposal for solution based on installation of flow conditioners, to relieve turbulence effects, are not allowed in flaring gas tubing, since such accessories obstructs the flow and flare lines are for intrinsic safety of operational plant.

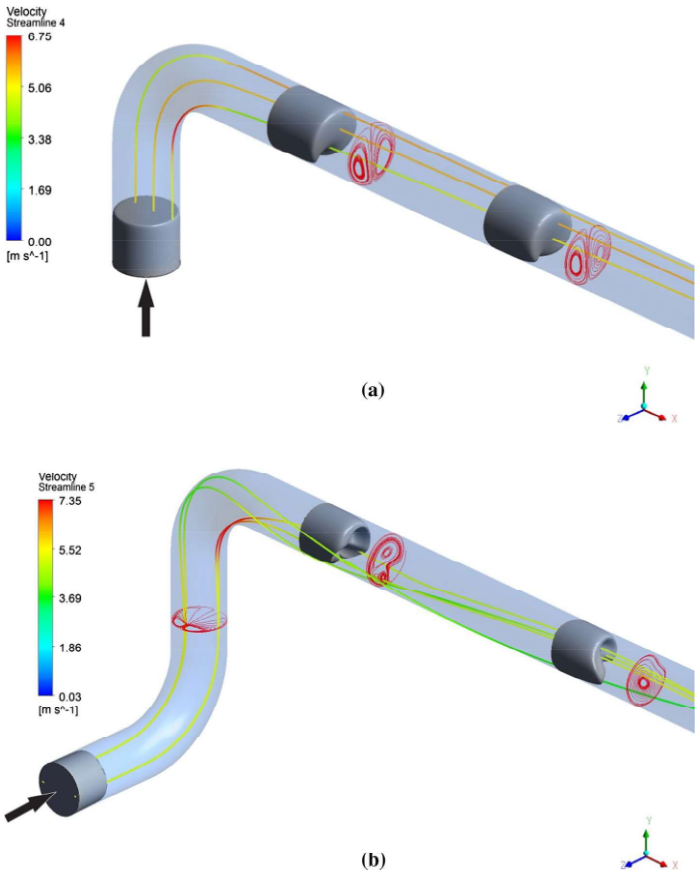

Figure 12 - Examples of profile disturbances downstream to single-elbow and a double elbow-configurations in flare gas flow conditions [66]

For this purpose, Mickan et al. [67] performed experiments comparing flow patterns downstream to several pipe geometries using laser doppler velocimetry (LDV), simulating a real gas industrial pipe facility. Aiming similar goal, Carlander and Delsing [48] examine flow rate measured by USFM under disturbed conditions and found increase of standard deviation up to 100% in measured velocity. The authors found, experimentally, differences below 4% comparing measured flow rate in case of one and two elbows [48].

Ultrasonic flow meter is also sensitive to transducers mounting, since mounting angle affects meter correction factor [59]. Ruppel and Peters [68] examined ultrasonic flow rate errors caused by flow patterns downstream single and double curves

installation. They conclude that error shift is very sensitive to mounting angle and straight tube length for a range of Reynolds number from $1.5x10^5$ to $3.0x10^5$.

More recently, computational numeric techniques, such as Computational Fluid Dynamics (CFD), are applied for evaluation of installation effects in USFM applications. Zheng et al. [69] perform three dimensional flow patterns downstream a single elbow pipe water flow. The article claims that downstream distance from installations effects and mounting angle disturb velocity profile.

Martins, Andrade & Ramos [52] examines deviations on profile factor induced by disturbed flow using atmospheric air via CFD methods. The authors found that for higher Reynolds number, higher is the relative deviation of profile correction factor comparing to fully developed reference flow. Moreover, profile factor is very sensitive to the mounting angle and behaviors are not linear.

The effect of pipe inner surface roughness should be considered, as studied by Mori et al. [59]. The profile correction factor changes 1.5% as the inner surface roughness changes from 1 μm to 95 μm.

On the other hand, multipath ultrasonic flow meters are recommended for applications under disturbed velocity profile. The velocities on each acoustic path are compared, providing information about the asymmetry of the velocity profile. Drenthen and Boer [70] reduced the uncertainty of an application from 1%, for a single path meter, to 0.4% using a three path meter.

Noise effects interfere in USFM performance, as well. As source, control valves with significant pressure drop can produce noise in the same ultrasonic frequency of ultrasonic transducers [71]. The power loss by control valves is much higher than transducers power. Once generated, the noise from valves travels both upstream and downstream direction. However, valves effect on flow metering performance shows to be greater installed upstream than downstream to flow metering cross section.

3.3.4 Signal processing

Signal processing technique in USFM should incorporate an adaptative filter that will give an ideal signal to noise ratio (SNR) performance. The first USFM applied radar detection principle. Basically, received signal are compared to bursts signals. The usage of chirp signals and a combination of chirp and continuous wave signals in USFM gives rise to high rangeability capability [1], [46]. Received signal is compared to burst signal, in a process of cross correlation.

One of the challenges of signal detection refers to flow induced noise, which is predominant below 50 kHz frequency on flare stack [46]. Another complexity in signal detection is the high absorption of sound energy.

3.3.5 Temperature effects

If USFM operates in low velocities and there is a large difference between gas temperature and atmospheric temperature, heat transfer by natural convection may occur, developing internal temperature gradients. This effect is called thermal stratification [49]. In case of multipath ultrasonic flow meter, it can be noticed a difference of sound speeds measured on each path, due to thermal stratification phenomenon.

3.3.6 Low velocity flow

Low flow presents two major challenges for the USFM. The first one is the resolution in velocity measurement by very short transit time (in the order of nanoseconds). The second challenge is the asymmetric flow, in which the velocity in the main flow direction is on the same order as non-axial flow.

The resolution in velocity measurement in ultrasonic flow meters is related to accuracy in measurement of transit time , as well as accuracy of dimensional geometrical parameters [2]. According to Matson et al. [2], longer path lengths results in lower inaccuracy in transit times measurements.

In low flow condition, non-axial velocity pattern contributes significantly to transit times measurements. In this case, asymmetric flow, originates from convection, heat transfer and stratification of gases with different densities [2].

Matson et al. [2] proposed solutions for accurate low flow applications. The basic option is one longer path, but it depends on gas composition and on piping diameter. Another option is installing two or more paths to achieve accuracy over a wide velocity range.

3.3.7 Recovery angle

The carry along effect on ultrasonic pulse packets is well known, especially at high speed applications, such as flare gas measurement.

For turbulent flow, the shift effect of wave trajectory on received pulse by USFM should be corrected. The trajectory of ultrasonic signal presents S shape and maximum shift get the magnitude order of Mach number [60]. The author shows that considering the trajectory shifts of ultrasonic pulses, the measured velocity is larger than if considering straight line trajectory.

Ray rescue angle, or recovery angle, is a proposal for high flow rate applications of transit time USFM [1]. As mechanical waves, ultrasonic pulses may blow away in high velocity flows, resulting in miss of the “perfectly aligned” target receiving transducer [2]. In this context, recovery angle can be implemented offset the beam drift effect in ultrasonic pulse packets in both upstream and downstream transducers [2].

In large dimensional pipes, ray rescue angle corrects the carry-along effect on upstream and downstream pulse packets [1], [2], [18]. The higher is flow velocity, the more prone may be the ultrasonic signal to this carry along effect. The same ray rescue angle prevents the formation of standing waves in small dimensional pipes [1].

For transit time ultrasonic flow meters, it is possible to calculate the downstream and upstream beam drift γ due to flow velocity [2]:

$$\gamma_{up} = \theta - \tan^{-1}\left(\frac{\sin\theta}{\cos\theta - M}\right) \tag{3.13}$$

$$\gamma_{down} = \theta - \tan^{-1}\left(\frac{\sin\theta}{\cos\theta + M}\right) \tag{3.14}$$

The upstream ultrasonic beam drift is more severe than downstream beam drift [2], [18]. Ray rescue number can be implemented in both upstream and downstream transducer [1], [18], as illustrated in Figure 13.

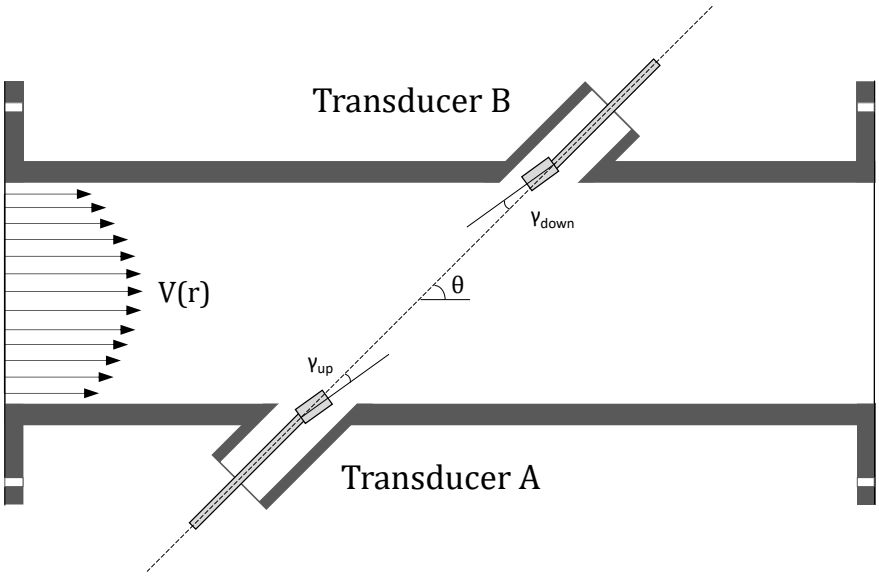

Figure 13 - Ultrasonic transducers with recovery angle

Matson, Sui and Nguyen [2] implement and test a 6° recovery angle on downstream transducer as a compromise of performance between high flow and low flow. This configuration is sold by a commercial flare gas USFM [65].

3.3.8 Attenuating media effects

Exploitation of unusual hydrocarbon sources lead to more diverse operating conditions. In the pre-salt petroleum reservoirs, for example, natural gas presents high CO_2 concentration. While standard applications deal with CO_2 below 5% [5], in pre-salt province carbon dioxide content may overtake 95% in high flare conditions [2].

CO_2 strongly affect ultrasonic flow meters performance, due to the absorption of ultrasonic waves energy, as typical in flaring gas transducers operational frequency

[2], [5], [36]. The molecular structure of CO_2 absorbs ultrasonic acoustical energy [4], [37]. In this context, received signal power is so weak that may induce failures in flow metering.

Due to wave propagation and attenuation, the harmonic acoustic pressure *p* decreases according to Lambert Beer law [20], as Equation (2.12). By observation of Lambert Beer equation, some considerations can be made in order to improve signal quality.

The first consideration is the power enhancement, increasing the acoustic pressure at the emitter [5], [23]. This can be made by providing a higher driving voltage to transducers. However, in flaring gas application transducers power is restricted due to intrinsic safety premise of the installation.

Secondly, the design of the transducer itself can increase the sound pressure level [5], improving the propagation of ultrasonic energy. The manufactures should assure efficiency in conversion of electrical energy into acoustical energy. It is called acoustic efficiency [5].

The third option is to reduce the path length, but it is generally not viable, since flaring gas flow meters are recommended to not obstruct the flow.

Lastly, transducers operation frequency is the major factor affecting the performance of flow metering. The attenuation of ultrasonic waves is frequency dependent. Low frequency is, normally, not practice in flare piping owing to the noise spectrum [46] of industrial facilities and due to impedance matching of transducer and fluid flow properties. Therefore, the frequency of a USFM transducer should be optimized for each specific application, in high CO_2 applications, for example.

In summary, to ensure accurate operation, the meter design and specifications related to the application need to be thoroughly evaluated prior to selecting the meter [5].

Matson, Sui and Nguyen [2] tested a USFM in natural gas between 1 bar and 3 bar up to 36 m/s in a 6 inches piping.

Helden et al. [5] examined flow metering performance in a reinjection application (62% CO_2 + 37% CH_4) using a 4 path ultrasonic flow meter with two operating frequency (135 kHz and 208 kHz). The difference between the tested USFM and the reference flow meter was 0.2%. However, this re-injection application had a pressure of 65 bar, that leads to a higher acoustical impedance. Consequently, the portion of ultrasonic energy which is transmitted to the gaseous medium is much higher than in atmospheric air. It means that the result from Helden et al. [5] cannot be extended to flaring gas applications.

Barros [8] evaluated a flare gas USFM in a wind tunnel with high CO_2 content, resulting in failures in flow metering. The transducers approximation shows to be

effective in reducing failure index. However, the procedure increases the variability of flow meter readings. The author established criteria for fault identification:

- *Criterion A* - Failure by negative flow readings.
- *Criterion B* – Failure by inconsistency between the measured sound speed and the theoretical sound speed estimated by state equations [72].
- *Criterion C* - Failure by signal loss, indicated by low signal strength.

Such criteria can be applied to develop a methodology to real-time data processing of operational flow rate measurement, identifying faults and presenting to the operator a less noisy flow rate information, without interfering in accumulated flow rate.

The effect of an attenuating medium, such as natural gas with high CO_2 concentration, is a challenge in ultrasonic flow metering process.

3.4 UNCERTAINTY AND ERROR SOURCES

Market models of flare gas ultrasonic flow meter generally achieves an accuracy better than 0.5% in long straight pipes, in a calibration lab [47]. The technological challenge is assuring similar accuracy in USFM installed in the field.

The requirements for ultrasonic flow measurement in flare gas applications is stated by some institutions (AGA 9 [6], API 14-10 [73], NBR 16777 [74], Portaria ANP/INMETRO [3])..

Operationally ultrasonic flow meter in field generally operates exposed to installation effects. As uncertainty sources:

- Nonideal upstream and downstream piping [52];
- Electronics and transit-time picking [70];
- Piping geometry [70]and roughness [59];
- Accumulation of oil on ultrasonic transducer;
- Shift of trajectory of ultrasonic pulses [60];
- Diffraction correction [55].

Lunde et al. [55] shown that especially for small-size meters (4”-12”) treatment of diffraction effects is highly recommended if high accuracy of the volumetric flow rate measurement is required.

3.5 DRY CALIBRATION

Currently, calibrating a flare gas USFM is impracticable. In addition to the absence of institutions capable to perform flow calibration in operating conditions, removing the ultrasonic flow meter from line implies in separate transducers from a unique device, associated to issues related to accessibility, costs, logistics and risks

[42]. In this context, the dry calibration procedure is widely used in performance check of USFM.

Dry calibration is a static verification of ultrasonic flow meters performance in a zero-flow arrangement, as illustrated in Figure 14. A dry calibration is not a flow calibration, but a verification of transit time measurement, flow calculation modulus, piping dimensions, electronics and transducers operation [70]. If necessary, meter's configuration is adjusted to ensure that meter performance matches dry calibration analysis.

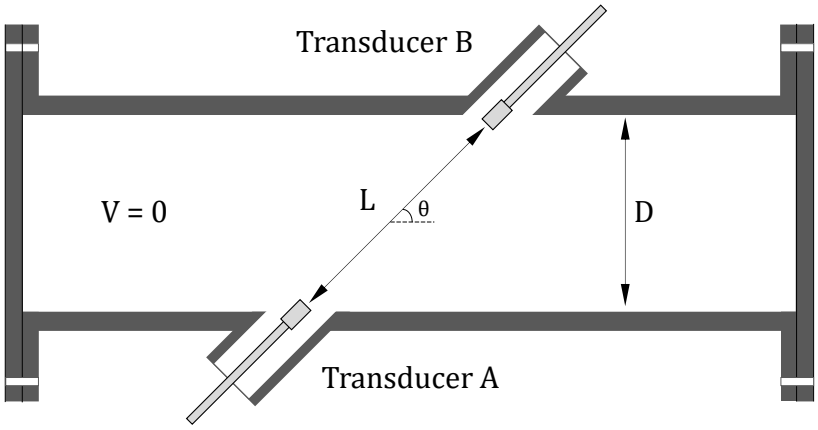

Figure 14 - Ultrasonic flow meter in a zero-flow arrangement (dry calibration)

The dry calibration procedure is especially attractive because does not require a meter to be sent to a calibration facility. The costs are very lower than the costs of a dynamic calibration. Dry calibration procedure should be performed prior to the meter commissioning and periodically verifying.

Among different types of dry calibration procedure [55] this study focus on the so-called "sound velocity method" [6]. A pair of transducers is mounted in a calibration chamber with a stabilized environment (pressure and temperature). The distance between transducers must be accurately measured. The chamber is filled with a known fluid (generally nitrogen or air) which the sound speed is precisely known. A zero point calibration can only be performed if the fluid is perfectly still and sound velocity is precisely known [61].

The measured sound speed using transit times of ultrasonic pulses are compared to the estimated thermodynamic sound speed. A zero-flow check is done to ensure that the meter indicate a null flow rate. Due to small differences in transducers, delay in electronics, diffraction effects and systematic effects [55], USFM exhibit small offset errors in the velocity measurement and sound speed measurements. So, if necessary, transit times are corrected in a dry calibration procedure.

4 THE DRY CALIBRATION PROCEDURE

4.1 INTRODUCTION

Regarding several acoustical phenomena involving ultrasonic flow measurement process (diffraction, refraction, attenuation and others), it is important to characterize a reference behavior for further comparison at actual operational flow conditions. This chapter examines the performance of an ultrasonic flow meter at zero-flow condition and high carbon dioxide concentration.

Firstly, flare gas ultrasonic flow meter is examined in the dry calibration arrangement in atmospheric air. Then, the flow meter is tested at attenuating media, composed by mixtures of air and carbon dioxide.

4.2 ZERO-FLOW VERIFICATION

In a calibration procedure, an instrument such as flow meter device, is adjusted so its indication in satisfactorily agreement to an adopted reference to a standard instrument [73]. Therefore, calibration processes are generally not applicable in flare gas ultrasonic flow meters applications due to:

(i) transducers must be removed from its working position, which prevents efficient calibration (due to the retractable rod arrangement);
(ii) lack of calibration facilities for such class of meters.

In this way, most legal laws and technical recommendations indicate a zero-flow verification as a way to ensure the performance of some parameters of metering process.

In ultrasonic flow metering process, the emitted signal is contaminated even before being transmitted to the acoustic media because of mechatronic effects in signal processing, such as cables, electronics and amplifiers [61]. The resulting systematical errors is a function of the signal delay time, leading to the so-called “zero flow error”. To perform a zero-flow verification, the fluid must stay perfectly still and the sound velocity in the media must be well known. This verification procedure is referred as dry calibration by manufactures and technical community [6], [55], [73]–[75].

The dry calibration represents a consolidated technique [55], [58], [70]. According to Drenthen & Boer [70], the stated performance of a USFM can be guaranteed based on a dry calibration, a practice widely accepted in orifice measurement. However, this procedure only verifies the performance of transducers, pipe’s geometry, signal processing, electronics, cables and capability of measure transit times. Yet, the authors did not consider other effects that impacts flow metering performance, for instance: turbulent effects, the beam drift effect typical in high speed applications, signal attenuation, as well as pulsating effects.

Even so, the dry calibration arrangement is widely applied for flare gas ultrasonic flow meters. The main advantage is that such procedure is an *in-situ* method for testing ultrasonic flow meters. Good engineering practice would be apply the procedure at the time of initial commissioning as well as periodically, in a work cycle [6], [73], [74], [76].

To perform a dry calibration procedure, ultrasonic transducers are submitted to a zero-flow check. Flow velocity in each acoustical path should be kept as zero (non-flow condition). Besides, sound speed obtained by measured transit times can be compared against the thermodynamic sound speed, estimated considering local pressure, temperature and fluid composition. Hence, small differences between speed of sound can be adjusted. However, large divergences indicate possibility of errors due to both: geometric assembly time-of-flight readings.

Others methodologies of zero-flow verification are applied for diverse other flow meters technologies, such as orifice plate [70] and mechanically-based flow meters [77]. Nilson & Delsing [77] suggest an *in situ* test method to examine the performance of flow meters, which has even the ability of distinguish the error sources.

But ultrasonic flow technology is unique in this sense, which is, in the same situation of reading zero-flow condition, a well-known thermodynamic property as sound velocity, that may be checked by thermodynamic state, which is independent from ultrasonic technologies.

4.3 DRY CALIBRATION METHODOLOGY

4.3.1 Experimental apparatus

The experimental apparatus of dry calibration is shown in Figure 15. It consists of a pair of transducers of the ultrasonic flow meter installed in a metallic spool, whose dimensions are well-known, blocked in both sides. In one extremity, there are injection of gases and a sample point to analyze the gas composition by a gas analyzer (Testo 350, in present case). In the other extremity, there is a purge valve and a temperature sensor.

One pair of welded nozzle and flanges are installed, that enables the assembly of ultrasonic transducers. The spool is sealed at both sides by an acrylic cap enveloped by a U-shaped rubber. The cap-rubber group gets inside the spool by interference, with gives a versatility capability to the experiment. Bolted internal brackets support and prevent possible movement of the acrylic caps in order to ensure the seal of the assembly.

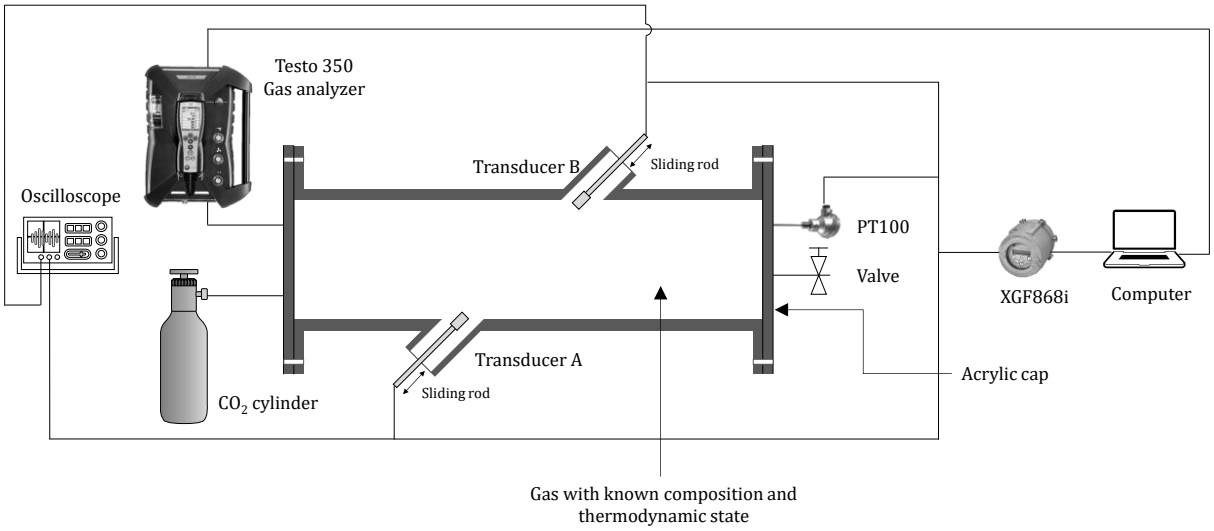

Figure 15 - Experimental apparatus: dry calibration set up (transducers in reference position)

As transmitter-receiver of sound waves, it is used a flare gas ultrasonic flow meter model GE XGF868i. It is a narrow-band piezoelectric transducer operating at 100 kHz. The 2-inch transducer flanges are connected to the 2-inch valve flanges, mounted on a 12-inch (284 mm) metallic spool.

But, since such arrangement by sliding rods transducers is usual for such flow meter application, the methodology is usable for any model available in market.

Once transducers are positioned at the desired distance, by sliding joint connection, the acoustical path length is set by a micrometer. This procedure provides accuracy in geometrical parameters, which are input for the USFM. Then, both sides of the spool are closed by acrylic caps. So, gas is injected and confined inside the spool without leakage. Moreover, the spool and the acrylic caps are covered by foam rubber as thermal insulator, aiming to reduce the heat exchange between external environment and gas inside the spool.

Temperature inside the spool is monitored by a PT100 sensor, so that gas temperature variation is detected. Room temperature and relative humidity are registered by a digital thermo-hygrometer. Environmental temperature is kept between 26°C and 30°C, and 70% of relative humidity.

4.3.2 Gas Injection

Since the spool dimensions are known, gas injection time can be predicted using the spool internal volume and the gas regulator flow rate indication. The procedure for gas injection follows the following steps:

i. Opening the purge valve of the spool, to keep constant the atmospheric pressure inside the spool.
ii. Turn on the gas analyzer Testo 350.

iii. Adjustment of the flow regulator of the CO_2 cylinder, to control the gas injection.
iv. Opening the CO_2 cylinder valve.
v. To clock the injection time aiming the estimation the gas concentration as a function of the internal volume of the spool.
vi. After stop injection, turn off the gas analyzer and close purge valve firstly, then the cylinder valve and the gas regulator.

The carbon dioxide utilized presents 99.99% purity.

After adjusting the carbon dioxide concentration to the desired value, the mixture is allowed to stand for 10 minutes to reach thermal equilibrium and uniformity. The gas composition is measured for 1 minute using Testo 350. Thereafter, tests are initialized.

4.3.3 Transducer approximation

In standard installation, as recommended by manufacturers, the transducers are positioned facing the inner wall tube. In such assembly, transducers do not obstruct the flow. However, transducers are mounted by sliding rods, which enables changes in the transducers distance, without the need to disassemble transducers.

The effect of acoustical path length may be evaluated in this dry calibration arrangement by ultrasonic transducers approximation.

Transducers positions are adjusted firstly by fixing one transducer and moving the other one to half of the desired distance. Then, micrometer is adjusted to full distance and the fixed transducer is now moved.

The desired positions are previously marked on transducer stem, so that the transducers can be moved to the desired distance without need to open the spool. Lastly, the current geometrical parameters are adjusted are in the meter software. All transducers positions are located in the so-called far field zone. Table 2 details transducers distances as a function of the reference distance.

Table 2 – Geometrical configurations of transducer approximation in dry calibration

#	% Reference distance	Acoustical path length [mm]	Axial length [mm]
1	100%	L_1 = 401.6	A_1 = 284.0
2	80%	L_2 = 321.3	A_2 = 227.2
3	60%	L_3 = 241.0	A_3 = 170.4
4	50%	L_4 = 200.8	A_4 = 142.0
5	40%	L_5 = 160.7	A_5 = 113.6

4.3.4 Examination of speed of sound performance

The main premise for the tests of the transit time ultrasonic flow meter is the realization of experiments in a known and steady state environment. In dry calibration

arrangement, it means that the experiment should present constant temperature, pressure and gas composition and non-flow condition.

The ultrasonic flow meter presents some diagnosis parameters, applied to identify failure events and to characterize the meter performance. In this context, the parameter “Signal Strength” is utilized in this work. According to the manufacturer, signal strength value must be above 50 in proper operation of the flow meter [62].

It may be verified if there is no significant gas leakage in the procedure of transducers approximation. So, after gas injection, the ultrasonic flow meter is examined at each transducer positions of Table 2.

In this context, after gas injection and positioning the transducers, it is adopted a period of 15 minutes test time for evaluation of the flow meter performance. Gas composition is measured before and after the USFM evaluation period, using Testo 350 to ensure the stability of gas concentration and spool sealing.

Main parameters examined by dry calibration procedure are: flow velocity and sound speed. Both are calculated independently using transit times readings.

In a zero-flow condition, the transit times upstream and downstream should be equal, if the flow meter is proper functioning. Hence, from Equation (3.5), flow velocity should be zero. Small velocity measured by USFM, typically less than 0.1 m/s, can indicate effects of natural convection currents.

Sound speed is a thermodynamic property of the medium. So, it is a function of temperature, pressure and chemical composition. In current work, the reference of sound speed in gases is the equation of natural gas by AGA10 [72], simulated through the software FlowSolv [78].

Differences between measured and reference speed of sound SoS_{USFM} versus SoS_{AGA10} are calculated by Equation (4.1).

$$\Delta c = \frac{\left| SoS_{AGA10} - SoS_{USFM} \right|}{SoS_{AGA10}}.100 \tag{4.1}$$

Through volumetric balance, it is found the gas composition using the measurements of Testo 350 and the dry air model adopted (79% N_2 + 21% O_2). The gas composition, atmospheric pressure and measured temperature are utilized to simulate the thermodynamic sound speed. Such theoretical sound speed (SoS_{AGA10}) is afterward compared to the measured sound speed by USFM using transit times (SoS_{USFM}).

Usually, market ultrasonic flow meters present diagnostic parameters to detect signal strength and signal quality. In this work, the diagnostic parameters are monitored during experiments to faults detection, but are not commented in the results section.

In order to monitor basic electrical signals produced by piezoelectric transducers, cables are placed at the terminal block electronics, connecting the transducers signal to an oscilloscope. This montage enables the monitoring emitted and received signal. These connections are important for academic researches, since the signal voltage can be utilized to predict acoustic parameters, as attenuation coefficient.

Data acquisition of ultrasonic flow meter model is done using the meter proprietary software [79]. The acquisition rate is 0.2 Hz. To increase this rate is necessary to implement a data acquisition system via Modbus protocol. However, in dry calibration arrangement is not necessary.

The temperature sensor is connected in a slot at the meter's electronics. So, temperature is integrated at flowmeter software. Gas concentration measured by Testo 350 XL is monitored at its own software EasyEmissions [80], with a data acquisition rate of 1 Hz.

4.3.5 Definition of reference state

The term "reference state" is referenced several times over this chapter. This condition is here defined as the standard installation of ultrasonic transducers, facing the inner wall of the duct. Besides, at reference state the spool is filled with atmospheric air at no flow condition. This is considered the optimum operating condition, since it presents minor acoustic attenuation condition.

4.4 RESULTS AND DISCUSSIONS

4.4.1 Ultrasonic flow meter performance in dry calibration condition

Before performing the evaluation of flow metering performance in high CO_2 level, it is necessary to perform a validation test of the ultrasonic flow meter at reference state. Thus, the meter is evaluated in the dry calibration arrangement with transducers positioned facing the inner wall of the duct and operating in atmospheric air. The flow meter is evaluated by 8 hours, approximately, at data acquisition rate of 0.2 Hz, totalizing 5780 readings.

The sound speed verification compares measured and estimated atmospheric air sound speed by perfect gas model. The sound speed of a perfect gas is calculated by Newton-Laplace equation [81]:

$$c = \sqrt{\frac{\gamma \overline{R} T}{M_{mol}}} \tag{4.2}$$

Where:

- γ [dimensionless] is the isentropic coefficient;
- $\overline{R}$ [J/Kmol.K] is the universal gas constant;

- M_{mol} [kg/kmol] is the molecular weight of the perfect gas;
- T [K] is the fluid temperature.

Readings are shown in Figure 16. Temperature inside dry calibration spool ranged from 21°C to 26°C. Then, sound speed of atmospheric air, considering perfect gas varied from 346.0 m/s to 347.5 m/s. On the other hand, experimental sound speed, reported by USFM, vary between 339.6 m/s to 341.1 m/s.

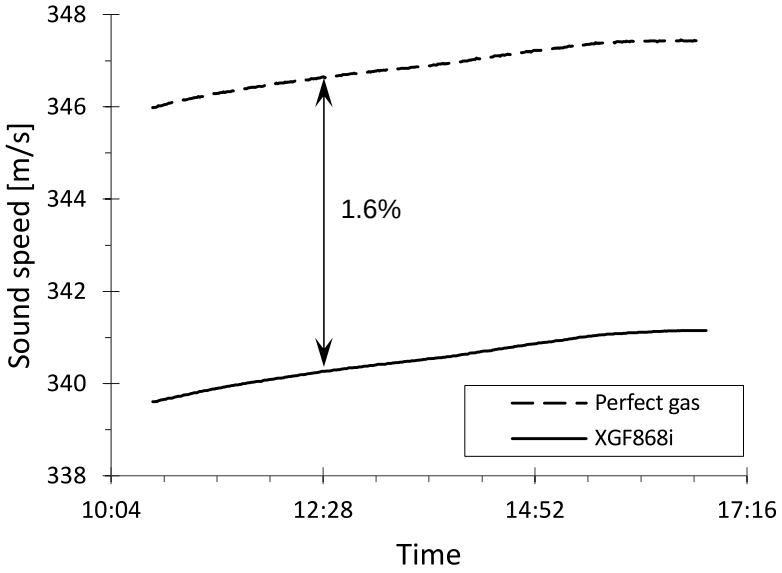

Figure 16 - Validation of the ultrasonic flow meter at reference

Differences of measured sound speed and reference sound speed, as Equation (4.1), remain constant in 5.3 m/s. This is equivalent to a percentual variation of approximately 1.6%. Even though there are differences between measured and theoretical values, the sound speed behavior remains relatively constant though out the test period. So, transit times can be adjusted so that meter's reported sound be coincident with the estimated speed of sound. However, this adjustment does keep the relative variation of sound speed constant when changing path length, propagation media and temperature.

Readings indicate that ultrasonic flow meter is sensitive to temperature variations. Considering the meter uncertainties (+/- 5% of flow rate), sound speed readings and estimated keeps a difference of 1.6%. Besides, flow rate measured by XGF868i are zero all over the validation test.

Considering that all diagnosis parameters during the validation experiment matches specified levels, the ultrasonic flow measurement is considered validated. Therefore, studies on the influence of CO_2 and transducer approximation on meter performance are continued.

4.4.2 CO_2 effect on speed of sound measurement

Acoustic absorption promoted by CO_2 leads to attenuation of ultrasonic waves emitted by transducers. Consequently, it is expected failure events in flow measurement process if operation in such condition. This can be monitored by diagnostic parameters.

Assessing carbon dioxide effect on sound speed measurement, ultrasonic transducers are facing internal tube wall, as reference position. This positioning is recommended by technical specifications. Besides, the manufacturer performed a dry calibration procedure to adjust transit time delays and electronic signals for commissioning of the flow meter in such reference position.

Figure 17 shows speed of sound readings, as well as reference speed of sound, according to AGA Report No. 10 (2002), that consider mixtures of dry air and carbon dioxide ($N_2 + O_2 + CO_2$). Mean values for speed of sound is obtained from 180 readings at stable CO_2 levels.

The thermodynamic speed of sound is inversely proportional to CO_2 concentration in air. The increase of carbon dioxide concentration decreases sound speed. The sound speed analysis indicate that flare gas ultrasonic flow meter is sensitive to high CO_2 levels according to AGA10 [72].

Regarding to sound speed measurement, the 100 kHz transducer evaluated could perform speed of sound readings with difference between 0.1% and 1.9% comparing to the AGA10 estimated sound speed up to 100% of CO_2. In such readings indications of flow velocity pointed out to zero. Considering technical specifications and legal requirements, tests with high carbon dioxide levels are considered validated.

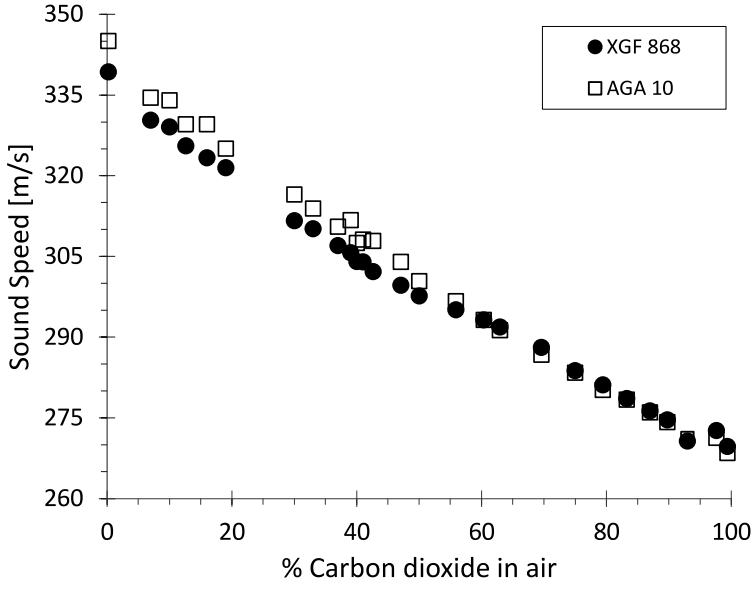

Figure 17 - Comparison between the measured sound speed and the reference value by AGA 10 with the presence of CO2

According to proprietary technical specifications, an appropriate transit time measurement process must present the signal strength parameters of the ultrasonic transducer above 50. Figure 18 shows the effect of CO_2 on signal strength. It is observed that the presence of CO_2 deteriorates signal strength of both transducers. There is no significant difference between signal strength upstream and downstream.

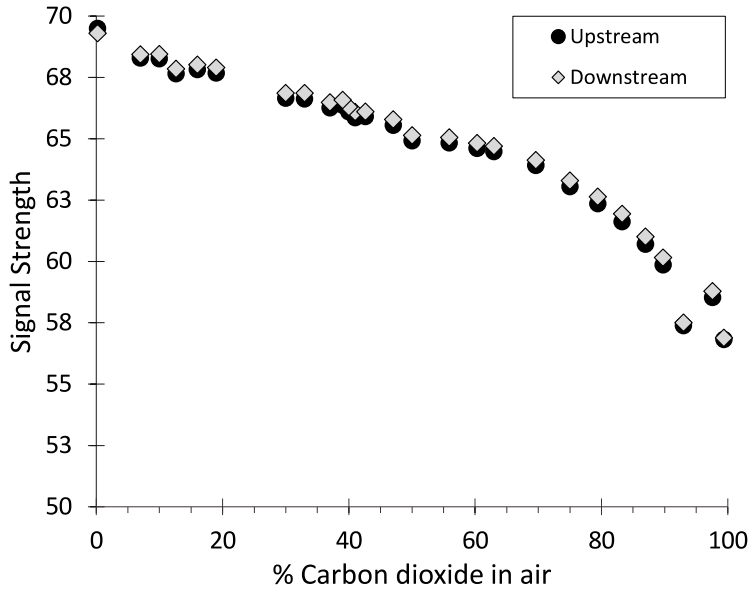

Figure 18 - Carbon dioxide effect on diagnostic parameter of ultrasonic flow meter

Signal strength fell from 69.5 in atmospheric air to 57 in approximately 100% CO_2. This is equivalent to a 18% reduction of signal strength.

Considering technical specifications and legal requirements, tests at high carbon dioxide levels are considered validated for measured speed of sound, as well as signal strength levels.

4.4.3 Transducers approximation effect

Considering Lambert Beer Law as Equation (2.12), path length reduction may be an alternative to improve performance of ultrasonic flow meters, since the procedure tends to increase the sound pressure. Hence, the meter is examined in dry calibration arrangement varying transducers distances according to Table 2, as well as at several mixtures of atmospheric air and carbon dioxide. The criteria for analysis of flow metering performance are: i) Flow rate; ii) Sound speed; iii) Signal strength and iv) Signal voltage amplitude.

In dry calibration procedure, ultrasonic transducers are examined under zero flow condition. Thus, it is expected that transit times upstream and downstream be equal whatever is fluid composition. Consequently, flow velocity, as well as flow rate, indications must be zero.

Flow velocity measurement for dry calibration tests with transducers approximation are show at Table 3.

Table 3 – Flow velocity in dry calibration experiments and transducers approximation

Path length [mm]	Flow velocity [m/s]					
	100% Air	15% CO_2 + 85% Air	30% CO_2 + 70% Air	50% CO_2 + 50% Air	70% CO_2 + 30% Air	100% CO_2
401.6	0.00	0.00	0.00	0.00	0.00	-0.03
321.3	-0.02	0.00	0.00	0.00	0.00	0.03
241.0	-0.04	0.00	0.00	0.00	0.00	0.14
200.8	-0.04	0.00	0.00	0.00	0.00	0.00
160.7	0.00	0.00	0.00	0.00	0.00	0.00

Tests with pure atmospheric air leads to small flow velocity readings, between -0.02 m/s and -0.04 m/s. This magnitude of flow velocity can be assigned to the inherent uncertainty of the process, as well as natural convection effects. Besides, dimensional differences between transducers and at electronics may lead to small offset errors at velocity in dry calibration [70].

Meanwhile, running's with CO_2 concentration between 15% and 70%, only zero indication of measured flow velocity is noticed. However, at approximately 100% of CO_2 flow velocity indication at the three longest transducer distance. In these cases, flow velocity measured using transit times is -0.03 m/s at 401.6 mm, 0.03 m/s at 321.3 mm and 0.14 m/s at 241.0 mm. Such behavior reinforces the influence of uncertainty and natural convection effects.

Except for the experiment indicating velocity of 0.14 m/s, flow measured are below the configured *cut off* value according to technical recommendations [62]. Thus, regarding to zero flow measurement, experiments with transducers approximation are considered validated.

Figure 19 illustrate transducer approximation effect on sound speed deviation. Especially for CO_2 levels higher than 70%, sound speed variations decrease with transducers approximation. It's also noticeable the increment differences between sound speed measured by USFM against reference sound speed by AGA10 as carbon dioxide is incremented in mixture.

Considering atmospheric air, sound speed difference is between 0.6% and 0.9%. Minimum difference is achieved in the reference path length. But, for 15% of carbon dioxide level, differences increase from 0.2% to 0.5%. For mixtures of air and carbon dioxide with 30% of CO_2. differences are between 0.1% and 1.1%.

For concentrations below 50% of carbon dioxide in air, the highest sound speed deviation is 1.1%. For 100% CO_2. differences are between 3.1% at L_1 = 401.6 mm and 1.8% at L_5 = 160.7 mm.

For others five different path lengths evaluated, maximum speed of sound deviations are achieved at 100% CO_2. That is an evidence of attenuating effects

induced by high CO_2 levels affects USFM transit time and, consequently, flow measurement performance.

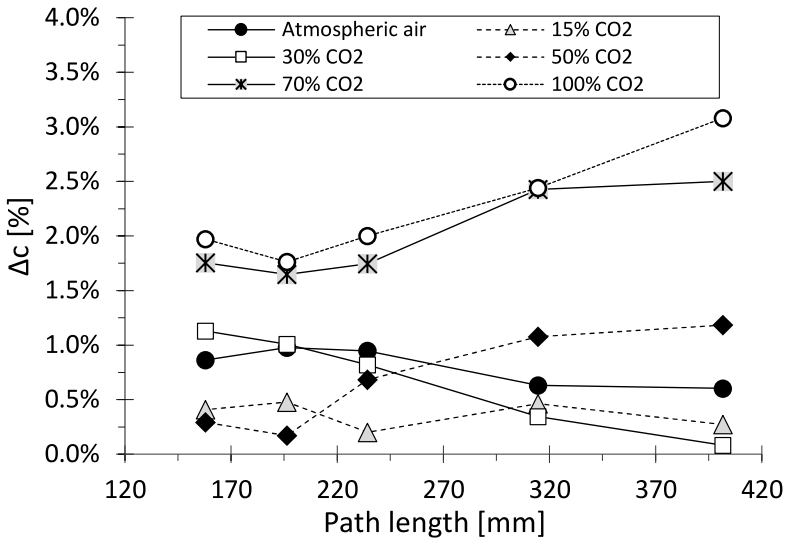

Figure 19 - Difference between USFM sound speed measurement and the reference sound speed according to AGA10

Transducers approximation effect on Signal Strength, which is an embedded diagnostic parameter of flowmeter in test, is shown in Figure 20, for several mixtures of atmospheric air and carbon dioxide.

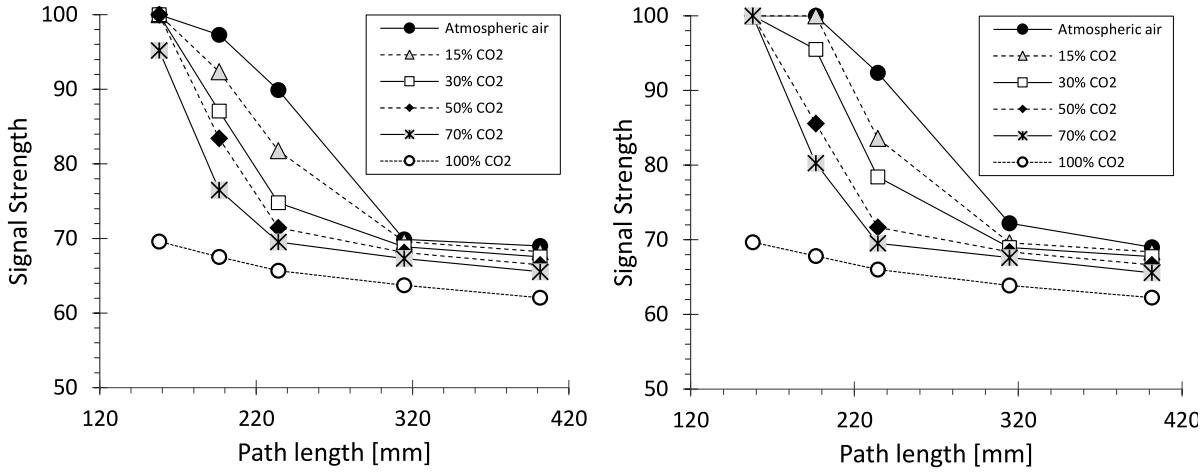

a) Upstream b) Downstream

Figure 20 - Signal Strength behavior with transducers approximation

Firstly, the behavior of Signal Strength exhibits similar behavior for both transducers. Such Signal Strength behavior is expected in dry calibration, because transducers are not submitted to flow rate effects, affecting signal reception.

Table 4 shows the deviation of signal strength relative to the reference state, which is ultrasonic flow meter operating in atmospheric air, facing the inner wall of the

tube. Since Signal Strength are similar for both transducers, the analysis is done with averaging Signal Strength of upstream and downstream transducer.

Table 4 - Signal Strength deviation relative to the reference state

Path length [mm]	Signal Strength deviation					
	100% Air	15% CO_2 + 85% Air	30% CO_2 + 70% Air	50% CO_2 + 50% Air	70% CO_2 + 30% Air	100% CO_2
401.6	0.0%	-1.0%	-2.0%	-3.6%	-5.0%	-9.9%
321.3	3.0%	0.9%	-1.1%	-1.1%	-2.2%	-7.5%
241.0	32.1%	19.8%	3.7%	3.7%	0.7%	-4.6%
200.8	43.0%	39.4%	22.5%	22.5%	13.6%	-1.9%
160.7	44.9%	44.9%	44.9%	44.9%	41.5%	0.9%

For concentrations analyzed, Signal Strength increases as path length is becoming shorter than original dimension. Maximum Signal Strength deviation is reached at the minimum transducers' distance. This is coherent with Lambert Beer law. Signal Strength presents an exponential behavior, which is also in agreement to Equation (2.12).

For CO_2 concentrations equal or lower than 50%, Signal Strength achieve the maximum value. At 70% of CO_2 in air, and minimal path length, averaging Signal Strength is 97.6, which is close to the maximum value.

For tests running executed with 100% of carbon dioxide, approximately, Signal Strength vary from 62.2 at L_1 = 401.6 mm to 69.7 at L_5 = 160.9 mm.

For each path length, the voltage amplitude of received signal is measured by oscilloscope. Figure 21 compare peak to peak voltage variations as transducers approximate and CO_2 content increase in atmospheric air.

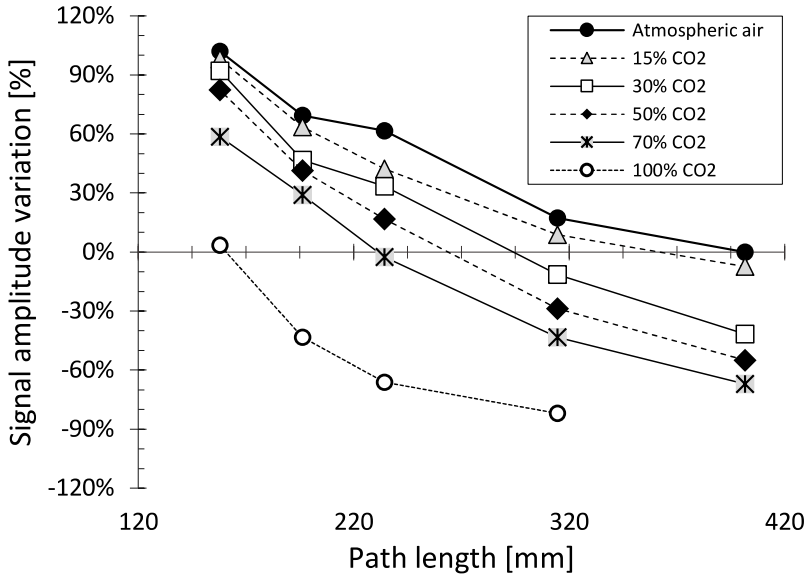

Figure 21 - Signal voltage amplitude variation from oscilloscope in dry calibration

In Figure 21, readings are compared to the reference state, i.e. ultrasonic transducers operating in atmospheric air with transducers positioned facing pipe wall.

Firstly, signal loss is directly proportional to CO_2 increment. So, fixing transducer distance, signal variation is minimum operating in atmospheric air, but increasing with the increment of carbon dioxide in mixture. Maximum signal variation is achieved at 100% of CO_2. It also noticeable that, for all gas mixtures evaluated, signal amplitude increases with transducers approximation, whatever CO_2 concentration.

Test readings with pure atmospheric air, transducers are only approximated, getting increasing respective signal. Figure 21 depicts oscilloscope voltage readings from transducers. It is observed that maximum signal variation in atmospheric air is 102% at L_5 = 160.7 mm.

At 15% of carbon dioxide in air, signal variation is -7.4% at L_1 = 401.6 mm, pointing signal loss. The signal variation become positive at L_2 = 321.3 mm, with an increase of 8.9% of the received signal voltage. At the minimum path length, signal enhanced 98%.

For mixtures of air and carbon dioxide at 30% CO_2. signal variation at reference position is -41.6%, indicating signal loss. At same concentration, it is observed signal loss of -11.3% at L_2 = 321.3mm. In this mixture, signal increase begun at the path length of L_3 = 241.0 mm. Maximum signal increase is also achieved at minimal path length, raising the signal in 92.1%.

In mixtures at 50% CO_2. it is observed signal loss -54.9% and -28.8% for, respectively, L_1 = 160.7 mm and L_2 = 321.3 mm. For transducers distance larger than L_3 = 241.0 mm, there is increase of signal amplitude, achieving maximum signal increment of 82.3% relative to the reference state.

For 70% of CO_2 in air, it is observed a signal loss from -67% at reference position to -2.4% at L_3 = 241.0 mm. Then, signal enhanced to a maximum of 58.6% at the minimum transducers distance evaluated.

Pure carbon dioxide presents such strong attenuation that, at transducers standard position, the resulting pulses at the receiver are below to detection threshold, so data could not be obtained in this case. But transducers approximation leads to signal amplitude variation between -82% at L_2 = 321.3 mm, which indicates signal loss, and 3.4% at L_5 = 160.7 mm, pointing out signal increase.

According to acoustics theory, sound pressure, sound power levels, as well as sound intensity can be calculated using experimental data of signal amplitude. Thus, results of signal voltage measurement can be related to the Signal Strength. In this context, a hypothesis testing is done, as described below.

The null hypothesis (denoted by H_0) is a statement that Signal Strength and signal voltage are related. The alternative hypothesis (H_1) is a statement in which the

parameters of interest differ from the null hypothesis, that is the case which Signal Strength and signal voltage are unrelated.

Data presented previously, in Figure 20 and Figure 21 are combined at Figure 22. It is important to emphasize that this analysis do not intend to come upon a correlation equation between Signal Strength and received signal voltage.

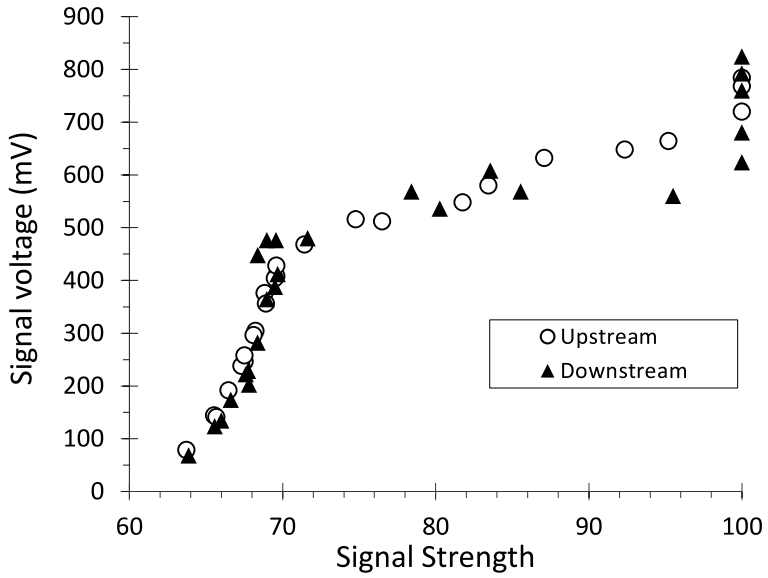

Figure 22 - Relation between Signal Strength and signal amplitude of the received signal

It's seen that signal strength and signal voltage measured by oscilloscope are correlated. Such correlation is not linear and can be decomposed as: a first data range bellows a Signal Strength value of 70 and a second range above a Signal Strength of 70.

The correlation is more likely for first data range (to Signal Strength below 72). The second range (Signal Strength above 72) also presents a correlation between Signal Strength and signal amplitude, but especially at values close to 100. This diagnostic parameter saturates, although signal amplitude of received signal remains increasing.

Analysis suggest that Signal Strength is somehow correlated to the voltage of received signal. Thus, the null hypothesis is true.

4.4.4 Experimental evaluation of the attenuation coefficient

For the experimental evaluation of acoustic attenuation, either pressure or frequency can be varied in same media. Ultrasonic transducers are tuned to an only one particular resonant frequency. On the other hand, pressure at offshore flaring gas system are atmospheric pressure, approximately. Since the aim of this study is to evaluate CO_2 effect on market flare gas ultrasonic flow meters, just gas composition and transducer distance are changed in the current research.

The measurement model assumed here is based on the study by Matson et al. [2], as shown in Figure 23. Taking advantage of piezoelectric properties, voltage at V_A level is supplied to Transducer A, which produces acoustic waves at ultrasonic frequency in a gaseous medium. Transducer B receives those ultrasonic waves, generating voltage at V_B level related to the received signal. Both transducers operate alternating as transmitter and receiver of ultrasonic waves. An oscilloscope is connected to transducers connections in USFM. So, both emitted and received signal can be recorded.

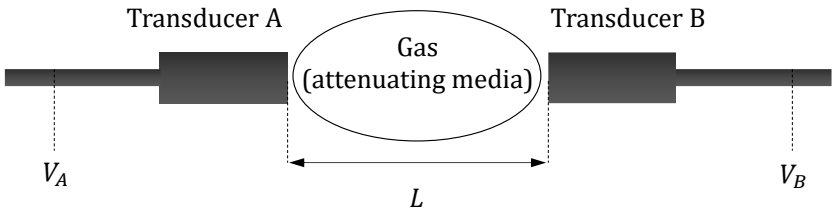

Figure 23 - Measurement model

Reference values for attenuation readings using ultrasonic flow meter is the empiric model [23] based on data for binary mixtures of N_2 and CO_2 [4], [27]. Measured attenuating coefficient is illustrated in Figure 24 and detailed in Table 5. The coefficient $\alpha\lambda$ characterizes the attenuation, as explained at Chapter 2.

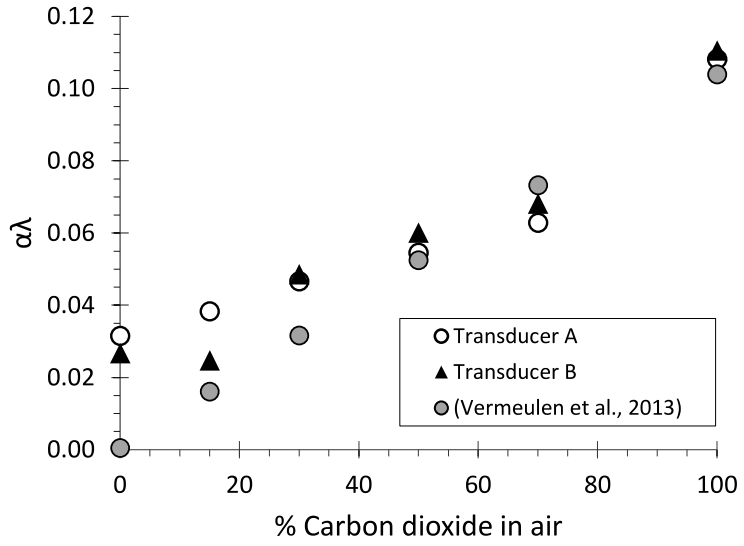

Figure 24 - Attenuation coefficient for several air + carbon dioxide mixtures

Table 5 - Comparison of experimental attenuation coefficient and the empirical model

Gas composition	α_{T1}	α_{T2}	Empiric	Δα [%]
Atmospheric air	0.032	0.027	-	-
100% N_2	0.030	0.029	0.0005	-5867%
85% air + 15% CO_2	0.038	0.025	0.016	-96%
70% air + 30% CO_2	0.047	0.049	0.032	-51%
50% air + 50% CO_2	0.055	0.060	0.052	-9%
30% air + 70% CO_2	0.063	0.068	0.073	11%
100% CO_2	0.108	0.111	0.104	-5%

Figure 24 and Table 5 analysis indicates that attenuation coefficient measured for pure air is 5787% higher than the estimated value by empiric model for 100% N_2. Although values of attenuation coefficient of dry air and N_2 have found to be similar [32], the empiric model applied in this study do not consider air humidity. The presence of air humidity strongly influence the absorption of ultrasonic waves [33].

The empiric model underestimates the attenuating coefficient until 50% of carbon dioxide in atmospheric air, especially for mixtures at low CO_2 levels, where the empiric model just considers N_2 and CO_2. Above 50% CO_2. experimental points are similar to empirical model, reaching differences between -9% and 11%.

The empiric model adopted as reference for comparison is limited to mixtures of N_2 and CO_2. Experimentally, the attenuation coefficient of pure N_2 is shown to be very similar to air. In this case, experimental values diverge from empirical values. Air humidity [17], [30] and impurity [22] significantly increases the absorption of ultrasonic waves.

The measurement model for predicting attenuating effects presents some limitations. The applied methodology does not regard transmission/reception efficiency factor and cables efficiency. Moreover, transducers were not modeled to acknowledge their dynamics. It was not applied correction for acoustical effects, such as scattering and diffraction. Besides, the energy loss due to impedance differences in transducers components were not accounted. On the other side, empirical attenuation coefficient is the intrinsic medium's attenuation, while experimental results are apparent attenuation result.

4.5 CONCLUDING REMARKS

Dry calibration procedure is a methodology to evaluate basic operational performance of ultrasonic flowmeter by transit time and presents the advantage of being low cost and easy to reproduce worldwide. Besides, it is reproducible in the field.

Analysis indicate that carbon dioxide attenuation affects USFM readings performance. Differences between measured speed of sound and estimated speed of sound by AGA10 becomes higher as concentration of CO_2 increases, reaching

maximum difference of 3.1% with ultrasonic transducers at reference position (section 4.4.3).

Transducers approximation procedure is proved to be effective to improve ultrasonic flow meter performance, as shown by reduction of sound speed difference and increasing amplitude of received signal (section 4.4.3). This procedure has the advantage of not changing the experimental setup, only the positioning of transducers, which typically are assembled by sliding rods in flare gas applications.

Dry calibration experiment is adapted for measuring the attenuation coefficient using procedures as indicated by literature [4], [38], [41]. Firstly, the experiments done is neither specify nor projected for attenuation prediction. Second, what is measured in current study is named as “apparent attenuation”, not the fluid medium's intrinsic attenuation [82], but including effects like diffraction, refraction, echoes, etc.. So, in this context, it is expected differences as reported between experimental attenuation coefficient and the data from literature.

Thus, it is expected higher differences in attenuating coefficient for low CO_2 content in air. Even so, experimental attenuation coefficient is consistent to empirical model for mixtures of atmospheric air and CO_2 for concentrations higher than 50%. The empirical model converges to experimental evaluation when CO_2 is substantially higher than air concentration.

5 VALIDATION OF WIND TUNNEL PROFILE

5.1 INTRODUCTION

This chapter describes the wind tunnel experimental facility, capable to operate at high flow speed and high carbon dioxide concentration, as well as characterizing its flow profile.

5.2 METHODOLOGY

5.2.1 Flow facility

The wind tunnel is located at Research Group of Oleo & Gas Flow and Measurement (NEMOG, in Portuguese), at Federal University of Espírito Santo (UFES). The wind tunnel, as shown in Figure 25, is especially designed to test flow metering technologies for flare gas applications at high speed flows and high carbon dioxide concentration.

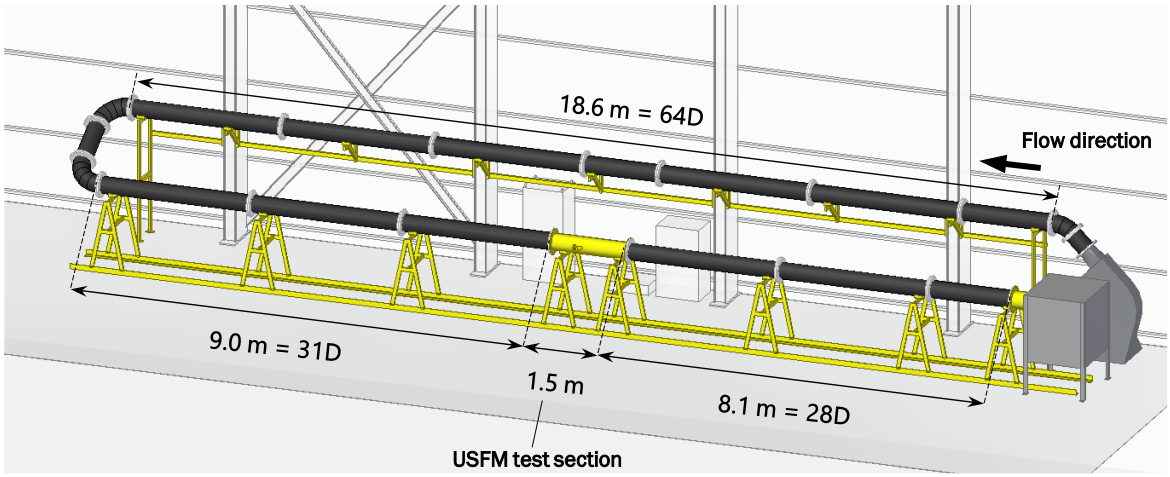

Figure 25 - Closed circuit wind tunnel

The wind tunnel consists of a set of plastic polypropylene tubes with different spool tube sections lengths, presenting nominal internal diameter of 12 inches (290.5 mm). The coupling between distinct tube sections is made by male-female (M&F) nylon flanges, in order to ensure stepless coupling. The advantage of this arrangement is the large-scale simulation of actual flow conditions, as those encountered in operational flaring gas at production plants.

NEMOG's wind tunnel is projected to allow pipe of different tubing configurations and size and to be easily altered in a short time. This setup enables interchangeability between straight section tubes and line accidents.

The maximum total length of each upper and lower horizontal segment is 18 meters, which corresponds to straight length of 60D, approximately. Considering ultrasonic flow meter test sections and the wind tunnel dimensions, there is 31D of

straight tube upstream of the test section and 26D downstream of the test section. In this context, this work uses two assembly configurations.

The “closed-circuit assembly” as illustrated in Figure 25. In this configuration, the flow rate is recirculated, enabling the evaluation of the ultrasonic flow meter after gas injection. In this work, carbon dioxide gaseous is injected. Due to high flow rate of the test circuit, the flow is heated by friction and blower power, reaching a steady state of temperature in about 85ºC, at maximum flow rate level.

The upper horizontal segment operates with internal pressure slightly higher than local atmospheric pressure, since it is located at the booster side of the blower. A standardized Pitot tube is installed at the upper segment, operating as reference flow meter for the closed loop control.

The lower horizontal segment is located on the suction side of the blower and operates with internal pressure slightly below local atmospheric pressure. The test section where the ultrasonic flow meter is evaluated is installed at the lower segment, as well as the laser doppler velocimeter equipment.

The flow is promoted by a centrifugal blower, with suction in the lower segment and return in the upper segment. A plenum box is installed between the blower and the lower horizontal segment, aiming to reduce the swirl effect generated by the blower.

The other wind tunnel mounting is so-called “open-circuit assembly”, where a bell-mouth type nozzle is installed upstream of the flow meter, at the inlet of the wind tunnel, aiming to stabilize the velocity profile at the entrance of the installation. In such configuration the ultrasonic flow meter is evaluated at several flow rate levels. This setup is especially suitable for establishing a turbulent and fully developed velocity profile at the test section, since it is a curve free configuration, as shown in Figure 26.

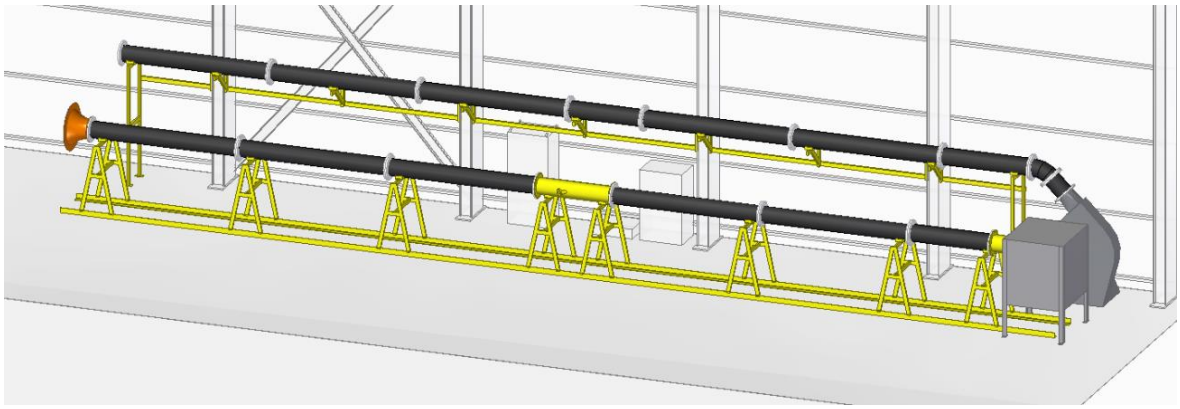

Figure 26 - Open circuit wind tunnel

Considering typical offshore flare gas operational conditions [83], the hydrodynamic similarity matches between NEMOG’s wind tunnel flow and typical offshore flare gas flow [84], [85]. Thus, experimental results in wind tunnel can be extended to the study of flare gas flow meters considering the same Reynolds number range.

5.2.2 Automation and instrumentation

Figure 27 displays the process and instrumentation diagram (P&ID) of NEMOG's wind tunnel.

The flow is promoted by an OTAM model RA1000 centrifugal blower. The blower is coupled to an electrical engine WEG 45 kW W22 (maximum speed: 1770 rpm). The engine-blower set is activated by a Siemens PM240-2 frequency inverter. A braking resistor (2.75 kW, 2.5Ω) is interconnected to the frequency inverter to absorb kinetic energy during the blower deceleration.

As reference flow measurement, a standardized Pitot Tube KIMO ITMP 120 is installed on the upper section on the wind tunnel. The Pitot tube pressure ports are connected to a differential pressure transmitter (PDT-1). The static pressure port of the Pitot tube is also connected to a static pressure transmitter (PIT-1).

The ultrasonic flow meter under performance test is installed on a metal spool, at the lower portion of the wind tunnel. The ultrasonic device is diametrical transit time type, with transducers angle of 45º relative to the pipe axis.

For velocity profile scanning, the laser doppler velocimetry (LDV) technique is used. So, a Laser Doppler Anemometer (LDA) model TSI PS-TM-1D-532 is installed downstream of the ultrasonic flow meter.

Downstream to the ultrasonic flow meter it is installed a static pressure transmitter (PIT-2) model Emerson 2051, and a temperature transmitter (TIT-1) model Iope HX11.

Carbon dioxide concentration, flowing inside the tubing, is monitored through a gas analyzer Keco 2605C. This instrument continuously evaluates CO_2 concentration by infrared technique and it is adapted to operate at wind tunnel low pressures.

For operational safety reasons, an analyzer KR7755 monitors environmental temperature, relative humidity and CO_2 concentration around the wind tunnel.

The experiment controlling, instrumentation, monitoring, as well as data acquisition are automated by a supervisory system based in LabView [86] platform. Figure 28 shows one supervisory system screen, indicating some monitored variables.

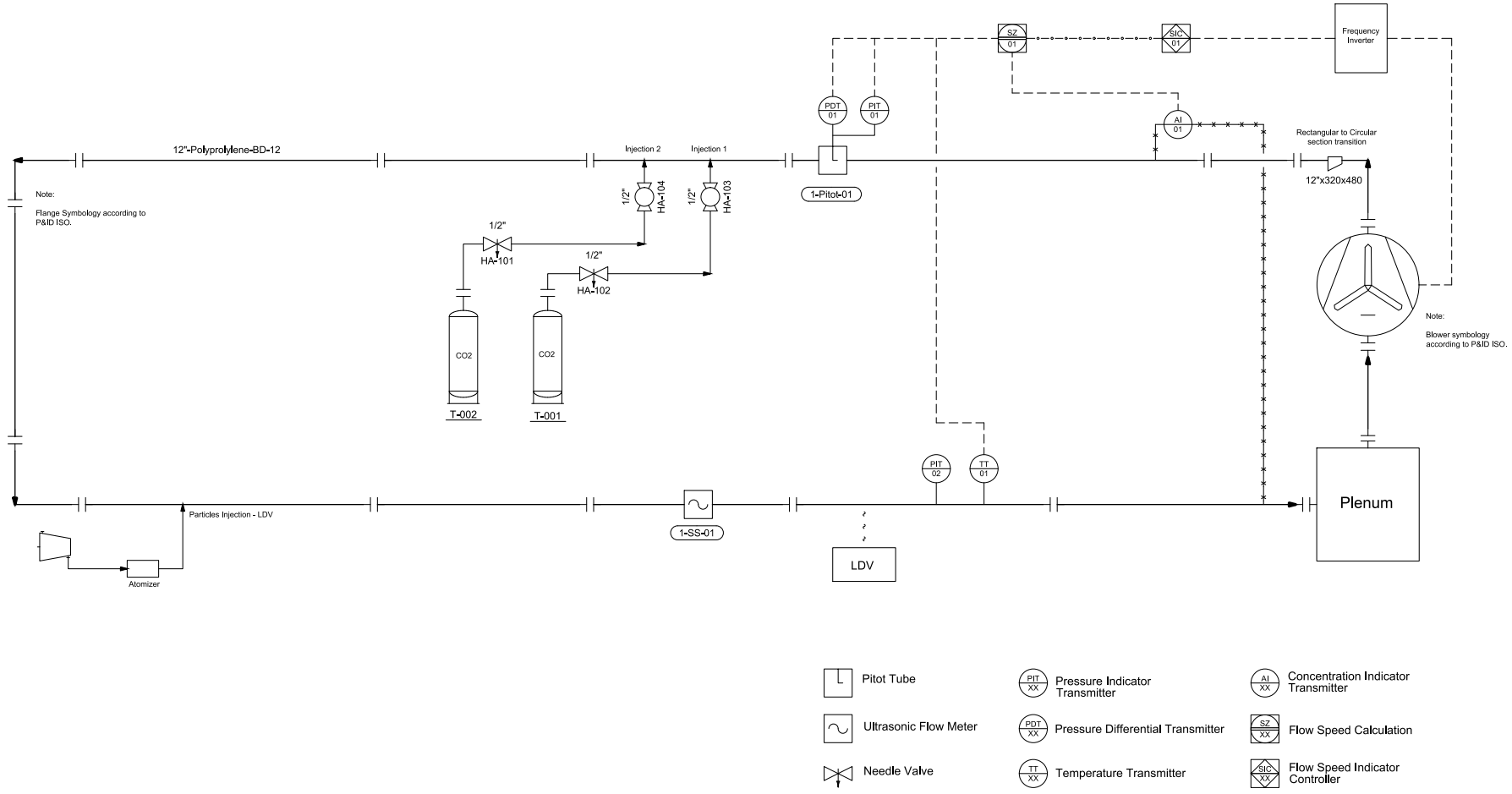

Figure 27 – P&ID diagram of NEMOG's wind tunnel

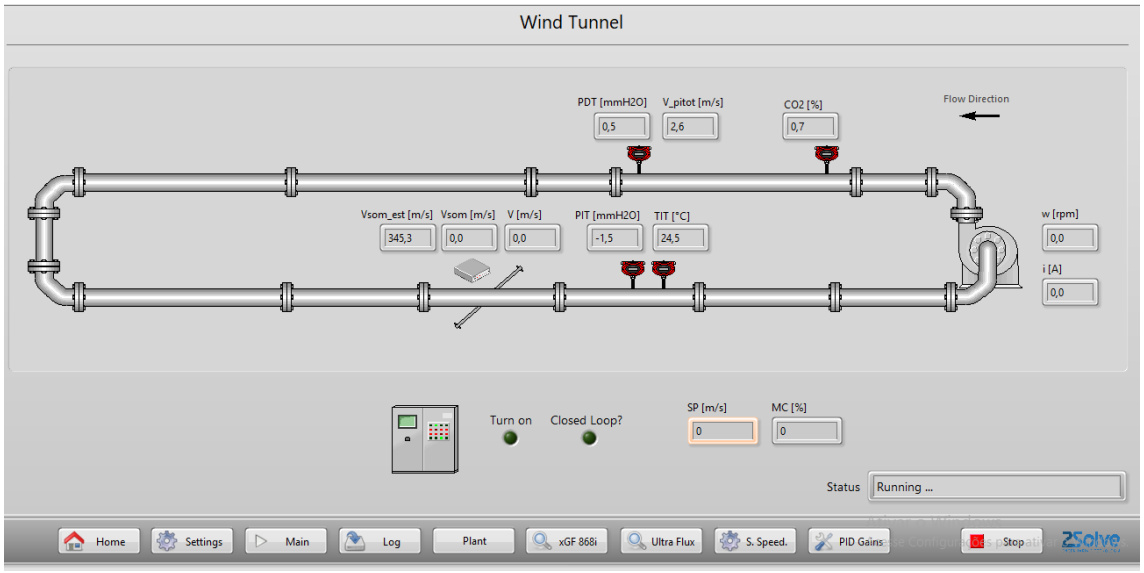

Figure 28 - Wind tunnel supervisory system screen

Data measurement readings, including the ultrasonic flow meter under tests, take place simultaneously at same data acquisition rate. Table 6 details the instrumentation and communication protocols installed.

Table 6 – Description of communication protocols

Instrumentation	Function	Communication protocol
PIT-1	Thermodynamic pressure	4 – 20 mA
PDT	Differential pressure	4 – 20 mA
PIT-2	Thermodynamic pressure	4 – 20 mA
TIT	Temperature	4 – 20 mA
Keco 2605C	CO_2 concentration	4 – 20 mA
PM240-2	Blower rotation	4 – 20 mA
xGF868I	Transit time ultrasonic flow meter	Modbus

The flow rate is regulated in the supervisory system, which allows operation in open loop control or closed loop control.

For control operation in open loop configuration, flow rate is defined by setting blower rotation. Thus, if the thermodynamic state and fluid are maintained constant, the open loop flow also stay constant.

However, for tests evaluating the effect of CO_2 on ultrasonic flow meters, carbon dioxide gaseous is injected, only operation in closed loop configuration is recommended. So, the gas corresponds of binary mixtures of local atmospheric air and carbon dioxide. Due to density and viscosity changes during gas injection, the open loop control operation is inadequate if the goal is to keep flow rate constant. In this context, the supervisory system may be changed to the option of operation in closed loop control.

So, for closed loop control, the controlled process variable is the average flow rate, as measured by the reference flow meter (Pitot Tube). The tuned controller is PID type, with proportional and integrative action. Once the Pitot Tube flow is defined and well stabilized, the controller adjusts the rotation of the motor-blower assembly in order to maintaining flow rate constant.

5.2.3 Carbon dioxide injection

The connection for carbon dioxide injection in the wind tunnel is located in the upper horizontal segment, as detailed in the P&ID diagram in Figure 27. The gas cylinder is connected to a ball valve, which is installed in the pipe connection by a silicone hose. Due to the high wind tunnel length and thus internal volume, two independent injection plugs are used.

The procedure for CO_2 injection into the wind tunnel begins with adjustment of the blower for closed loop control operation at the desired flow rate. Data acquisition begin in stationary atmospheric air. After flow rate and temperature are stabilized, the flow rate of the rotameter at the CO_2 analyzer KECO 2605C is adjusted to 1.5 SCFM, as indicated by the manufacturer. Afterward, ball valves, connected to the wind tunnel tubing, are opened. Gas injection starts with opening the CO_2 cylinder valve.

First, the valves of gas cylinders are fully opened, until the CO_2 analyzer indicates concentrations up to 80%, aiming to get high carbon dioxide concentration inside tunnel tubing. Then, CO_2 injection is reduced, in order to compensate gas leakage by connections.

On the other hand, for personal safety, environmental CO_2 concentration is monitored by a meter KR7755. Over this subject, it is follow the recommendations of The American Conference of Governmental Industrial Hygienists [87], which defines maximum CO_2 values in the environment as 5000 ppm over 8 hours (TWA – Time Weighted Average) and 30000 ppm over 15 minutes (STEL). Thus, alarms are configured in the KR7755 meter for the TWA and STEL limits.

5.2.4 The reference flow meter

A Pitot tube L-shaped model Kimo ITMP 120 is installed as reference flow meter. The geometry dimensions [84], installation and operation of the Pitot tube are in accordance to standard ISO/FDS 3966:2008 [88].

The Pitot Tube is installed on upper horizontal segment of wind tunnel. The meter is located along the cross section with the total pressure port on the pipe axis. The straight tube position upstream to Pitot tube is 7.8 m (26D), while the straight tube position downstream is 10.5 m (36D).

The general relationship between the velocity of the fluid stream and the differential pressure, caused by the fluid moving over the Pitot tube, is given by:

$$v_{Pitot} = \alpha \cdot (1 - \varepsilon) \cdot \sqrt{\frac{2.P_D}{\rho}} \quad (5.1)$$

Where:

- v_{Pitot} [m/s] is the local velocity measured by the Pitot tube;
- α [dimensionless] is the calibration factor (or discharge coefficient) for Pitot tube;
- ε [dimensionless] is compressibility correction factor;
- P_D [Pa] corresponds to the differential pressure measured;
- ρ [kg/m³] is the density of the fluid.

Maximum Mach number, achieved is Ma_{max} = 0.16. at maximum blower flow rate. So, the wind tunnel flow is subsonic. Thus, the compressibility factor is considered null. On the other side, the manufacturer of the Pitot tube indicates the discharge factor of 1.0015 [89].

Operational flow rate Q_{Pitot} [m³/h], measured by the Pitot tube, is calculated as Equation (5.2).

$$Q_{Pitot} = v_{Pitot}.A \quad (5.2)$$

Where A [m²] is the internal cross section area.

Due to operational conditions of pressure and temperature, perfect-gas hypothesis is valid (compressibility factor: Z = 1), so gas density can be estimated using the perfect gas equation. It is important to emphasize that the perfect gas equation has its fundamentals based in the kinetic theory of dilute gases [90].

$$\rho = \frac{P}{Z \cdot R \cdot T} \quad (5.3)$$

Where

- ρ [kg/m³] is the gas density;
- P [Pa] is the gas pressure;
- Z [dimensionless] is the compressibility factor;
- T [K] is the gas temperature;
- R [kJ/kg.K] is the gas constant.

The gas constant R is the ratio of the universal gas constant $\overline{R}$ to the molecular weight of the gas M_{mol} :

$$R = \frac{\overline{R}}{M_{mol}} \quad (5.4)$$

The universal gas constant value is $\overline{R}$ = 8.3114 kJ/kmol.K.

For a mixture of perfect gases, the gaseous mixture density can be estimated by summing the product of the mole fraction x_i of each gas by its density ρ_i.

$$\rho_{mixture} = \sum_{i=1}^{n} x_i \cdot \rho_i \tag{5.5}$$

The viscosity of gases can be approximated by Sutherland law, resulted from the kinetic theory using an idealized intermolecular-force potential [90]. The equation is:

$$\frac{\mu}{\mu_0} = \left(\frac{T}{T_0}\right)^{\frac{3}{2}} \left(\frac{T_0 + S}{T + S}\right) \tag{5.6}$$

Where:

- μ [Pa.s] is the estimated gas viscosity;
- T [K] is the gas temperature;
- T_0 [K] is the reference temperature
- S [K] is an effective temperature, called Sutherland constant, which is characteristic of the gas;
- μ_0 [Pa.s] is the reference viscosity, which is also characteristic of the gas.

The model for predicting the viscosity of a mixture of gases is Grahan's model [91], in which the viscosity of a mixture is approximated by summing the product of mole fractions x_i of each gas component by the individual's viscosities μ_i:

$$\mu_{mixture} = \sum_{i=1}^{n} x_i \cdot \mu_i \tag{5.7}$$

Table 7 presents the fluid properties for estimation of density and viscosity of gaseous mixtures of air and carbon dioxide.

Table 7 - Thermodynamic properties of dry air and carbon dioxide

Fluid	**M_{mol} [kg/kmol]**	**S [K]**	**T_0 [K]**	**μ_0 [Pa.s]**
Air	28.97	110.4	273.0	1.716×10^{-5}
CO_2	44.01	222.0	273.0	1.370×10^{-5}

Equations (5.1) to (5.7) are implemented in supervisory wind tunnel system.

5.3 LASER DOPPLER ANEMOMETRY

A detailed discussion about Laser Doppler Anemometry – LDA technology is beyond the scope of this text. However, aiming to characterize the use of this

technology for the determination and validation of the flow velocity profile, it is necessary to present some aspects of measurement by LDA.

The characterization of the velocity profile is important to characterize the flow measurement error by the ultrasonic flow meter. Hence, the velocity distribution is measured using Laser Doppler Anemometry (LDA) technique, installed downstream to flare gas flow meter test section

5.3.1 Laser Doppler Anemometry Technology

The LDA hardware setup consists of: i) Transmission system of the Solid-State Laser; ii) Receiving unit for the light signal scattered by the tracking particle and iii) Signal processor. Figure 29 illustrates LDA sketch, as installed at wind tunnel.

The LDA consists of a two-beam fiber optic probe that collects data in backscatter mode, in which the gaussian laser beams emitted thought the LDA *PowerSight* Module and the signal scattered by the particle is received by the same lens though the LDA head. The received signal is processed in the Photodetector and Signal Processor unit. The most advantage of such system is the consistency of the optical alignment between the transmitting and receiving unit [92].

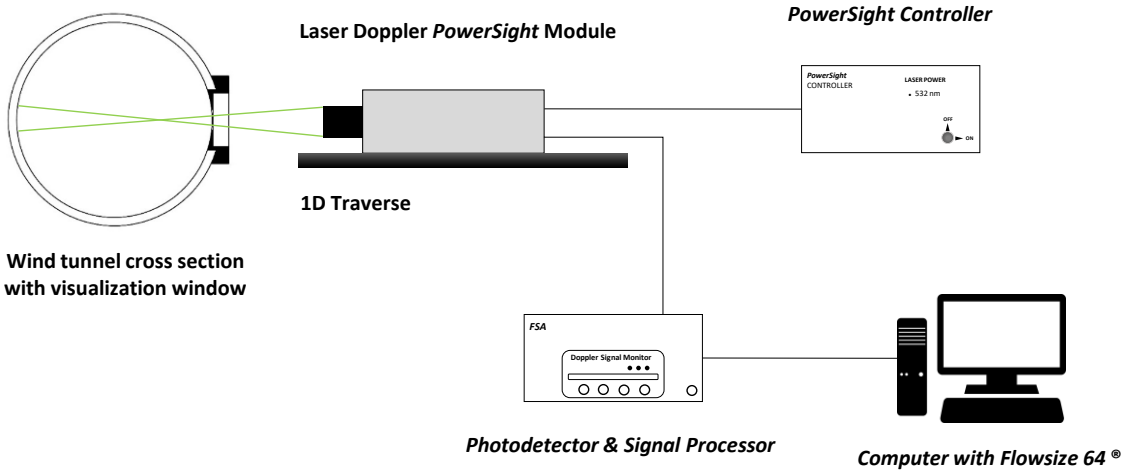

Figure 29 - LDA assembly at wind tunnel

5.3.2 Particle injection

LDA technique require tracer particles, suspended in the flow, to scatter the laser light. Particles have to be traceable, being able to follow the flow, including turbulent effects. The tracer particles to be applied in the NEMOG's wind tunnel should have a reduced diameter, suitable to achieve the required traceability of the flow. Particles are generated by an atomizer, capable to turn a specific liquid into particles of the diameter order of 6 μm.

The atomizer presents 6 ejector nozzles. Operator may select the nozzle arrangement, providing a flexible choice of the quantity of particles. The number of particles needed is particular to each application. The specific liquid for atomization

selected to flow in the wind tunnel is Bis (2-ethylhexyl) Sebacate 90%, which presents density of 0.914 g/mL and reasonable time-life.

The tracer particles injector is placed at 10.5 meters (36.2D) upstream to the LDA measuring section. Particles injection and LDA mounting in NEMOG's wind tunnel are shown in the P&ID diagram at Figure 27.

5.3.3 Visualization window

The LDA is non-intrusive technique for velocity measurement. It requires a transparent window to allow the transmission of light beam emitted by the Laser unit. The design of such window depends on the test facility characteristics. It's necessary to take in account minimization of light diffraction effects.

In this context, a special nylon made holder is designed and manufactured. This element fits the internal curvature of wind tunnel tubing. An orifice in the nylon holder allow the installation of a flat glass visor, as shown on Figure 30. Therefore, both the internal and external surface of the window are flat, which reduces diffraction effects.

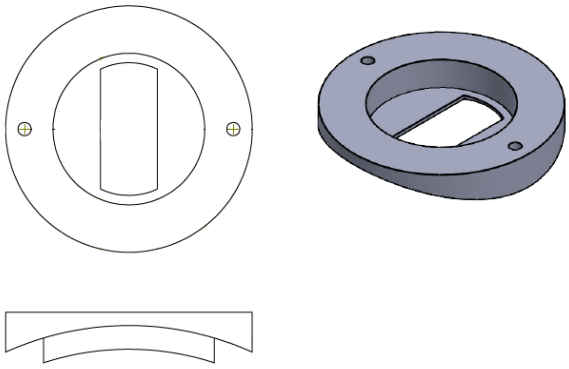

Figure 30 - Transparent window holder sketch

A special feature of the window is that it allows the glass visor to be easily changed, when necessary, even during a high flow experiment. This is an attractive characteristic because the fluid for atomized particles presents oleic characteristics, resulting in loss of transparency of the visor, as the particles attach the surface. Figure 31 shows the holder installed at wind tunnel.

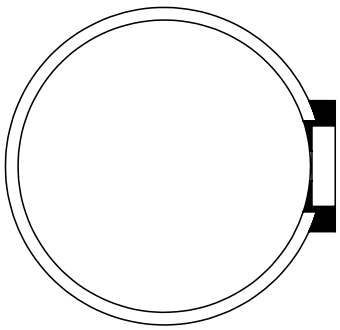

Figure 31 - Window holder installed at wind tunnel cross section.

5.3.4 Flow Velocity Profile measuring procedure

Before performing each set of experiment, the LDA is calibrated to guarantee that the intersection of the laser beams matching photodetectors.

The calibration is done using a calibration wheel, presenting a specific micro roughness on its surface, simulating particles that pass through the measurement volume. The tangential velocity of the wheel is constant, as a function of the wheel's diameter and the electrical line frequency. Measured velocity is adjusted to match the tangential velocity of the calibrator.

LDA technique can perform the velocity measurement of the flow on a single point. To get a complete scan of the velocity profile, it is necessary to move the measurement volume over the tubing internal diameter. Thus, the flow velocity is measured at selected discrete point along the transversal section. The motion of the LDA transmission unit is provided by an automated unidimensional traverser, as indicated in Figure 29.

Before start readings, it is necessary to define a matrix with the measurement points position. Then, it is defined the settings for data treatment on the software Flowsizer 64 [93]. These settings include, for instance, digital filters, laser power and laser voltage.

Due to the relatively large diameter of wind tunnel tubing, it is needed to define three distinct regions for LDA configurations settings, because light scattering happens in different ways among them.

For the near surface region, the viscous forces are more intense resulting in a high velocity gradient and a high turbulence intensity in this section. However, the core flow region is in the so-called "logarithmic region". Hence, at 1 mm distance it is used for the first two sections and at 2 mm is used for the central area.

After the system calibration, positioning the transmission unit and selecting the proper settings for each discrete point to be measured, the measurement is initialized and the LDV system scans automatically the diameter. The measurement takes about 40 minutes to be completed. The data is further processed.

5.4 RESULTS AND DISCUSSIONS

5.4.1 Operational characterization

The wind tunnel facility is a measurement facility for examination of flare gas flow meter performance. Technical specifications of wind tunnel facility are summarized in Table 8.

Table 8 - Main parameters of NEMOG's wind tunnel

Internal diameter	290.5 mm
External diameter	325.5 mm
Pipe wall	17.5 mm
Pipe roughness	1.7 μm
Pressure range in upper horizontal segment	101.3 – 105 kPa
Pressure range in lower horizontal segment	92.3 – 101.3 kPa
Temperature range	20°C – 90°C
CO_2 concentration	Up to 100%
Fluid Density	0.98 – 1.83 kg/m³
Fluid Dynamic viscosity	14.6 – 21.1 μPa.s
Flow rate	1,000 – 12,000 Nm³/h
Upstream straight section from testing section	9.0 m (31D)
Downstream straight section from testing section	7.6 m (26D)

Due to the high flow rate (velocity up to 50 m/s) and compression functioning of the blower, the gas inside the wind tunnel is heated. Heat transfer between wind tunnel tubes and the environment is not enough to keep the flow temperature unchanged. Thus, if operating in closed circuit, the flow achieves steady state at temperatures higher than room temperature. This relation depends on the blower flow rate level, gas properties and room temperature. Running tests executed the wind tunnel, reached maximum steady state temperature of 90ºC.

Thus, the difference between temperature of the gas flow T_{TIT} and environmental temperature T_{RT} , is calculated as Equation (5.8). Results are shown in Figure 32.

$$\Delta T_{flow} = T_{TIT} - T_{RT} \tag{5.8}$$

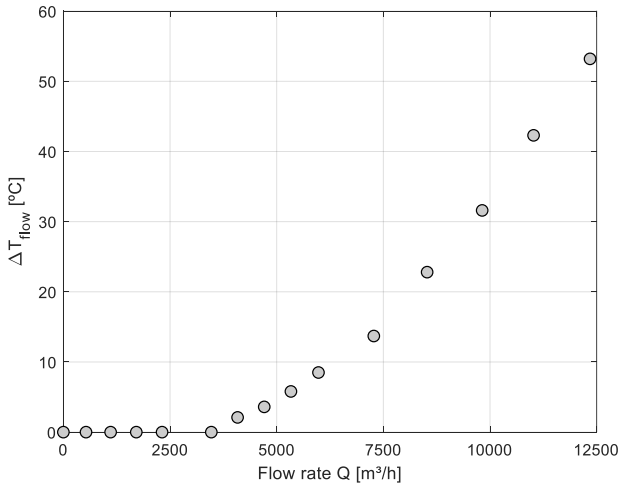

Figure 32 – Steady state temperature variation in wind tunnel for several flow rate levels

Since both local atmospheric air and carbon dioxide are working fluids, it is necessary to estimate density and viscosity considering temperature, pressure and gas composition. Equations (5.5) and (5.7) are utilized for that. Considering typical operating temperature and pressure, density varies between 0.98 kg/m³ and 1.83 kg/m³. On the other hand, viscosity range is between 14.6 μPa.s 21.1 μPa.s.

Maximum flow rate, supplied by the blower, is 12,000 Nm³/h. Currently, minimal level of operational flow rate is limited by the capacity of the refence flow. Experimentally, the minimal reliable Pitot tube flow rate is 1,000 Nm³/h. The first reason of this is typical low operational range of Pitot tube meters. Moreover, noise disturbance affects the instrumentations signal, which effects on the meter uncertainty are higher at low differential pressures. Consequently, noise effects reduce the flow measurement reliability at low flow rates due to high measurement uncertainties.

5.4.2 Velocity profile

To check the presence of any flow disturbances, the velocity distribution is measured downstream to the ultrasonic flow meter testing section. The velocity distribution is measured by laser doppler anemometry (LDA) at 155 selected points distributed along horizontal diameter.

Experimental velocity profile measured obtained by LDA technique is shown in Figure 33 for three Reynolds number. For this analysis, ultrasonic transducers are positioned facing inner wall of the tube, so reducing flow disturbances. Besides, the wind tunnel is operating in closed circuit arrangement. Flow rate examined is the same that the ultrasonic flow meter is evaluated at several CO_2 concentrations in Chapter 6.

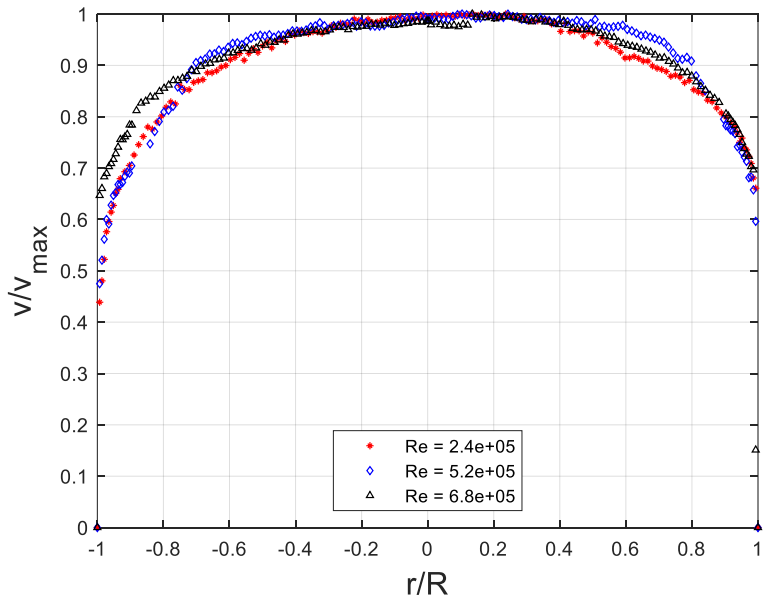

Figure 33 - Experimental velocity profile varying Reynolds numbers

In Figure 33, in order to observe the effect of Reynolds number on the shape of the flow profile, the local velocity is normalized in relation to v_{max}, which is maximum

measured velocity. Each measuring point in the graph correspond to the average from a database, which corresponds to $1x10^4$ and $5x10^5$ readings, approximately.

The velocity profile shape is similar to the theoretical turbulent fully developed flow profile [64], [94], especially in the core region. In the area at radial position r/R between -0.4 and +0.4 the experimental velocity profiles points are visually coinciding, with maximum relative deviation in relation to Nikuradse's velocity profile [64] between 1.4% and -1.9% at Re_1, between 1.0% and -2.0% at Re_2 and between 1.1% and -2.3% at Re_3. It is noticeable that near the boundary region there are differences in velocity profiles behavior.

Near the transparent window (r/R = -1), the velocities points at Reynolds number $Re_1 = 2.4x10^5$ and $Re_2 = 5.4x10^5$ overlaps between $-1 < r/R < -0.75$. At the opposite radial edge (r/R = 1), it is observed that, for three Reynolds number evaluated, the velocities measured by LDA technique are almost coinciding.

The velocity profile at highest Reynolds $Re_3 = 6.8x10^{5.}$ is fuller compared to other velocity profiles. This phenomenon agrees with Nikuradse's study [64], which noticed that velocity profile becomes fuller as Reynolds number increases. Nikuradse's velocity profile as Equation (3.9) indicates that the higher is the Reynolds number, higher will be the value of the exponent "n", predicted as Equation (3.10). Therefore, highest Reynolds numbers leads to fully developed profiles closest to uniform shape.

Due to the results similarity between experimental velocity profiles at different Reynolds numbers, it is necessary to make specific analysis of the parameters of interest related to ultrasonic flow measurement subject. Therefore, the velocity profile is numerically integrated in order to obtain the average velocity along the cross section and the profile factor as well. Turbulence intensity measured is also analyzed.

The quadrature of experimental velocity profile is done numerically, by Trapezoidal Rule. To accomplish this analysis, all of 155 velocity profile points measured are used. Then, the profile factor k is calculated as Equation (3.7).

On the other hand, Nikuradse [64] performed experimental investigations into the velocity profile and law of friction in several Reynolds numbers up to $3x10^6$. The ratio between mean to the maximum velocity can be easily derived combining Equation (3.9) and Equation (3.10), leading to:

$$\frac{\bar{v}}{v_{max}} = \frac{2n^2}{(n+1)(2n+2)} \tag{5.9}$$

For any turbulent fully developed flow, the profile factor can be calculated based on Nikuradse's empirical velocity profile at Equation (3.11). This recommended by AGA 9 [6] and NBR 16777 [74].

On the other hand, turbulent motion is characterized by random fluctuations of velocity and pressure over time [95]. It is convenient to separate the turbulent motion into a mean values and fluctuations. Considering a main velocity component u:

$$u = \bar{u} + u' \tag{5.10}$$

Where $\bar{u}$ [m/s] is the average velocity and u' [m/s] is the fluctuating velocity.

The turbulent intensity TI [%] in the main flow direction is:

$$TI = \frac{\sqrt{(u')^2}}{\bar{u}} \tag{5.11}$$

Table 9 summarizes the main interest parameters related to measured velocity profile analysis.

Table 9 - Specific parameters of the experimental velocity profile

Parameter	Q_{min}	Q_{middle}	Q_{max}
Reynolds number	$2.4x10^5$	$5.2x10^5$	$6.8x10^5$
Flow rate [Nm³/h]	2974.7	6834.2	9692.3
Steady state temperature T [°C]	25	40	80
Internal pressure P [kPa]	101.3	100.5	100
Friction factor	0.01518	0.01313	0.01256
Average velocity [m/s]	12.7	30.8	49.6
K factor experimental	0.9406	0.9437	0.9520
K factor analytical	0.9421	0.9460	0.9472
K factor variation [%]	0.15	0.24	-0.51
Average turbulent intensity [%]	7.7	7.2	8.1
Average asymmetry [%]	4.7	5.0	3.2

One can notice that operating temperature and pressure varies with flow rate increasing. They are both considered for prediction of density and viscosity, consequently Reynolds number and friction factor. Temperature and pressure are also used to convert flow rate into normalized condition (20ºC, 1.01325 MPa).

Differences between experimental profile factor and AGA 9 value considering turbulent fully developed flow is between 0.15% and -0.51%. It means that the velocity profile pattern measured is near the fully developed.

Average turbulent intensity are: 7.7% at $Re_1 = 2.4x10^5$, 7.2% at $Re_2 = 5.2x10^5$ and 8.1% at $Re_3 = 6.8x10^5$. The knowledge of turbulent intensity is relevant in the realization of numeric simulation, because different boundary conditions leads to different simulation results.

From comparison between velocity profile points symmetrical in relation to the pipe axis, asymmetry may be calculated. Main asymmetry are: 4.7% at $Re_1 = 2.4x10^5$, 5.0% at $Re_2 = 5.2x10^5$ and 3.2% at $Re_3 = 6.8x10^5$.

This analysis only considered the main velocity component axis direction, since the available LDA system is a unidimensional. If other velocity components are considered, probably the profile factor, as well as turbulent intensity, may increase.

5.4.3 Law of the wall analysis

The non-dimensional form of a turbulent velocity profile is given by the “law of the wall” [95], [96]. Turbulent flows may be distinguished among three distinct regions:

i) The inner layer is located adjacent to the wall, where the flow is predominant viscous;
ii) A transition region, where the flow is turbulent, but still influenced by viscosity;
iii) An outer layer, which includes most flow regions, where the viscous effect is negligible.

In the inner layer is located the viscous sublayer. The follow equation is valid:

$$u_+ = y_+ \tag{5.12}$$

In the outer region, the velocity distribution has a logarithmic form. For smooth pipes, the universal velocity-distribution law [95] has the form:

$$u_+ = 2.5 \cdot \ln(y_+) + 5.5 \tag{5.13}$$

Another way to calculate the law of the wall is by using the empirical velocity profile proposed by Nikuradse [64].

$$u_+ = 8.74 \cdot (y_+)^{1/n} \tag{5.14}$$

Viscous sublayer is valid until $y_+ = 5$. as calculated by Equation (5.12), where purely laminar friction dominates the flow forces. In the range of $5 < y_+ < 70$ [95], the law of the wall takes the form of transition region, where law of the wall is a mix of laminar and turbulent friction. For y_+ values larger than 70, laminar friction turns negligible compared to turbulent friction, and u_+ behaves as a logarithmic function of y_+ as Equation (5.13). Other authors considers that $y_+ = 30$ as upper limit for transition region [96].

For evaluation of the law of the wall, considering experimental velocity profile measured by LDA technique, it is necessary to calculate the dimensionless form of the velocity scale $u_{+_{exp}}$ and length scale y_{exp}.

The dimensionless form of the measuring position along the cross section is predicted by the viscosity as Eq. (5.6), density as Eq. (5.3), the position $y(r)$ from the piping wall and friction velocity u_t.

$$y_{+_{exp}} = \frac{y(r) \cdot u_t}{\left(\mu / \rho\right)} \tag{5.15}$$

Experimental dimensionless velocity is estimated relating measured velocity profile $u(r)$ and friction velocity u_t.

$$u_{+_{exp}} = \frac{u(r)}{u_t} \tag{5.16}$$

The shear stress, at the piping wall τ_{wall}, is a sum of laminar and turbulent shearing stress. Since the LDA system is unidimensional, measuring only the information about the main velocity component, the shear stress is calculated by the average velocity along the cross section [95].

$$\tau_{wall} = \frac{f \cdot \rho \cdot \bar{u}}{8} \tag{5.17}$$

Where f is the friction factor, ρ [kg/m³] is the fluid density and $\bar{u}$ [m/s] the average velocity along the cross section.

The friction factor is a dimensionless variable calculated by the Colebrook-White equation using Reynolds number Re, pipe roughness e and internal diameter of the pipe D. For turbulent flows, it is calculated as:

$$\frac{1}{\sqrt{f}} = -2 \cdot \log_{10}\left(\frac{e}{3.7D} + \frac{2.51}{\mathrm{Re}\sqrt{f}}\right) \tag{5.18}$$

Finally, the friction velocity u_t is characteristic of the turbulent fluctuating motion, measuring the intensity of turbulent eddying and of the transfer of momentum due to these fluctuations [95]. It prediction follows Equation (5.19).

$$u_t = \sqrt{\frac{\tau_{wall}}{\rho}} \tag{5.19}$$

This work uses the law of wall for analysis of the velocity profile of NEMOG's wind tunnel. The adopted model is the relation for smooth pipes, since the pipe roughness is very low (1.7 μm).

Figure 34 shows the dimensionless form of the experimental velocity profile in law of the wall analysis at Reynolds number of 2.4×10^5. The minimum y_+ achieved is 35. Thus, the velocity profile in near boundary condition is apart from viscous sublayer. Maximum y_+ reached is 5,100.

Throughout the law of the wall it is possible to infer some information about the symmetry of flow profile. At low flow rate level, it is noteworthy that the velocity profile is asymmetrical, especially for y_+ below 2,000. As the velocity profile approaches the tube axis, the velocity profile tends to be axially symmetric in the core flow region. As y_+ increases, both halve of the velocity profile have a tendency to converge with Logarithmic-Law as Equation (5.13).

The law of the wall analysis indicates that the velocity profile at $Re_1 = 2.4x10^5$ is neither fully developed nor symmetric.

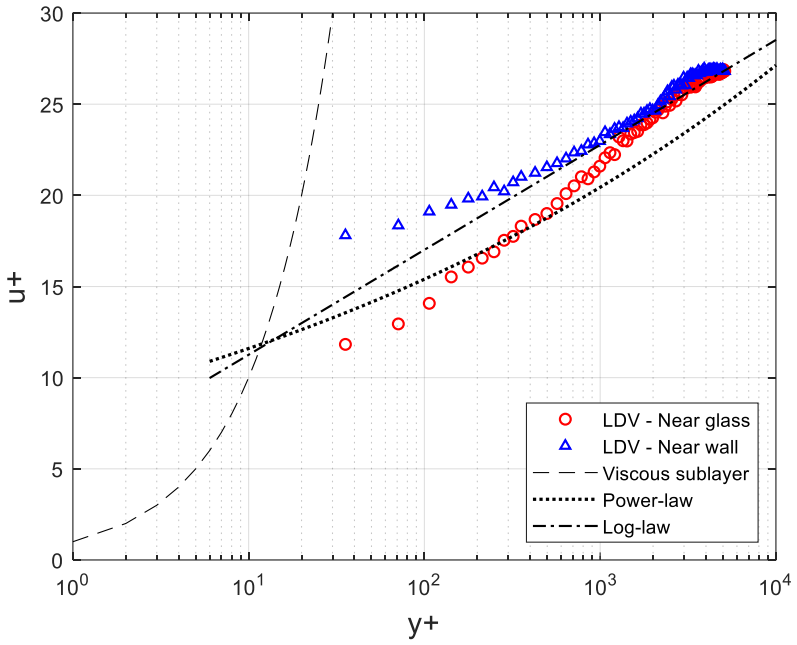

Figure 34 - Law of the wall, $Re_1 = 2.4x10^5$

The law of the wall analysis for $Re_2 = 5.2x10^5$ is shown in Figure 35.

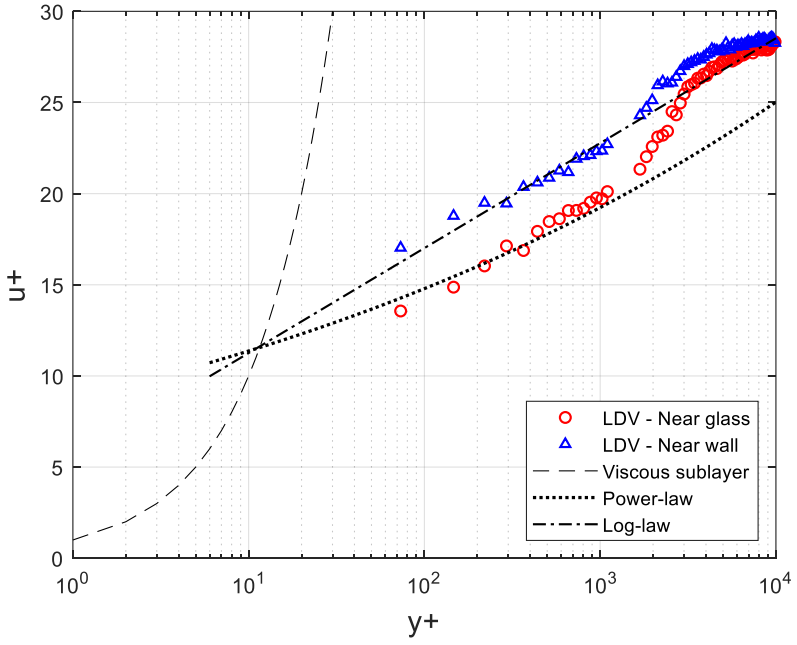

Figure 35 - Law of the wall, $Re_2 = 5.2x10^5$

Minimal experimental is $y_+ = 80$. Thus, it is already at fully turbulent layer. For y_+ values between 80 and 1,000. The dimensionless velocity profile at near wall region, which corresponds to the velocity profile region between $0 < r/R < 1$, follows the log-

law curve. However, in this same y_+ range, but near the visualization window, the experimental dimensionless velocity u_+ pattern behaves as the Power-law of Equation (5.14).

From y_+ = 1,000. the dimensionless velocity profile tends to converge closest to the pipe axis, matching the wall function.

The divergences between the experimental law of the wall analysis indicates that the velocity profile is neither symmetric nor fully developed at $Re_2 = 5.2x10^5$.

Figure 36 presents the law of the wall analysis at the highest flow rate evaluated, which corresponds to an average $Re_3 = 6.8x10^5$.

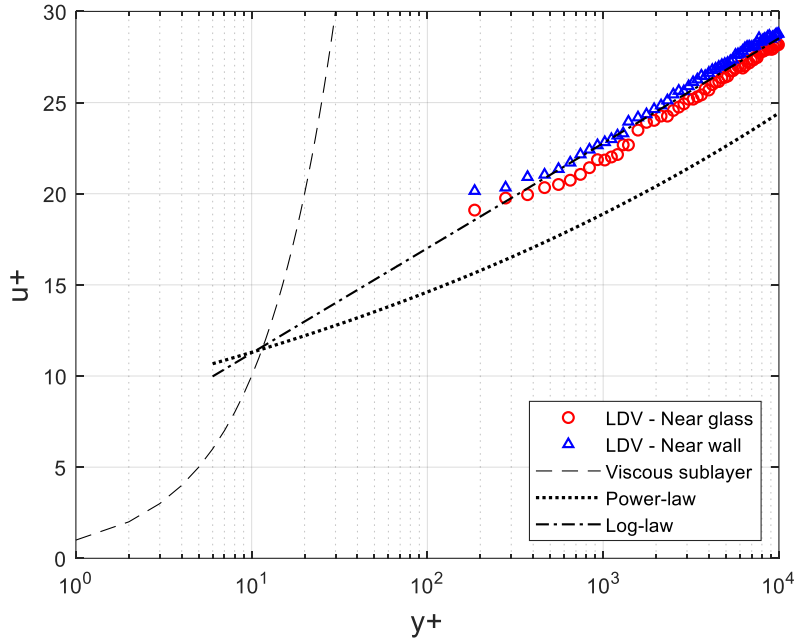

Figure 36 - Law of the wall, $Re_3 = 6.8x10^5$

Minimal y_+ achieved is 185. Thus, the velocity profile is already in fully turbulent sublayer. The velocity profile is almost symmetrical at this flow rate. The two halves of the velocity profile are since the nearest boundary point with similar value. Both flow profiles are very similar to the theoretical law of the wall using logarithmic law for smooth pipes, calculated as Equation (5.13).

Divergences between the theoretical law of the wall for turbulent fully developed flow and experimental dimensionless velocity profile can be explained by the straight tube length upstream to the LDA measuring section. The upstream straight tubes length from the LDA hardware from curves is approximately 36 internal diameters (36D).

According to Nikuradse [64], the turbulent fully developed flow profile exists after an inlet length from 25 to 40 internal diameters (20 – 40D) from the inlet flow. However, this assumption does not consider curves and line accidents as well. On the other hand, Martins [66] used Computational Fluid Dynamics (CFD) method to find that it is

necessary 80 internal diameters (80D) from the inlet to achieve a turbulent fully developed flow.

5.5 CONCLUDING REMARKS

This chapter presents the experimental set up and characterizes the operation of NEMOG's wind tunnel. This facility is one of the few in the world capable to evaluate flare gas ultrasonic flow meters due to its semi-industrial scale as well as instrumentation capability. The wind tunnel features enable researches about the worldwide technological challenge related to flare gas flow measurement: high flow rate levels with high concentration of carbon dioxide.

The experimental velocity profile and law of the wall analysis indicate that the velocity profile varies with Reynolds number. Turbulent intensity, asymmetry magnitude and profile factor are also defined for several Reynolds number.

Analysis indicates that the velocity profile is not turbulent fully developed yet. However, at Reynolds number of 6.8×10^5 the law of the wall analysis shows that velocity profile is almost symmetrical and approaching the logarithmic law of the wall for smooth pipes.

The velocity distribution after the LDA test section may develop more, but there are only 36D upstream from the measuring section. Results shows that there will not be a symmetric and undisturbed flow pattern unless if flow conditioners be installed.

6 ULTRASONIC FLOW METER PERFORMANCE IN WIND TUNNEL

6.1 INTRODUCTION

Performance of ultrasonic flowmeter is affected by several factors, as installation effects and attenuating media. Most studies about ultrasonic flow measurement performance up to date focused on installation effects. For flare gas flow measurement in typical conditions, signal attenuation occurs in presence of high concentration of carbon dioxide, leading to flow readings faults. However, little research exists specifically on this subject [2], [9], [23], [36], [97], mainly because experimental flow facilities operating at high carbon dioxide demands large and expensive installations.

This chapter analyze flare gas ultrasonic flow metering in a wind tunnel designed to operate with high flow rate and high carbon dioxide content, as described in Chapter 5.

6.2 METHODOLOGY

6.2.1 The ultrasonic flow meter installation

The flow meter device under evaluation is a flare gas ultrasonic flow meter, model GE XGF868i. The meter is suitable for gaseous applications up to 150°C. The USFM demand inlet and outlet straight tube sections of 20D upstream and 10D downstream. Such meter is the same analyzed in Chapter 4, but now evaluated at NEMOG's wind tunnel, as characterized in Chapter 5.

A major benefit of testing ultrasonic flow meters at NEMOG's wind tunnel is that the experimental arrangement allows precisely positioning of transducers. In operational flaring gas flow meters at production plants, dimensional verification must be done without accessing to the inside of the pipe, due to safety and operational reasons. The procedure for transducers approximation is the same as described in Chapter 4, for dry calibration in that case.

The ultrasonic device is mounted in a spool equipped with two pairs of transducers. Both transducers pairs present the same specifications, only installation is modified. Transducers in Channel 1 are positioned on horizontal plane, while Channel 2 transducers are positioned on vertical plane. Thus, Channel 1 and Channel 2 are orthogonal. Figure 37 illustrate Channel 1 and Channel 2 location along pipe's cross section.

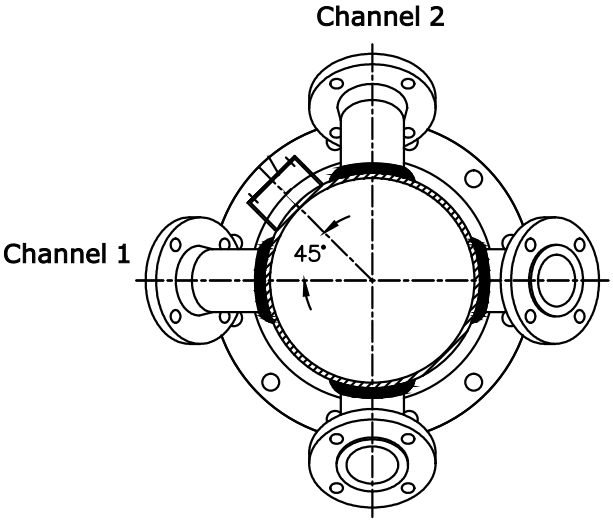

Figure 37 – Installation of dual channel ultrasonic flow meter along pipe's cross section

Aiming to analyze different transducers installation arrangement, transducers in Channel 2 remains unchanged, i.e., acoustical path length remains unalterable. On the other hand, transducers in Channel 1 may be approximated and examined with recovery angle, as well. This arrangement allows real time comparison between modification of transducers installation and a reference configuration, provided by Channel 2.

Dimensions of ultrasonic flow meter spool in wind tunnel are different from those at dry calibration spool. Thus, geometrical configurations in standard installation of transducers changed: L_{ref} = 410.8 mm in wind tunnel against L_{ref} = 401.6 mm in dry calibration.

On the other hand, same transducers are tested against approximation distances, as done in dry calibration analysis, but now, considering flow effects. Table 2 details transducers distances tested in Channel 1 related to the reference distance.

Table 10 – Geometrical configurations of transducer approximation in wind tunnel

#	% Distance approximation	Path length [mm]	Axial length [mm]
1	100%	L_1 = 410.8	A_1 = 290.5
2	78.2%	L_2 = 321.3	A_2 = 227.2
3	58.7%	L_3 = 241.0	A_3 = 170.4
4	48.9%	L_4 = 200.8	A_4 = 142.0
5	39.1%	L_5 = 160.7	A_5 = 113.6

6.2.2 Failure criteria

For evaluation of failure readings events in ultrasonic flow measurement operation in high CO_2 levels, the criteria proposed by Barros [9] are adapted

considering typical operation characteristics of NEMOG's wind tunnel. The first approach for the failure criteria are following:

- *Criterion A* - Failure by flow readings deviation higher than 20% relative to a stable reference flow meter in wind tunnel.
- *Criterion B* – Failure by inconsistencies between the measured sound speed and the theoretical sound speed estimated by state equations [72].
- *Criterion C* - Failure by signal loss.

Such criteria are analyzed and quantified along the text.

According to Resolução Conjunta ANP/INMETRO nº1 [3], flare gas volume should be daily reported by operators. Thus, the main parameter evaluated in wind tunnel experiments that should be measured flow by ultrasonic flow meter Q_{USFM} . So, the failure criterion *A* evaluates the parameter δQ , analyzing the absolute percentual variation between the flow rate Q_{USFM} and the flow rate of the Pitot tube Q_{Pitot} .

$$\delta Q = \frac{|Q_{USFM} - Q_{Pitot}|}{Q_{Pitot}} \tag{6.1}$$

On criterion *A,* δQ limit is defined as the maximum difference between ultrasonic flow meter and Pitot tube at low flow rate and without applying digital filters. Figure 38 exemplifies the occurrence of failure A in CO_2 concentration above 60%.

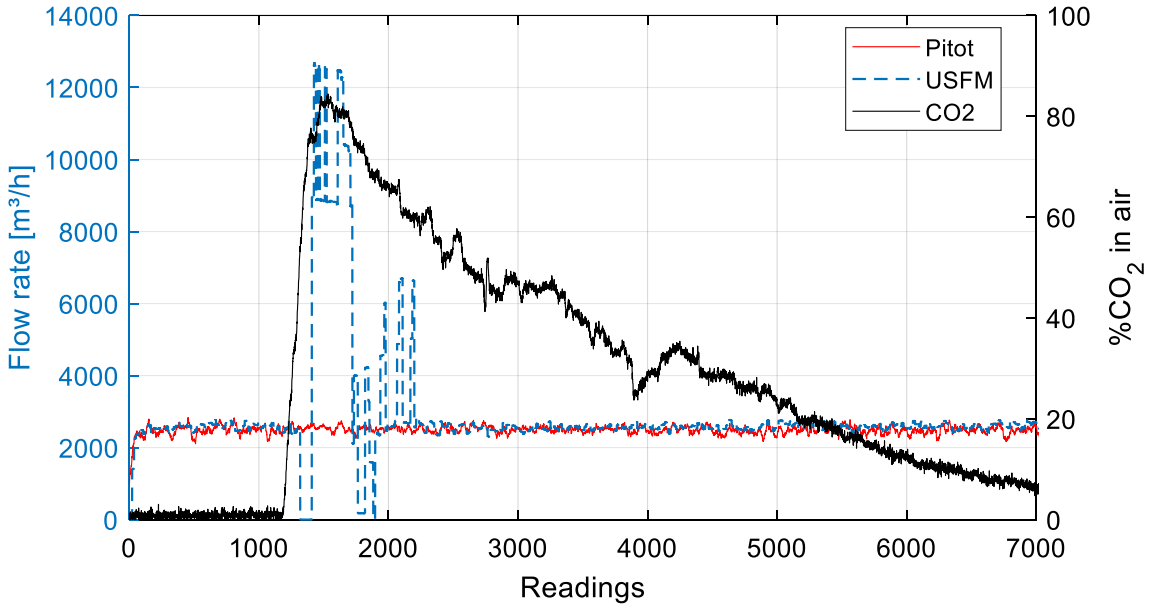

Figure 38 - Occurrence of failure A in a test with CO_2

Criterion *B* analyze sound speed readings behavior. Thus, an acceptable difference must be defined. The lowest limit corresponds to the sound speed at 100% CO_2 at 20ºC. The highest limit is the sound speed for atmospheric air at 90ºC, which is maximum steady state temperature recorded in closed loop operation. The highest

and lowest limits present 5% of acceptable variation, as a first guess, since ultrasonic flow meters are not calibrated to speed of sound measurement. So, the resulting reasonable range for sound speed is stablished between 250 m/s and 400 m/s. Figure 39 illustrates failure by criterion B.

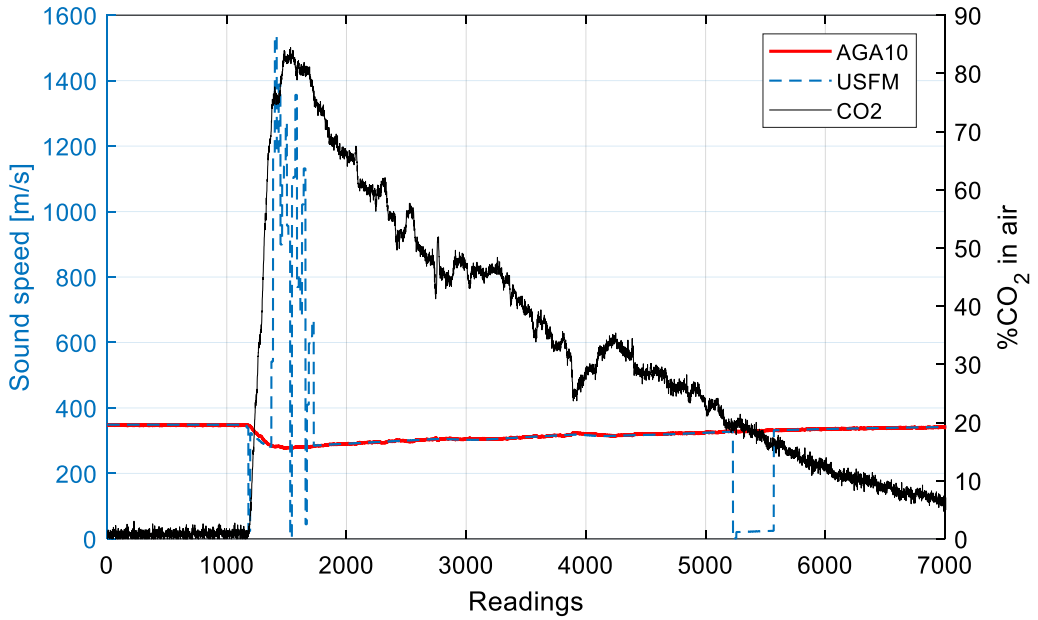

Figure 39 - Occurrence of failure B in a test with CO2

The application of Criterion *C* evaluates technical diagnostic of proprietary parameters. These values are indicated in datasheets of the meter, as well as operators experience. According to manufacturer's recommendation, Signal Strength must register upper than 50. Figure 40 shows failure by low Signal Strength for CO_2 concentrations above 75%.

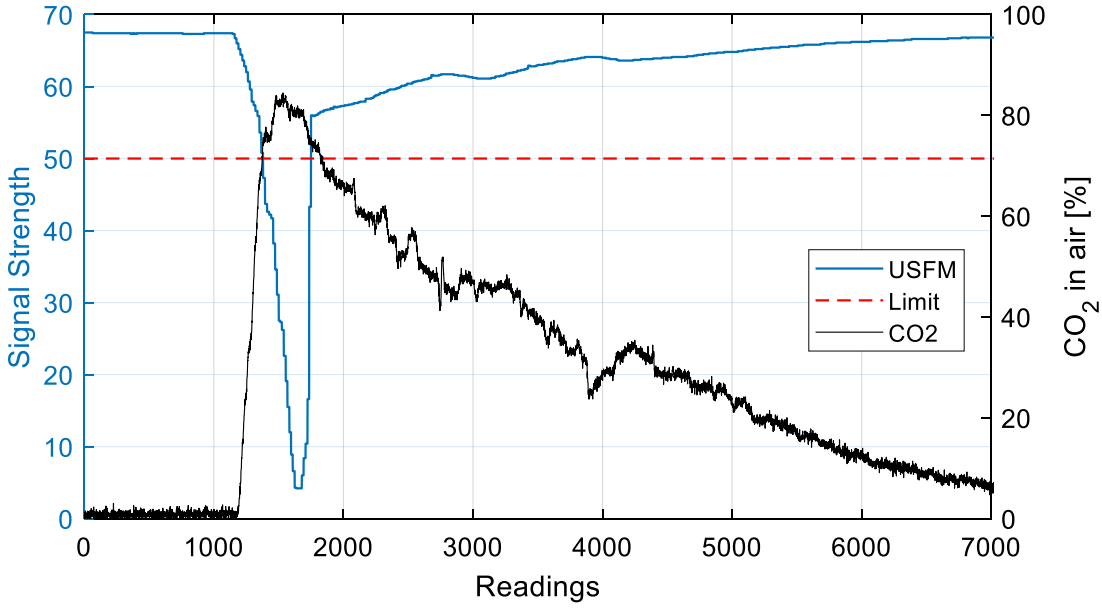

Figure 40 - Occurrence of failure C in a test with CO_2

6.2.3 Design of experiments

In any experimental scientific research, the influential variables might act independently or in tandem. Considering a simple case of two variables affecting a given result, the traditional strategy is fixing one parameter and optimizing the other, than repeating this optimization inverting the variables. In simple cases, it may work but in complex cases this traditional procedure may not lead to the overall optimum response for the experiment. Besides, traditional method may present high cost.

A process variable is affected by controllable factors and uncontrollable factors, such as noise and environmental process. This is illustrated in Figure 41, where a process variable is submitted by an input. The output is a consequence of the interaction between input, controllable and uncontrollable factors.

In order to characterize which factor (controllable and uncontrollable) most affects process output, a screening experiment is done especially designed for magnitude and direction of each factor.

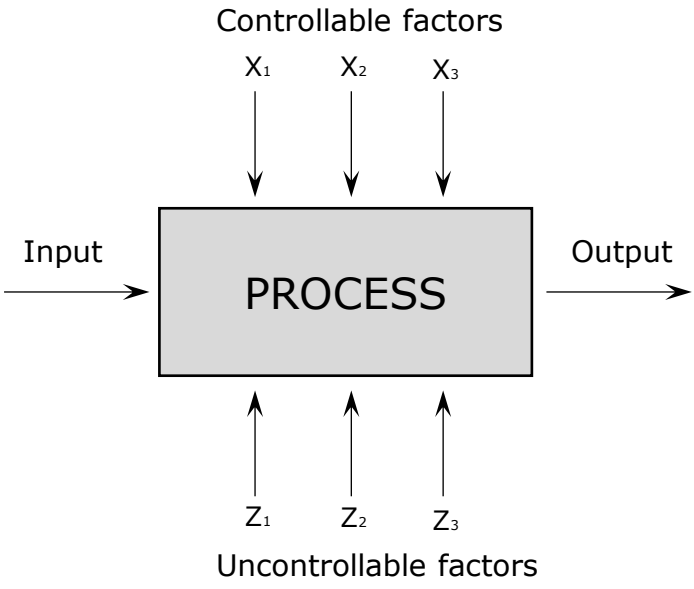

Figure 41 - Experimental process

Montgomery [98] states that it is possible to reach better results comparing to tradition common sense method by varying all variables simultaneously using the design of experiments (DOE) technique. Design of Experiments is a statistical tool to describe the variation between parameters affecting the process and its output. The main advantage of DOE is that it allows to gather maximum information with a minimum number of experiment trials.

DOE has been widely accepted in industry for product performance improvement, process capability and yield. It has also been increasingly used in oil and gas industry. Almeida et al. [99] use DOE to evaluate the influence of water dissolved in crude oil and meter factor on ultrasonic flow meter uncertainty.

A full factorial design is a type of planning that the number of experiments *n* is given by b^k, where *b* is the number of levels and *k* is the number of factors. The simplest case is a two-level experiment.

Factorial design with three factors and two levels can be understood as a cube whose vertices represents factors levels. This experimental design results in a total of $2^3 = 8$ experiments or 8 treatment combination. Geometrically, this design is represented by a cube, in which each corner represents a test run, as Figure 42(a).

The higher level is designated as plus (+) and the lower level is designated as minus (-). Figure 42 lists the eight runs of the 2^3-factorial design.

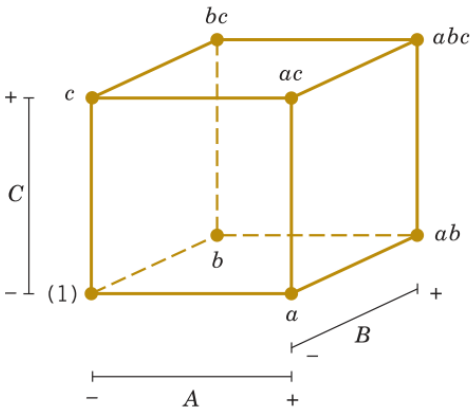

(a) Geometric view

Run	A	B	C
1	−	−	−
2	+	−	−
3	−	+	−
4	+	+	−
5	−	−	+
6	+	−	+
7	−	+	+
8	+	+	+

(b) 2^3 design matrix

Figure 42 - Factorial design 2^3 [8]

The design of trial runs (in coded form) for 2^3 factorial design is summarized in Table 11. The interaction effects of second order and higher order is obtained by the product of the controlled variable signals (+) and (-).

Table 11 - Design of trial runs for 23 factorial design

Test	**Code**	**Variable**			**Interaction**			
		x_1	x_2	x_3	x_1x_2	x_1x_3	x_2x_3	$x_1x_2x_3$
1	1	-	-	-	+	+	+	-
2	x_1	+	-	-	-	-	+	+
3	x_2	-	+	-	-	+	-	+
4	x_3	-	-	+	+	-	-	-
5	x_1x_2	+	+	-	+	-	-	+
6	x_1x_3	+	-	+	-	+	-	-
7	x_2x_3	-	+	+	-	-	+	-
8	$x_1x_2x_3$	+	+	+	+	+	+	+

This work adopted two levels and three factors, resulting in a full factorial design 2^3. The factors under analysis are: average flow rate, CO_2 concentration and transducers installation, as detailed in Table 12.

The low level (+) is defined as transducers in reference position (facing internal wall of tube), operating in atmospheric air, at low flow rate. The high level (+) is transducers installation modified (either approximated or recovery angle arrangement), at high flow rate operating and high carbon dioxide level. It is defined a minimum CO_2 concentration of 30%, because lower CO_2 concentration might present neglectable effect.

Table 12 - Factors specification

Factor	Description	Low (-)	High (+)
x_1	Average velocity [m/s]	11	45
x_2	CO_2 concentration [%]	Atmospheric air	46% of CO_2
x_3	Transducers installation [mm]	410.8	200.8

In order to estimate factorial design analysis reliability, each test is replicated for five times. Additionally, it is defined a minimum sample size of 40 data in each test to guarantee a normal distribution. The significance level adopted is 5%. Finally, analysis of variance (ANOVA) is applied to analyze the experimental design adopted.

6.3 UNCERTAINTY ANALYSIS

The aim of this section is to provide tools for predicting the uncertainty of flare gas ultrasonic flow meters according to API MSM 14-10 [73].

Uncertainty evaluation characterizes the range of values of a measurand is expected to keep a specific confidence level. According to API MSM 14-10 [73], uncertainty prediction for flare flow meters can be estimated only by primary uncertainties related to: i) Temperature; ii) Pressure; iii) Gas composition; iv) Meter performance; v) Installation effects.

According to GUM 1995 [100], combined uncertainties u_c for an output quantity can be determined as a summation of the contribution of standard uncertainty of each input source, as Equation (6.2). This analysis assumes that individual input quantities are uncorrelated.

$$u_c^{\,2} = \sum_{i=1}^{n} \left(\frac{\partial f}{\partial x_i} \right)^2 u^2(x_i) \tag{6.2}$$

When performing data readings, an important issue is the knowledge of the probability that the true value of actual measurand lies in a *U* interval around the value of the measurement performed. The resulting combined uncertainty as Equation (6.2) represents standard uncertainty, which presents an associated confidence level of about 68%. In practice, the confidence level is particular to each application.

The expanded uncertainty for the value of *U* is associated to the chosen probability. Generally, to obtain the expanded uncertainty, the standard uncertainty of

the measurand is multiplied by a factor called the coverage factor k_{CL}, as Equation (6.3).

$$U = k_{CL}.u_C \tag{6.3}$$

Taking a gaussian random distribution variable as a reference, the relationship between the probability and respective factor is given in Table 13.

Table 13 - Coverage factor [100]

Confidence level p [%]	Coverage factor k
68.27	1
90	1.645
95	1.96
95.45	2
99	2.576
99.73	3

Flow rate measured by ultrasonic flow meter in standard conditions, according to ANP (P_{ref} = 1.0325 MPa, T_{ref} = 293 K) is calculated as:

$$Q_{Std} = Q_{USFM}\left(\frac{P}{T}\right)\left(\frac{T_{ref}}{P_{ref}}\right) \tag{6.4}$$

Where:

- Q_{Std} [Nm³/h] is standardized flow rate;
- Q_{USFM} [Nm³/h] is the flow rate in operational conditions;
- P [kPa] is line pressure;
- T [K] is line temperature.,

Flow rate measured by ultrasonic flow meter is given by Equation (6.5).

$$Q_{USFM} = \bar{v} \cdot A = \frac{\pi D^2}{4} \cdot \bar{v} \tag{6.5}$$

Where $\bar{v}$ [m/s] is the average velocity measured along the cross section and A [m²] the cross-section area related to internal diameter D [m].

Combining Equations (6.4) and (6.5):

$$Q_{Std} = \frac{\pi D^2}{4} \cdot \bar{v} \cdot \left(\frac{P}{T}\right)\left(\frac{T_{ref}}{P_{ref}}\right) \tag{6.6}$$

The invariable terms in Equation (6.6), which are constants, are summarized into Equation (6.7):

$$C_1 = \frac{\pi}{4}\left(\frac{T_{ref}}{P_{ref}}\right) \tag{6.7}$$

Thus, resulting expression for standardized flow rate is:

$$Q_{Std} = C_1 \cdot D^2 \cdot \bar{v} \cdot \left(\frac{P}{T}\right) \tag{6.8}$$

The combined uncertainty of the standardized flow rate is described in Equation (6.9).

$$\left[u(Q_{Std})\right]^2 = \left(\frac{\partial Q_{Std}}{\partial C_1}u(C)\right)^2 + \left(\frac{\partial Q_{Std}}{\partial D}u(D)\right)^2 + \left(\frac{\partial Q_{Std}}{\partial \bar{v}}u\left(\bar{v}\right)\right)^2 + \left(\frac{\partial Q_{Std}}{\partial P}u\left(P\right)\right)^2 + \left(\frac{\partial Q_{Std}}{\partial T}u\left(T\right)\right)^2 \tag{6.9}$$

Applying the partial derivatives:

$$\left[u(Q_{Std})\right]^2 = \left(0\right)^2 + \left(C_1 \cdot \bar{v} \cdot 2D \cdot \frac{P}{T} \cdot u(D)\right)^2 + \left(C_1 \cdot D^2 \cdot \frac{P}{T} \cdot u\left(\bar{v}\right)\right)^2 + \left(C_1 \cdot \bar{v} \cdot D^2 \cdot \frac{1}{T} \cdot u(P)\right)^2 + \left(C_1 \cdot \bar{v} \cdot D^2 \cdot \frac{P}{(-T)^2} \cdot u(T)\right)^2 \tag{6.10}$$

Dividing Equation (6.10) by Equation (6.8), results Equation (6.11).

$$\left(\frac{u(Q_{Std})}{Q_{Std}}\right)^2 = \left(\frac{2.u(D)}{D}\right)^2 + \left(\frac{u\left(\bar{v}\right)}{\bar{v}}\right)^2 + \left(\frac{u\left(P\right)}{P}\right)^2 + \left(\frac{u\left(T\right)}{T}\right)^2 \tag{6.11}$$

The resulting expression for combined uncertainty of flare gas flow rate measured by ultrasonic flow meter is estimated by Equation (6.11).

Flow rate predicted by Pitot tube is also a product of average velocity along the cross section measured by Pitot tube and cross section area, as shown in Chapter 5. So, by analogy of Equation (6.5) and (6.11), the combined uncertainty for Pitot tube flow rate Q_{Pitot} is:

$$\left(\frac{u(Q_{Pitot})}{Q_{Pitot}}\right)^2 = \left(\frac{2.u(D)}{D}\right)^2 + \left(\frac{u\left(v_{Pitot}\right)}{v_{Pitot}}\right)^2 + \left(\frac{u\left(P\right)}{P}\right)^2 + \left(\frac{u\left(T\right)}{T}\right)^2 \tag{6.12}$$

Since NEMOG's wind tunnel is subsonic, reaching maximum Mach number lower than 0.3, the compressibility factor can be neglected in Pitot tube velocity equation. Besides, fluid density is estimated using the thermodynamic state of a known gas. These assumptions leads to a simplified expression for predicting the velocity measured by Pitot tube, as Equation (6.13):

$$v_{Pitot} = \alpha\sqrt{\frac{2.P_D}{\rho}} \Rightarrow v_{Pitot} = \alpha\sqrt{\frac{2.P_D}{P/RT}} \tag{6.13}$$

The uncertainty of terms in Equation (6.13) that can't be neither measured nor predicted are neglected in current analysis. These terms are summarized into a constant factor C_2:

$$C_2 = \alpha\sqrt{2R} \tag{6.14}$$

Combining Equations (6.13) and (6.14):

$$v_{Pitot} = C_2\sqrt{\frac{2.P_D T}{P}} \tag{6.15}$$

Resulting expression for combined uncertainty of Pitot tube velocity is described in Equation (6.16).

$$\left[u(v_{Pitot})\right]^2 = \left(\frac{\partial v_{Pitot}}{\partial C}u(C_2)\right)^2 + \left(\frac{\partial v_{Pitot}}{\partial P_D}u(P_D)\right)^2 + \left(\frac{\partial v_{Pitot}}{\partial P}u(P)\right)^2 + \left(\frac{\partial v_{Pitot}}{\partial T}u(T)\right)^2 \tag{6.16}$$

Applying the partial derivatives in Equation (6.17):

$$\left[u(v_{Pitot})\right]^2 = (0)^2 + \left(C_2.\frac{1}{2}\left(\frac{T}{P.P_D}\right)^{\frac{1}{2}}u(P_D)\right)^2 + \left(C_2.\frac{1}{2}\left(\frac{P_D}{P.T}\right)^{\frac{1}{2}}u(P)\right)^2 + \left(C_2.\frac{1}{2}(P_D T)^{\frac{1}{2}}\left(\frac{1}{P}\right)^{\frac{3}{2}}u(T)\right)^2 \tag{6.17}$$

Dividing Equation (6.17) by Equation (6.15), the general expression for combined uncertainty of Pitot tube velocity is:

$$\left(\frac{u(v_{Pitot})}{v_{Pitot}}\right)^2 = \left(\frac{1}{2}\frac{u(P_D)}{P_D}\right)^2 + \left(\frac{1}{2}\frac{u(P)}{P}\right)^2 + \left(\frac{1}{2}\frac{u(T)}{T}\right)^2 \tag{6.18}$$

Replacing Equation (6.18) in Equation (6.12), the expression for predicting the uncertainty of Pitot tube flow rate in standard conditions is:

$$\left(\frac{u(Q_{Pitot})}{Q_{Pitot}}\right)^2 = \left(\frac{2.u(D)}{D}\right)^2 + \left[\left(\frac{1}{2}\frac{u(P_D)}{P_D}\right)^2 + \left(\frac{1}{2}\frac{u(P)}{P}\right)^2 + \left(\frac{1}{2}\frac{u(T)}{T}\right)^2\right]^2 + \left(\frac{u(P)}{P}\right)^2 + \left(\frac{u(T)}{T}\right)^2 \tag{6.19}$$

Current analysis applied uncertainty Type A, which involves all components whose uncertainty may be calculated from a series of observations, generally applying statistical methods. For a type A uncertainty, the standard uncertainty of the component is defined as equal to one standard deviation of the series of observations. This work applied a 95% confidence level on all uncertainty's analysis.

6.4 RESULTS

6.4.1 Validation of flow metering performance

As flow metering process by ultrasonic technology is based on correlation between emitted and received ultrasonic pulse signals, a huge signal processing is applied. The signal processing process should to be suitable to overcome the low signal-to-noise ratio, especially at high velocities, besides should measure small transit times differences at low velocities [1]. After signal processing, data statistics are applied on flow readings, to increase the flow metering accuracy.

The ultrasonic flow meter allows the user to select some data statistics on the flow measurement, such as moving average filter and cutoff limit. Moving average filter implies in setting the response time of the flow meter after a step change in flow rate. Technical specification recommends moving average filter of 30 samples to ensure most stable signal [62].

In order to validate flow metering performance, the moving average filter is turned off. For first analysis, the ultrasonic flow meter is installed in wind tunnel open-circuit assembly, as described in Chapter 5.

The performance test is accomplished by comparing ultrasonic readings measurement and reference flow by Pitot tube, at 10 different flow rate steps. Uncertainty is analyzed, as well.

Figure 43 presents the performance test for flow rate behavior, regardless statistics analysis in both measurement in Channel 1 and Channel 2. Each point corresponds to an average of sample populated by, at least, 300 readings. The uncertainty analysis for ultrasonic flow metering follows Equation (6.11), while the uncertainty bars for Pitot tube is calculated as Equation (6.19).

Aiming comparison of ultrasonic flow meter and Pitot tube readings, a correlation line ($y = x$) is plotted. This line is theoretical and represent and ideal correlation, if the flow measured by the reference flow meter and by the ultrasonic flow meter under test would be equal. Additionally, and average line is plotted, representing the average flow rate on both transducers pairs.

In Figure 43 it is observed that Pitot tube uncertainty presents higher values than ultrasonic flow readings, especially at low flow rate.

Table 14 details the ratio of Pitot tube and ultrasonic readings uncertainty.

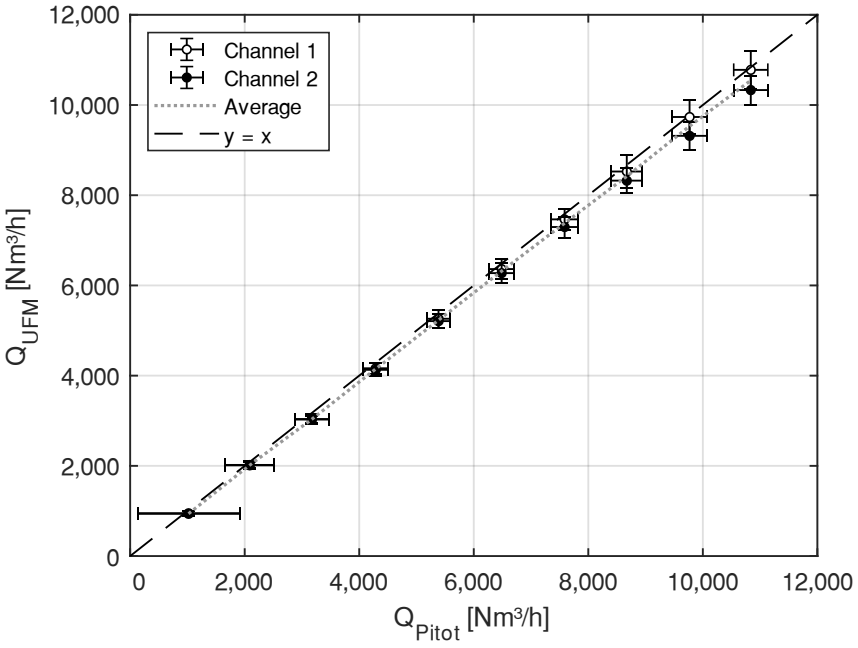

Figure 43 - Flow rate analysis in open loop configuration, Average = 1

Table 14 - Uncertainty of the Pitot tube with 95% confidence level

Q_{Pitot} [Nm³/h]	$U(Q_{Pitot})$ [Nm³/h]	$U(Q_{Pitot})/ Q_{Pitot}$ [%]
1,018.9	890.7	87.4
2,087.4	432.3	20.7
3,171.5	296.3	9.3
4,287.1	221.3	5.2
5,384.2	203.6	3.8
6,486.5	223.8	3.5
7,586.3	236.0	3.1
8,671.9	271.7	3.1
9,768.3	300.2	3.1
10,837.1	298.1	2.8

PDT calibration starts at 0 mmca, which corresponds of an analogic signal of 4 mA. Signal noise typically presents low variation amplitude. As in low flow rates, differential pressure is low and standard deviation is almost constant, while mean value is low. So, ratio is higher compared to high flow rate levels, where mean value is high.

Due to Pitot tube uncertainty levels and remembering that Pitot tube flow rate feed the closed loop control, the evaluation of ultrasonic flow metering performance in wind tunnel is done only for flow rates higher than 2,000 Nm³/h.

Table 15 compares the flow rate and uncertainty of the ultrasonic flow meter for Channel 1 and Channel 2. If velocity profile is turbulent and fully developed and both transducers pair are identical, flow rate readings would be identical, ideally speaking. However, as can be seen in Figure 43 and detailed in Table 15, average values of flow rate between both channels are different.

Table 15 - Comparison of flow rate measured by ultrasonic flow meter on Channel 1 and Channel 2 and reference

Q_{Pitot} [Nm³/h]	Q_{Ch1} [Nm³/h]	$U(Q_{Ch1})/Q_{Ch1}$ [%]	Q_{Ch2} [Nm³/h]	$U(Q_{Ch2})/Q_{Ch2}$ [%]
1,018.9	936.7	5.8	950.7	4.8
2,087.4	2,011.9	4.3	2,020.6	3.5
3,171.5	3,038.4	3.7	3,026.6	2.9
4,287.1	4,163.1	3.0	4,129.0	3.4
5,384.2	5,261.2	3.8	5,208.9	3.1
6,486.5	6,362.8	3.5	6,273.1	3.5
7,586.3	7,464.9	3.2	7,295.2	3.2
8,671.9	8,525.5	4.3	8,323.4	3.3
9,768.3	9,734.2	3.9	9,316.5	3.3
10,837.1	10,779.3	3.9	10,331.5	3.1

Considering only average flow rate, both transducers pairs underestimates flow measurement. For reference flow rate of 1,018.9 Nm³/h and 2,087.9 Nm³/h, measurements performed in Channel 2, presents relative difference of -6.7% and -3.2%, respectively (closest to reference value). These same relative difference values for Channel 1 are -8.1% and -3.6%. Considering uncertainties (95% confidence level), flow rate on both channels are overlapping.

As wind tunnel flow rates increases, flow rate measured by Channel 1 are closest to Pitot tube readings and relative difference diminish as average flow rate increases, achieving a minimum difference of -0.3% at 9,768.3 Nm³/h. On the other hand, flow rate measured by Channel 2 achieve a minimum relative difference of -3.3% at a reference flow rate of 5,384.2 Nm³/h.

One can observe from Figure 43 that flow rate measured by each transducers pair diverges as flow rate increases, especially for flow rates higher than 6,500 Nm³/h. It is also noteworthy that the dashed grey average line deviated from the ideal correlation line y = x as flow rate increases.

Multipath ultrasonic flow meters are indicated to increase the reliability of flow measurement. This configuration is recommended for USFM installation close to line accidents, such as curves, due to its capacity to detect asymmetries in flow profile. Therefore, it is important to take into account flow rate information supplied by both transducers, as an average value. Thus, a linear regression is proposed for average flow rate from ultrasonic channels coincide with reference flow rate. The linear regression presents the form:

$$y_c = B_1 + B_2.x \tag{6.20}$$

Linear regression parameters are detailed on Table 16. The coefficient of determination "R^2" is 0.9999, which means that regression model account 99,99% of the variability in data.

For evaluation significance of linear regression proposed, an analysis of variance (ANOVA) method is used, which results are on Table 17. Considering a 95% confidence level, the linear regression proposed is considered validated, since p-value is less than 0.025.

Table 16 - Linear regression parameters

Predictor	**Coefficient**	**Standard Error**	**F-Test**	**p-value**
Linear B_1	-46.9427	10.3800	- 4.5224	0.0019
Angular B_2	0.9788	0.0015	632.9635	4.34E-20
R^2	99,99%	**R^2 adjusted**	99,99%	

Table 17 - ANOVA for testing significance of regression

Source of variation	**Degrees of freedom**	**Sum of squares**	**Mean Square**	**F-Test**	**P**
Regression	1	94,738,973.4	94,738,973.4	400,642.8	4.34E-20
Residual error	8	1,891.7	236.4		
Total	9	94,740,865.1			

As detailed on Chapter 3, sound speed is a thermodynamic property, which depends of chemical composition of fluid and thermodynamic state and it is independent of USFM operation, so flow rate should not affect sound speed readings by ultrasonic flow meter ideally speaking. Measured sound speed behavior is shown in Figure 44. Sound velocity measured on Channel 1 and Channel 2 are analyzed considering respectively uncertainties. Speed of sound for atmospheric air as perfect gas is the reference for comparison, represented by the black "x" symbol.

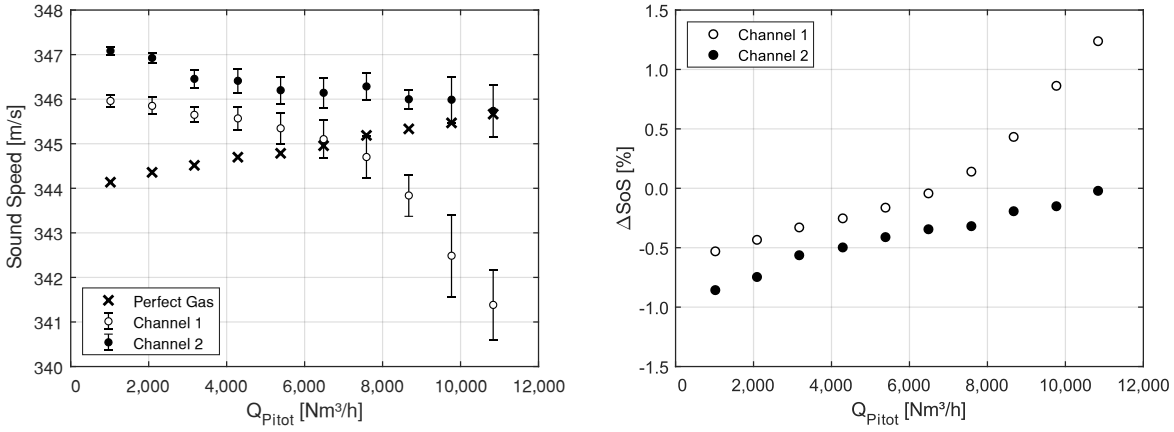

a) Sound speed b) Sound speed variation

Figure 44 - Sound speed analysis in open loop configuration, Average = 1

Flow temperature increased in the validation experiment. So, sound speed predicted by perfect gas model also increase. Reference sound speed range is between 344.1 m/s (at minimum flow rate) and 346.7 m/s (at maximum flow rate), therefore a variation of 0.75%.

On the other hand, measured sound speed calculated by transit times of each transducers pair, are different and diverges as flow rate increases. At Channel 1, flow rate uncertainty with 95% confidence level presents minimum value of 0.13 m/s at the lowest flow rate and maximum value of 0.92 m/s at an average flow rate of 9,768.3 Nm³/h, which is the second largest flow rate under test. Sound speed maximum value is 345.9 m/s at lower flow rate and the lowest sound speed achieved value is 341.4 m/s at the highest flow rate.

At Channel 2, the highest sound speed value measured is 347.1 m/s at the lowest flow rate. Minimal sound speed measured is 345.7 m/s at the highest flow rate. The uncertainty on sound speed measurement by Channel 2 presents the same behavior as on Channel 1: minimal uncertainty presents magnitude of 0.09 m/s at the lowest flow rate, in this case with magnitude of 0.09 m/s, and maximum uncertainty at the highest flow rate, which corresponds to an uncertainty of 0.58 m/s.

Mean values of sound speed measured by USFM are compared to reference sound speed following perfect gas model, as Equation (6.21). Figure 44.a illustrates the results.

$$\Delta SoS = 100.\frac{\left(SoS_{USFM} - SoS_{ref}\right)}{SoS_{ref}} \tag{6.21}$$

Where SoS_{USFM} is calculated according to Equation (3.4) and SoS_{ref} according to Newton Laplace law, as Equation (4.2).

In Channel 1, minimal sound speed variation is -0.5% at the lowest flow rate. Maximum variation is 1.2% at the highest flow rate. In Channel 2, these values are, -0.8% and 0%, respectively.

Lastly, the diagnostic parameter Signal Strength is analyzed in Figure 45. According to technical specifications, appropriate transit time measurement process must present the signal strength parameters of the ultrasonic transducer higher than 50.

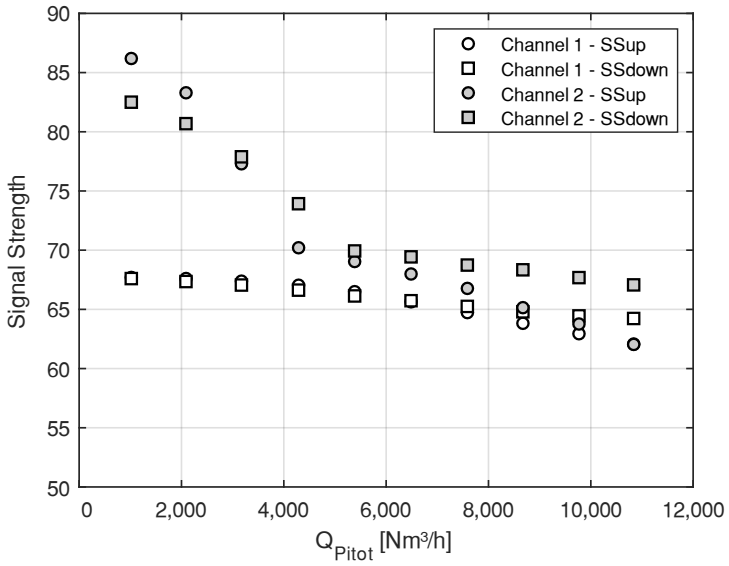

Figure 45 - Signal Strength analysis in open loop configuration

It is remarkable that Signal Strength measured is different on Channel 1 and on Channel 2. Both transducers pairs are same model, but different batches. So, differences on Signal Strength behavior can be attributed to constructive differences.

In Channel 1, signal strength upstream fell from 67.7 (at lowest flow rate) to 62.0 (at highest flow rate), corresponding to 8.5% reduction. These same values on downstream transducers are 67.6 and 64.2, respectively, which represents a reduction of 5%.

As shown in Figure 45, Channel 2 presents higher Signal Strength, especially in low flow rates. At lowest flow rate, signal strength upstream is 86.2 and signal strength downstream is 82.5. At highest flow rate, these values fell to 62.0 and 67.0, respectively. Considering these values, signal strength reduction on Channel 2 is 28% in upstream transducer and 18% in downstream transducer.

6.4.2 Transducers approximation procedure

One proposal to improve flow metering performance of ultrasonic flow meter is the transducers approximation, since path length reduction increase the sound pressure, as predicted by Lambert-Beer law, as Equation (2.12). Transducers approximation is proved effective in dry calibration process, as detailed in Chapter 4.

In this this context, the performance of transducers approximation procedure is examined in wind tunnel, as well. Transducers from Channel 1 are approximated, while transducers from Channel 2 remains facing the inner wall of the tube. Relative

transducers distances are detailed in Table 2 and wind tunnel is mounted in open loop circuit configuration.

The performance of transducers approximation procedure is evaluated by following criteria: i) Flow rate variability and ii) Signal voltage amplitude, as produced by piezoelectric transducers. Signal strength and sound speed are also monitored and assessed, as well. Minimal signal strength reached is 62, so higher than the specified minimum value of 50, according to technical specifications. Sound speed measured by USFM are evaluated as Equation (6.21), varying less than 2%.

The analysis of flow rate variability is important to evaluate turbulence effects and vortices induced by transducers intrusion in core flow. Equation (6.22) calculates flow rate variability, as a ratio between standard deviation from flow rate measured "$\sigma(Q)$" [Nm³/h] and average flow rate "$\overline{Q}$".

$$\Delta Q = \frac{\sigma(Q)}{\overline{Q}} \tag{6.22}$$

Variabilities, as calculated by Equation (6.22) are shown in Figure 46, varying flow rate. Considering distances key, as stablished in Table 10, L_1 represents variability behavior for no-intrusive assembly (transducers facing internal tube wall). In such position, maximum flow rate variability reaches 2.5%, at Q_{Pitot} = 3,100 Nm²/h and minimum variability of 1.8%, at Q_{Pitot} = 7,400 Nm³/h.

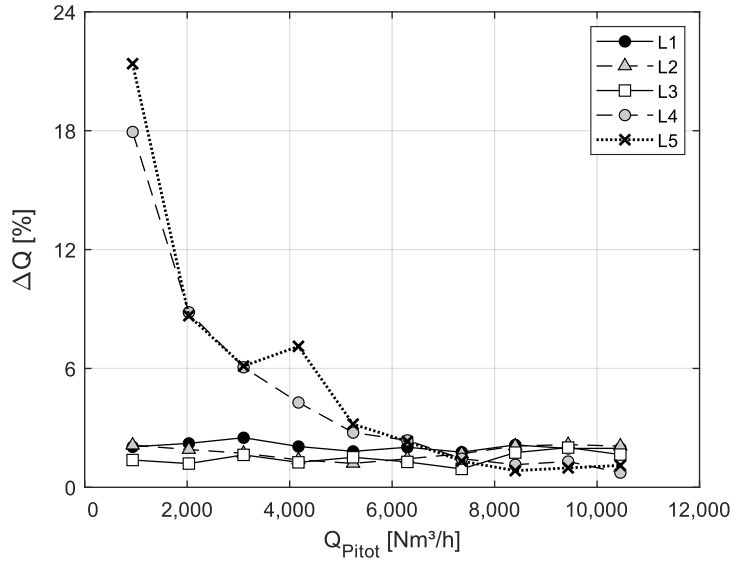

Figure 46 - Flow rate variability at several transducers approximation distances

Average flow rate variabilities of L_1, L_2 and L_3, are similar: 2.0%, 1.8% and 1.5%, respectively. Average flow rate variability increases at L_4 = 200.8 mm to 4.7% and 5.3% at L_5 = 160.7 mm.

Flow rate variability at L_2 = 321.3 mm is between 1.2% at Q_{Pitot} = 5,200 Nm²/h and 2.2% at Q_{Pitot} = 9,500 Nm²/h.

At L_3 = 241.0 mm, minimum flow rate variability is 1.0% at Q_{Pitot} = 7,400 Nm³/h, while maximum variability is 2.0% at Q_{Pitot} = 9,500 Nm²/h.

For L_4 = 200.8 mm and L_5 = 160.7 mm, flow rate variability is inversely proportional to flow rate. As can be seen in Figure 46, ΔQ is higher at the lowest flow rate, with variability of 17.8% at L_4 and 21.4% at L_5. Overall, flow rate variability reduced with the increase of flow rate, except in Q_{Pitot} = 4150 Nm³/h where flow rate variability increased from 6.1% to 7.1%. Minimum ΔQ is 0.7% at L_4 and 1.1% at L_5. Comparing two shorter transducers distances, flow rate variability is minor at L_4.

Flow rate variability shows to be less sensitive to transducer distance for flow velocities above 6,000 Nm^3/h.

Then, signal voltage amplitude is analyzed. Signal amplitude of received signal is measured by oscilloscope, as done in dry calibration procedure, detailed in Chapter 4. Thus, considering a steady state Pitot tube flow rate as reference flow meter, peak-to-peak signal voltage is measured. Readings are shown in Figure 47.

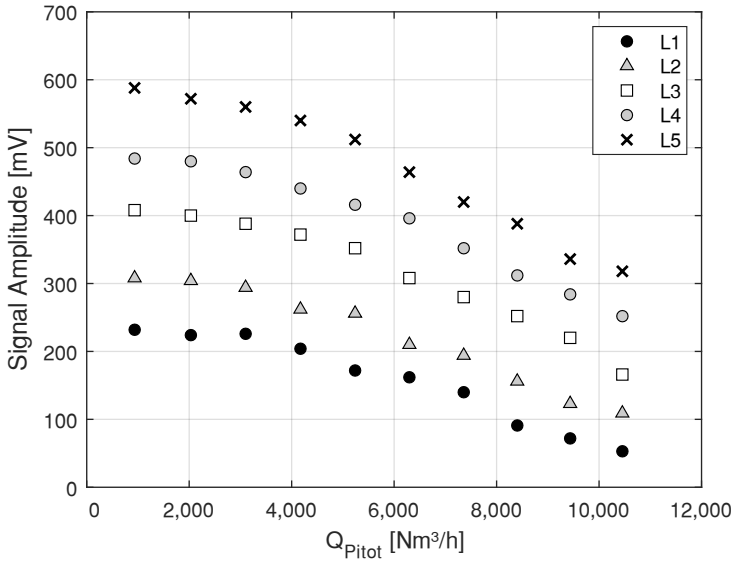

Figure 47 - Voltage from received signal at several flow rate levels

For each flow rate level, signal amplitude is minimum in reference position L_1, which is the largest transducer distance, and increases as path length is reduced. Therefore, maximum signal is at L_5 (shortest transducers distance).

On the other hand, signal voltage is maximum at the lowest flow rate and minimum at highest flow rate. This phenomenon is due to the carry along effect, typical in ultrasonic flow meters [1], [2], [18], in which velocity profile interferes the propagation of sound pressure emitted from a transducer. The carry along effect may be minimized with the application of the recovery angle assembly [1], [2], [18].

At L_1 = 410.8 mm, signal amplitude is between 232 mV and 53 mV. At L_2, these values increase to minimum of 308 mV and maximum of 109 mV. At L_3, voltage of received signal is between 408 mV and 166 mV.

At 50% reduction of path length, signal amplitude at L_4 is 484 mV at minimal flow rate and 252 mV at maximum flow rate. At the lowest acoustic path length L_5, signal voltage is between 588 mV and 318 mV.

At flow rate of 900 Nm³/h, signal amplitude increased 150% with the reduction of path length from 410.8 mm to 160.9 mm. At flow rate of 10,500 Nm³/h, signal amplitude increased 500% with 60% of path length reduction (from L_1 to L_5).

Reading's analysis indicate that transducers approximation may be a viable alternative to improve ultrasonic flow meter performance. Thus, this technique will be examined in wind tunnel operating with high carbon dioxide concentration. The path length distance chosen is L_4 = 200.8 mm, which corresponds to 50% reduction.

Despite transducers be intrusive at L_4, probably disturbing velocity profile, this path length distance chosen to verify improvements in flow metering performance with high CO_2 concentration. Shorter acoustic path lengths distances than L_4 (so close to reference position) reduces significantly the variability transducers approximation effects.

6.4.3 Temperature effect on flow metering performance

In closed circuit assembly, fluid temperature inside NEMOG's wind tunnel is heated on some flow rate levels, due to viscous effects, but mainly to compression work. Thus, it is necessary to characterize temperature effect on the performance parameters of ultrasonic flow meter, since tests at high CO_2 concentration must be executed in closed circuit mounting. According to technical specifications [65], ultrasonic transducers can be operated up to 150 ºC.

Sound speed is a thermodynamic property that is temperature dependent. Given a gas with uniform chemical composition, which follows the perfect gas hypothesis, sound speed is only a function of temperature (Newton-Laplace Equation). Figure 48 compares temperature effect on sound speed for the heating process at high flow rate level in NEMOG's wind tunnel.

Estimated reference sound speed by perfect gas model, presents minimal value of 351.5 m/s at 35ºC and maximum of 377.6 m/s at 80ºC.

Considering sound speed measured by USFM transit times, minimal sound speed is 343.3 m/s in Channel 1 and 348.9 m/s in Channel 2. Additionally, maximum sound speed is 374.6 m/s in Channel 1 and 377.9 m/s in Channel 2.

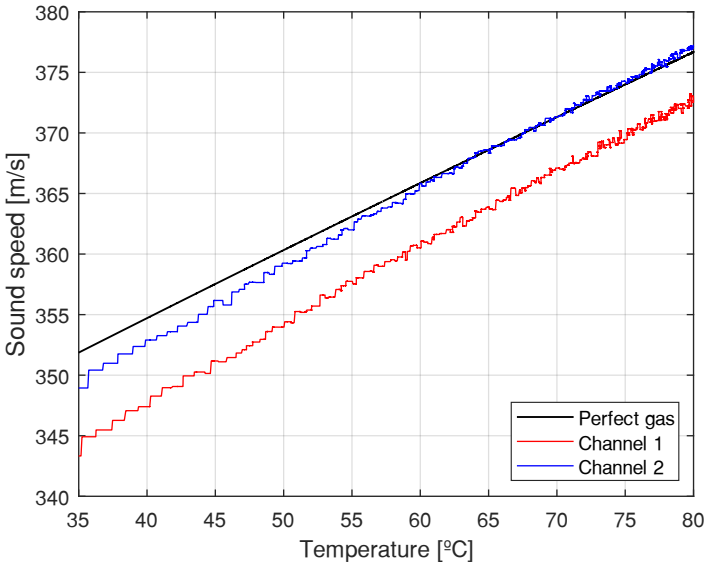

Figure 48 - Performance of sound speed measurement by ultrasonic flow meter with temperature increase

Sound speed variation from the ultrasonic flow meter and reference perfect gas model can be calculated as Equation (6.21). Considering Channel 1, *ΔSoS* starts in 2.4%, which is the highest value, at 30ºC and reduces as temperature approaches to steady state regime, reaching minimum value of 0.8% at 80ºC. Mean *ΔSoS* variation in Channel 1 is 1.2%

For Channel 2, *ΔSoS* presents maximum value of 0.9% at 30°C. This variation reduces as temperature increases, achieving minimum of 0%. Mean *ΔSoS* variation in Channel 1 is 0.2%.

Sound speed analysis indicate the relevance to reach steady state temperature regime before initiating experiments with carbon dioxide injection, because each meter presents it owns dynamics.

The influence of temperature on Signal Strength is shown in Figure 49 for highest wind tunnel flow rate. It can be noticed that, for both channels, Signal Strength upstream presents lower value than Signal Strength downstream.

In Channel 1, minimum SS_{up} is 60.7 at 45ºC and maximum SS_{up} is 62.6 at 75°C. Signal Strength downstream remains virtually unchanged: minimum of 63.2 and maximum of 63.7.

In Channel 2, minimum signal strength values are: 60.5 at 35ºC for SS_{up} and 65.6 at 64°C for SS_{down}. Maximum signal strength are: 62 at 56°C for SS_{up} and 66.7 at 66°C for SS_{down}.

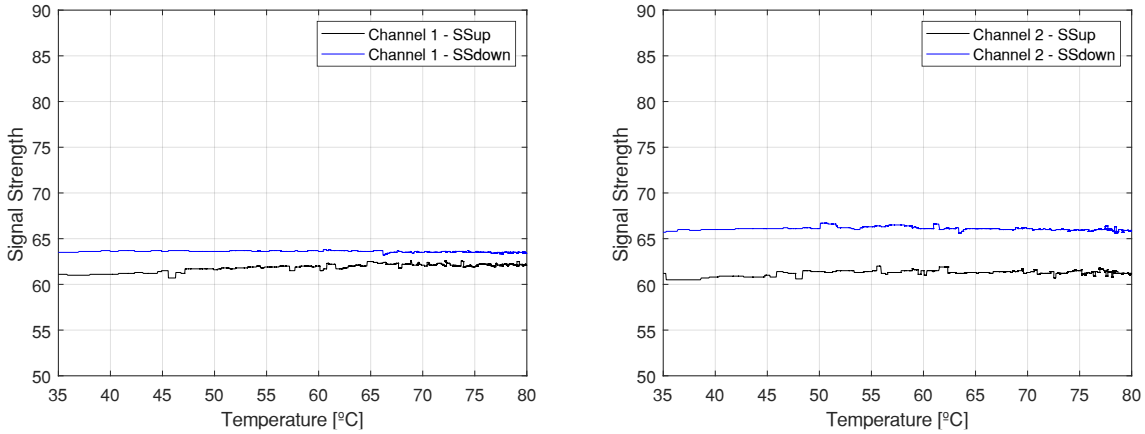

a) Channel 1 b) Channel 2

Figure 49 - Temperature effect on performance parameters

Analysis indicate that temperature up to 80°C do not affect signal strength, as a performance parameter of the ultrasonic flow meter under evaluation.

6.4.4 CO_2 effect on flow metering performance keeping transducers in reference position

In following analysis, wind tunnel is mounted in closed loop circuit configuration

For evaluation of carbon dioxide effect on ultrasonic flow metering performance, three flow rate levels are examined:

Table 18 - Velocity steps examined in experiments with high carbon dioxide concentration

Flow rate level	Symbol	Average velocity [m/s]
Minimum	Q_{min}	11
Intermediate	Q_{int}	28
Maximum	Q_{max}	45

These selected velocities steps consider operational capacities of wind tunnel instrumentation and power, as detailed in Chapter 5 and in Section 6.4.1.

Minimum flow rate is determined by the sensing capacity of the gas analyzer Keco 2605C and by an acceptable variability of Pitot tube uncertainty. Maximum flow rate is determined by the blower capability to keep the flow rate constant at closed loop control in high CO_2 level. Intermediate flow rate is established to be a simple averaging of minimum and maximum values.

After the gas temperature reaches steady state regime, tests begin with carbon dioxide injection. The evaluation of flow metering performance at high CO_2 concentration is performed in steady state intervals of volumetric concentration. Thus, molecular composition should present maximum standard deviation from 1, at a minimum sampling time of 40 readings (40 seconds). This methodology guarantees a

normal distribution of experimental readings and its adequate for not presents dynamic effects for different technologies. Then, failure criteria are analyzed in an algorithm developed in Matlab [101].

Firstly, transducers of both Channel 1 and Channel 2 are assembled in reference position, which means, facing the inner wall of the tube. Figure 50 presents the flow rate results at three flow rate levels.

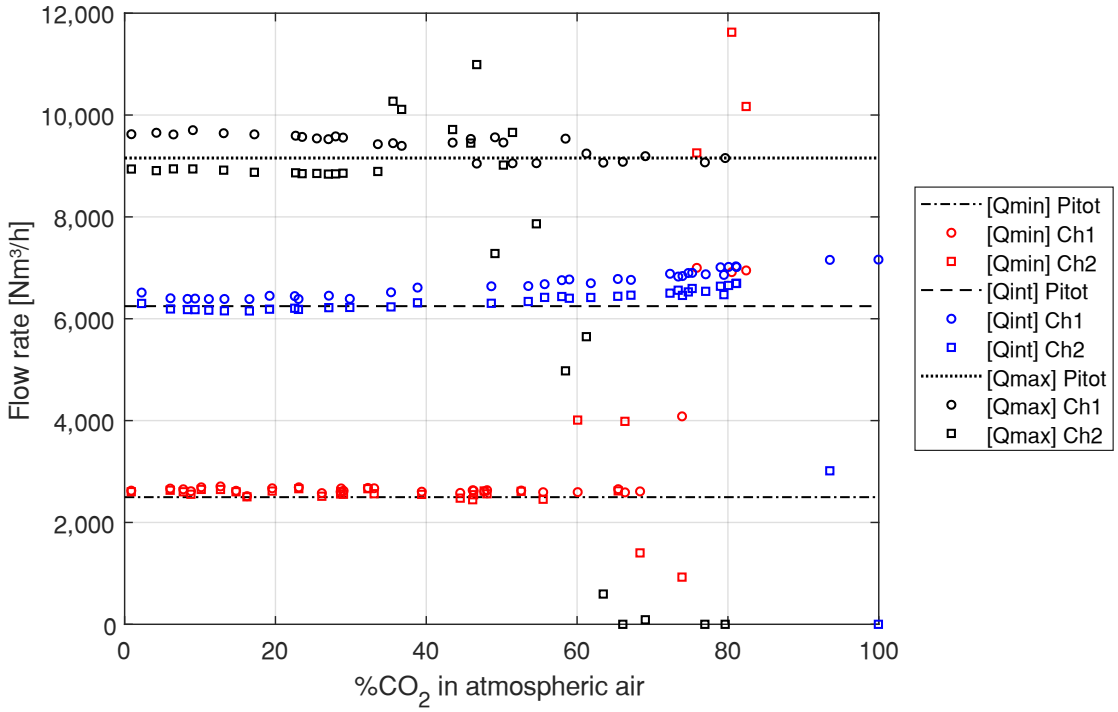

Figure 50 - Carbon dioxide effect on flow rate measurement with transducers in reference position

Failure criterion type *A* evaluates the relative difference between the ultrasonic flow meter flow rate and reference flow rate, as Equation (6.1). Maximum δQ allowed in this criterion is 20%, which is maximum difference between ultrasonic flow meter and Pitot tube flow rates, regardless application of filter or calibration curves.

At the lowest flow rate level Q_{min}, at average reference flow rate of 2,500 Nm³/h, failure type *A* is identified in Channel 1 at 74% of CO_2. In Channel 2, failure criterion type *A* starts intermittent at 60% of CO_2. At 74% of CO_2, all flow rate reading by both Channel 1 and Channel 2 are in failure.

At intermediate flow rate level Q_{int}, at average reference flow rate of 6,300 Nm³/h, there is no indication of failures type *A* in Channel 1 up to 100% of CO_2. On the other hand, failure type *A* begun internment at Channel 2 in 93% of CO_2, fails in 62% of flow rate readings. At 100% of CO_2, 100% flow measurement readings in Channel 2 fails.

At the highest flow rate level evaluated Q_{max}, at average reference flow rate of 9,200 Nm³/h, there are no indication of failure type *A* from Channel 1 measurements. However, from the analysis of criteria type *B* and *C*, it is notice that, actually, flow rate from Channel 1 is unchanged because it is frozen. This stresses the relevance of having additional criteria regardless of flow rate to characterize flow metering failures of ultrasonic flow meters.

In Channel 2, failures type *A* begin at 47% of CO_2 in atmospheric air, with 15% of failure. Above 58% of CO_2, 100% flow readings fail.

Failure criterion type *B* consider sound speed measured by ultrasonic flow meter. Since temperature, pressure and molecular composition are well known in NEMOG's wind tunnel, it is defined an expected level for sound speed. Inferior limit corresponds to pure carbon dioxide at 20°C, with corresponds to sound speed of 250 m/s, approximately. On the other side, upper limit is 400 m/s, the sound speed for atmospheric air at 90°C. Results are shown in Figure 51.

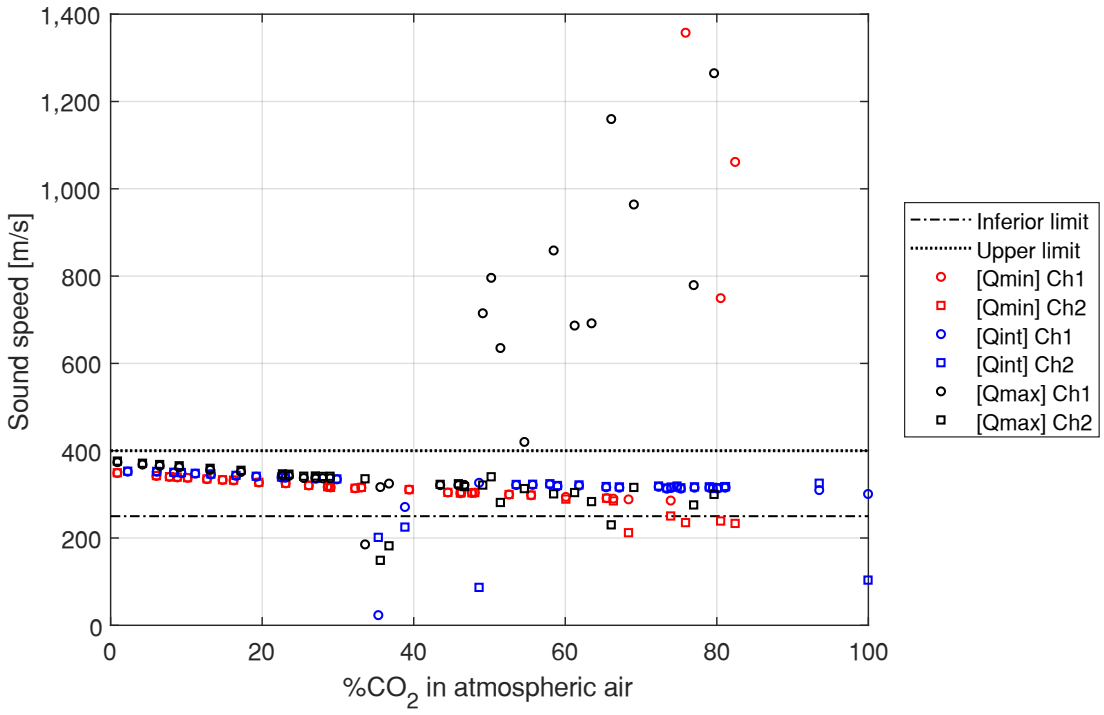

Figure 51 - Carbon dioxide effect on sound speed measurement with transducers in reference position

At the lowest flow rate experiment Q_{min}, failure type *B* starts on Channel 1 on 76% of CO_2. The start of failures type *B* coincides with failure detected by criterion *A*, as described above. In Channel 2, sound speed failures reach 48% of readings failing, at 69% of CO_2. Above 76% of CO_2, 100% sound speed readings for measurements in Channel 2 fails by criterion *B*.

At intermediate flow rate, there is an indication of one punctual failure type *B* in Channel 1, at 35% of CO_2. However, flow rate measured is acceptable and

performance parameters keeps as recommended by technical specifications, indicating that flow readings are not failing. There is no indication of failures type *B* in Channel 1, up to 100% of CO_2.

Still at intermediate flow rate, there are punctual indication of failure type *B* on Channel 2 in concentrations between 35% of CO_2 and 48% of CO_2. Similar as detected in Channel 1, flow readings and performance parameters are in accordance to the limits stablished by failure criteria type *A* and *C*. Above 48% of CO_2 in atmospheric air, there is no additional indication of failure type *B* up to 100% of CO_2.

At the highest flow rate evaluate, which corresponds to an average velocity of 45 m/s, failure type *B* starts on Channel 1 at 34% of CO_2. Above 50% of CO_2, all readings indicate failure type *B*.

Channel 2 presents punctual failure type *B* events: 60% of readings meets failure criterion type *B* at 36% of CO_2. At 51% of CO_2, 13% of readings from Channel 2 fails. In 70% of CO_2, this value drops to 20% of failures type *B*. This analysis indicate that attenuation presents non-linear effects in flow metering performance.

Failure criterion type *C* evaluates flowmeter parameters accordance to technical recommendations. For the ultrasonic flowmeter analyzed, Signal Strength is analyzed. Figure 52 presents results for Channel 1 and Channel 2. A reference dashed line is plotted to emphasize Signal Strength inferior limit of 50.

At the lowest flow rate, failure type *C* in Channel 1 begin at 75% CO_2. At intermediate flow rate, there is no indication of failure type *C* in both Channel 1 and Channel 2. At the highest flow rate of tests, failure by low Signal Strength begin in Channel 1 at 45% CO_2. There is no indication of failure type *C* in any flow rate at Channel 2.

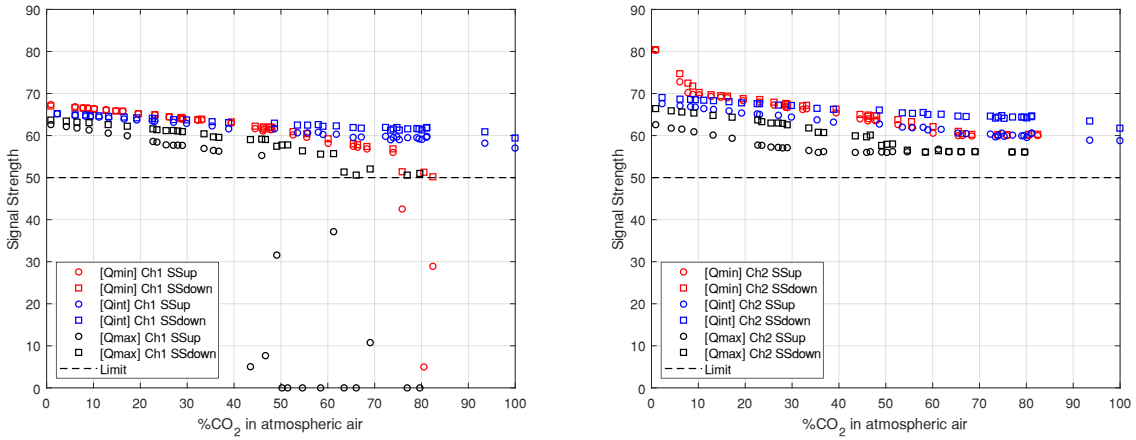

a) Channel 1 b) Channel 2

Figure 52 - Carbon dioxide effect on Signal Strength with transducers in reference position

From experiments performed at high carbon dioxide concentration, flow rate variability can be analyzed to examine flow rate variability with transducers in reference

position (facing the inner wall of the tube). Thus, Equation (6.22) is used in results from Channel 1. This analysis only considers readings in which any failure criterion is detected. At Q_{min} = 2,300 Nm³/h, flow rate variability lies between 0.68% and 3.79%. At Q_{int} = 6,300 Nm³/h, minimum flow rate variability is 0.21% and maximum ΔQ_{int} is 1.06%. At Q_{max} = 9,000 Nm³/h, flow rate variability is between 0.18% and 1.12%.

Combining fail readings by criterion *A*, *B* and *C*, failure index F_{index} is calculated as Equation (6.23).

$$F_{index} = \frac{n_{failure}}{n_{total}} = \frac{n_A + n_B + n_C}{n_{total}} \tag{6.23}$$

Where n_A is the number of failure readings by criterion A, n_B the total of failure readings by criterion B, n_C is the total of failure readings by criterion C and n_{total} the total flow metering readings.

Results from Figure 50, Figure 51.and Figure 52 are summarized in Table 19 to four intervals of carbon dioxide concentration. The critical carbon dioxide concentration, in which all readings are in fault, is also shown.

Table 19 - Summary of failure index of flow metering process with transducers in reference position

%CO_2	**Channel 1**			**Channel 2**		
	Q_{min}	Q_{int}	Q_{max}	Q_{min}	Q_{int}	Q_{max}
0 – 25	0.0%	0.0%	0.0%	0.0%	0.0%	0.0%
25 – 50	0.0%	18.5%	38.6%	0.0%	34.4%	14.0%
50 – 75	4.4%	0.0%	100.0%	40.3%	0.0%	45.8%
75 – 100	100.0%	0.0%	100.0%	100.0%	41.8%	100.0%
%CO_2 failure limit	73.9	100	46.7	68.3	100	50.2

6.4.5 Performance analysis of transducers approximation procedure in high CO_2 concentration

Previous analysis executed in dry calibration procedure, shows that transducers approximation increases ultrasonic signals up to 100% of CO_2, as shown in Section 4.4.3. Additionally, wind tunnel experiments show that transducers approximation also increase signal power at several flow rate levels, in atmospheric air. Thus, transducers approximation is here examined in wind tunnel with high carbon dioxide concentration. This procedure mitigates molecular attenuation promoted by carbon dioxide.

Before starting experiments with path length variation technique, in wind tunnel and high carbon dioxide concentration, it is necessary to evaluate transducers approximation effect in velocity profile. Thus, velocity profile is measured downstream to the ultrasonic flow meter test section, which transducers from Channel 1 approximated. Channel 1 transducers are installed on horizontal position, same plane of LDA measurement section. Channel 2 is installed on vertical plane.

In this context, velocity distribution is measured by Laser Doppler anemometry – LDA technique, at 155 selected points distributed along horizontal diameter, applying same methodology as detailed in Chapter 5. Wind tunnel operates in closed circuit arrangement. Experimental velocity profile is measured at three Reynolds numbers, which corresponds to three flow rates examined during tests with high carbon dioxide concentration.

Figure 53 shows the dimensionless velocity profiles at three Reynolds number. In order to observe the effect of Reynolds number, local velocities are normalized in relation to maximum velocity measured v_{max}.

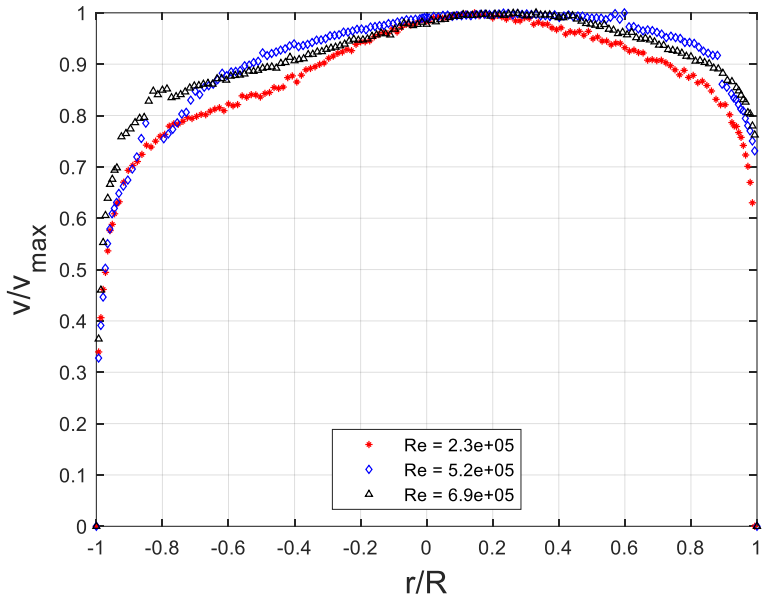

Figure 53 – Experimental velocity profile with transducers approximation

It is observed that at three Reynolds number evaluated, maximum velocity v_{max} is located approximately in radial position r/R = 0.2. For a turbulent fully developed velocity profile, it is expected that maximum velocity be located in the pipe's axis, as occurred in velocity profile with transducers in reference position. Thus, radial position of maximum velocity indicates that transducers approximation increases velocity profile asymmetry.

In the region between the window (r/R = -1) and pipe's shaft (r/R = 0), local velocities are lower than symmetrical radial length (0 < r/R < 1). By observation, it is concluded that transducers approximation procedure has retarded flow velocity profile at -1 < r/R < 0. It is noticeable that, for no Reynolds number, the velocity profile is neither symmetrical nor fully developed.

From Figure 53, it is verified discontinuities in adjacent experimental velocities readings, especially at $Re_2 = 5.2 \times 10^5$ and $Re_3 = 6.9 \times 10^5$. Such discontinuities coincide with changing glass window events. This procedure is necessary, due to the loss of transparency of the glass window, because of evaporation of the LDA fluid at higher flow temperatures.

Considering data provided by flow profiles, as shown in Figure 53, Table 20 details the main parameters of interest, related to velocity profile analysis with transducers approximation. The methodology to obtain such parameters is the same as described in Chapter 5.

Table 20 - Specific parameters of the experimental velocity profile with transducers approximation

Parameter	Q_{min}	Q_{int}	Q_{max}
Reynolds number	$2.4x10^5$	$5.2x10^5$	$6.8x10^5$
Flow rate [Nm³/h]	2891.6	6802.6	9752.6
Steady state temperature T [°C]	25	40	80
Internal pressure P [kPa]	101.3	100.5	100
Friction factor	0.01526	0.01314	0.01255
Average velocity [m/s]	12.3	30.7	49.9
K factor experimental	0.9361	0.9476	0.9575
K factor analytical	0.9419	0.9460	0.9472
K factor variation [%]	0.62	-0.17	-1.09
Average turbulent intensity [%]	8.1	8.6	7.1
Average asymmetry [%]	12.2	11.4	9.9

Considering approximation of ultrasonic transducers, the difference between experimental profile factor and in relation to analytical value, according to AGA 9 [6], is 0.62% at $Re_1 = 2.4x10^5$, -0.17% at $Re_2 = 5.2x10^5$ and -1.09% at $Re_3 = 6.8x10^5$. For transducers at reference distance, these differences are between 0.15% and -0.51%. Thus, transducers approximation increases the profile factor divergence in relation to analytical value considering turbulent and fully developed velocity profile.

Average turbulent intensity are: 8.1% at $Re_1 = 2.4x10^5$, 8.6% at $Re_2 = 5.2x10^5$ and 7.1% at $Re_3 = 6.8x10^5$. Comparing these values with results with transducers in reference position, turbulent intensity increased 5% at Re_1 and 20% in Re_2.

Comparing experimental velocity profile to faced transducers profile, average turbulent intensity increases 5% for $Re_1 = 2.4x10^5$ and increases 20% for $Re_2 = 5.2x10^5$. At Re_3, average turbulent intensity is reduced by -12%.

For asymmetry analysis, measured velocity points symmetrical in relation to pipe axis are compared. Average asymmetry are: 12.2% at $Re_1 = 2.4x10^5$, 11.4% at $Re_2 = 5.2x10^5$ and 9.9% at $Re_3 = 6.8x10^5$. Comparing these asymmetries to the case of transducers in reference position, transducers approximation procedure increases average asymmetry in 157% at Re_1, 125% at Re_2 and 206% at Re_3.

Concluding, as experimental velocity profile indicates, transducers approximation procedure increases flow turbulence, turbulent intensity and asymmetry as well.

Finally, transducer approximation procedure is evaluated at high carbon dioxide concentration at NEMOG's wind tunnel. Channel 1 transducers are approximated to L_4 = 200.8 mm, which corresponds to 51% of path length reduction comparing to reference transducers position. Channel 2 transducers remains in reference position. After the experiments, failure criteria are applied.

Failure criterion *A* examines flow rate USFM readings under test with reference flow rate by Pitot tube. Figure 54 shows flow measurement readings.

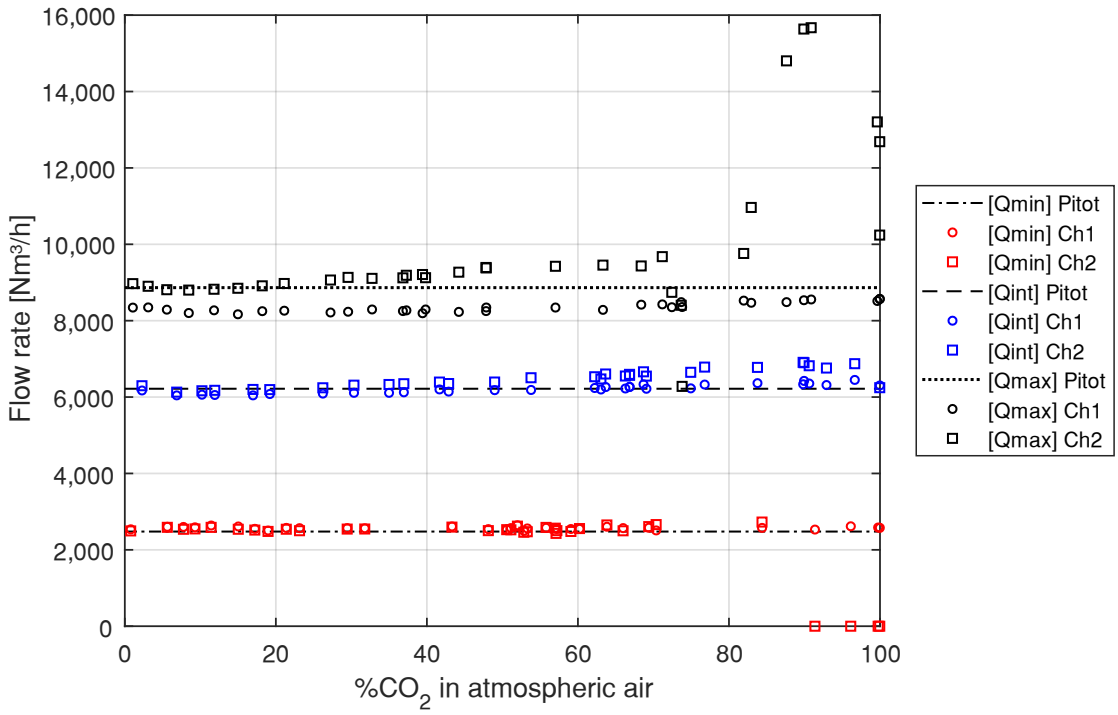

Figure 54 - Carbon dioxide effect on flow rate measurement with transducers approximated

At lowest flow rate evaluated (which corresponds to an average reference flow rate of Q_{min} = 2,500 Nm³/h), there is no indication of failure type *A* up to 100% of CO_2. Channel 2 (which is kept in reference position), failure by flow measured starts above 90% of CO_2 in atmospheric air.

At intermediate flow rate level Q_{int} = 6,300 Nm³/h, there is no indication of failure type *A* in Channel 1 up to 100% CO_2, similarly as occurred during experiments with Channel 1 transducers at the reference position. Considering Channel 2, 18% of failure readings fails at 100% of CO_2.

At the highest flow rate Q_{max} = 9,200 Nm³/h, there is no indication of failure type *A* up to 100% of CO_2. However, in Channel 2 failure type *A* starts intermittent above

72% of CO_2. Failure events increases as carbon dioxide concentration increases, so that all readings above 85% of CO_2 present failure.

In order to apply failure analysis by criterion *B*, Figure 55 shows the behavior of sound speed, as measured by approximated transducers of Channel 1. Measured sound speed is compared to speed of sound through reference AGA 10 [72], considering chemical composition and thermodynamic state.

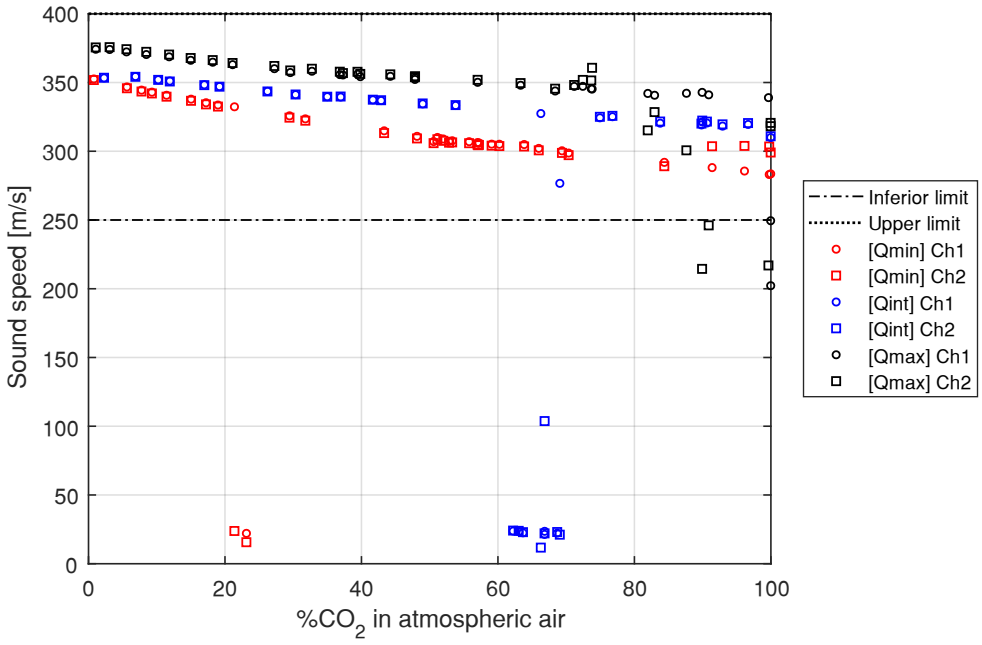

Figure 55 - Carbon dioxide effect on sound speed measurement with transducers approximated

At minimum flow rate (Q_{min} = 2,500 Nm³/h), there are isolated indication of failure type *B* in Channel 1 at 23% of CO_2. Similarly, there are indications of sound speed failure in Channel 2 at 21% and 23% of CO_2. However, flow rate measured is acceptable and performance parameters are in accordance to technical specifications, indicating that flow readings are not frozen. There is no additional indication of failure criterion *B* up to 100% of CO_2.

At intermediate flow rate Q_{int}, both Channel 1 and Channel 2 indicate failure by sound speed in values of 60-70% of CO_2. Technical performance parameters, as well as flow rate, does not indicate failure type *A* or type *C*.

At the highest flow rate under test, 30% of readings from Channel 1 at 100% of CO_2 are classified as failure by criterion *B*. At experiments with transducers at reference position, this limit was 50% of CO_2. On the other hand, transducers from Channel 1 fails at 90% of CO_2.

Failure criterion *C* analyze performance parameters of the flow meter. Figure 56 presents transducers approximation readings. At three flow rate levels under test, there is no indication of failure by low Signal Strength either in Channel 1 or Channel 2.

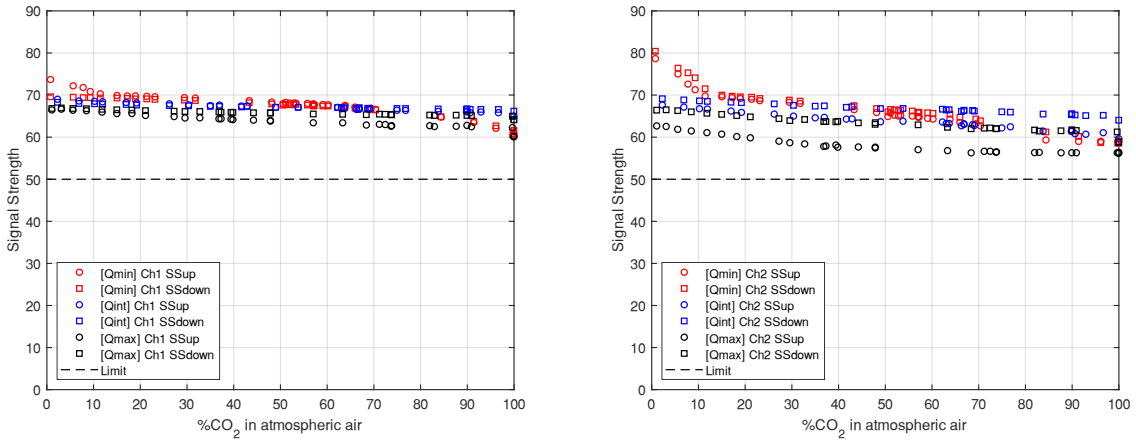

a) Channel 1 b) Channel 2

Figure 56 - Carbon dioxide effect on Signal Strength with transducers approximated

Considering analysis from Figure 52, at low flow rate Q_{min} failure by low signal strength is indicate at 75% of CO_2. At the highest flow rate, all flow readings above 45% of CO_2 presents low Signal Strength. This comparison indicates that transducers approximation is effective in failure reduction in ultrasonic flow measurement applications.

In Channel 2, (which keeps acoustic path length unchanged), presented the same Signal Strength behavior comparing to results of Figure 52, indicating repeatability.

From experiments performed with high carbon dioxide concentration, flow rate variability can be analyzed to examine the effect of transducers approximation on flow rate variability. Thus, Equation (6.22) is used in results from Channel 1. This analysis only considers readings in which any failure criterion is detected. At Q_{min} = 2,500 Nm³/h, flow rate variability lies between 0.71% and 2.85%. At Q_{int} = 6,300 Nm³/h, minimum flow rate variability is 0.31% and maximum ΔQ_{int} is 1.31%. At Q_{max} = 9,300 Nm³/h, flow rate variability is between 0.43% and 1.33%.

Lastly, failure index is calculated by Equation (6.23), combining results failure criteria A, B and C. Results are summarized in Table 21.

Table 21 - Summary of failure index of flow metering process with transducers approximation

%CO_2	**Channel 1**			**Channel 2**		
	Q_{min}	Q_{int}	Q_{max}	Q_{min}	Q_{int}	Q_{max}
0 – 25	6.9%	0.0%	0.0%	11.0%	0.0%	0.0%
25 – 50	0.0%	0.0%	0.0%	0.0%	0.0%	0.0%
50 – 75	0.0%	64.7%	0.0%	0.0%	95.6%	19.3%
75 – 100	0.0%	0.0%	19.6%	100.0%	10.4%	79.2%
%CO_2 failure limit	100.0	100.0	100.0	84.3	96.6	82.9

In order to evaluate which factor most affects flow metering performance, a two-level factorial design type 2^k is performed with n = 5 replicates. Thus, the defined controllable factors are: Blower rotation (factor x_1); CO_2 concentration (factor x_2) and acoustical path length (factor x_3).

The two levels examined are low (-) and high (+). The outputs evaluated are: flow rate variation, speed of sound variation, signal strength upstream and signal strength downstream. The significance level adopted is α = 0.05.

Table 22 presents ANOVA result for flow rate variation. The numerical estimates of effects indicate that the only factor that significantly affects flow rate variation is blower rotation level (factor x_1), with p-value smaller than 0.05. Factor x_1 has a positive direction, i.e. increasing blower rotation level increases flow rate variation. Others primary factors, as well as second-order interaction, do not present significantly effect since its p-value is higher than 0.05.

Table 22 - ANOVA result for factorial design analyzing flow rate variation

Term	Effect	Coefficient	Std. Error	F-Test	p-value
Constant	-	5.689	0.302	18.869	0.000
x_1	1.648	0.824	0.302	2.733	0.012
x_2	-0.448	-0.223	0.302	-0.742	0.299
x_3	-0.941	-0.470	0.302	-1.561	0.118
x_1x_2	-0.935	-0.467	0.302	-1.551	0.120
x_1x_3	-1.143	-0.571	0.302	-1.896	0.068
x_2x_3	0.380	0.189	0.302	0.630	0.323
$x_1x_2x_3$	-1.923	-0.961	0.302	-3.189	0.004

ANOVA result for sound speed variation is detailed in Table 23. Term x_2 presents larger effect value of 1.932, indicating that the effect of increasing carbon dioxide concentration increases sound speed variation. The effect of x_1 is 1.396, pointing that sound speed variation increases with blower rotation. The second order term x_1x_2, which indicates interaction between factors x_1 and x_2, presents second major effect (x_1x_2 = 1.693), which means that at high blower rotation level and high carbon dioxide effect, sound speed variation increases.

Table 23 - ANOVA result for factorial design analyzing speed of sound variation

Term	Effect	Coefficient	Std. Error	F-Test	p-value
Constant	-	1.6075	0.084	19.060	0.000
x_1	1.396	0.6980	0.084	8.276	0.000
x_2	1.932	0.9662	0.084	11.456	0.000
x_3	0.912	0.4562	0.084	5.409	0.000
x_1x_2	1.693	0.8463	0.084	10.034	0.000
x_1x_3	-0.164	-0.0819	0.084	-0.971	0.245
x_2x_3	0.863	0.4316	0.084	5.118	0.000
$x_1x_2x_3$	0.281	0.1407	0.084	1.668	0.100

Table 24 detailed ANOVA results for Signal Strength of upstream transducer (SS_{up}). The first order terms x_1 and x_2 presents effects of same magnitude order: x_1 = -5.793 and x_2 = -5.392. The negative value indicates that SS_{up} decreases with the increasing of blower rotation or carbon dioxide level. On the other hand, x_3 = 6.266, which is the highest effect value, showing that Signal Strength upstream increases with transducers approximation.

Table 24 - ANOVA result for factorial design analyzing Signal Strength from upstream transducer

Term	Effect	Coefficient	Std. Error	F-Test	p-value
Constant	-	64.879	0.052	1247.378	0.000
x_1	-5.793	-2.896	0.052	-55.686	0.000
x_2	-5.392	-2.695	0.052	-51.830	0.000
x_3	6.266	3.133	0.052	60.236	0.000
x_1x_2	0.209	0.104	0.052	2.011	0.056
x_1x_3	-0.267	-0.133	0.052	-2.563	0.018
x_2x_3	1.167	0.583	0.052	11.214	0.000
$x_1x_2x_3$	0.959	0.479	0.052	9.221	0.000

ANOVA for Signal Strength from downstream transducer (SS_{down}) is detailed in Table 25. Differently from results for Signal Strength upstream, first order terms do not present highest effect values. The highest effect value is 3.430, from the interaction x_2x_3 between high carbon dioxide concentration (factor x_2) and transducers approximation (factor x_3), resulting in increasing of SS_{down}.

Nevertheless, reference flow rate (factor x_1) and sound speed concentration (factor x_2) present negative effect, demonstrating that Signal Strength downstream decreases with the increasing of factors A and B. On the other hand, SS_{down} increases with path length reduction (factor x_3).

Table 25 - ANOVA result for factorial design analyzing Signal Strength from downstream transducer

Term	Effect	Coefficient	Std. Error	F-Test	p-value
Constant	-	64,3055	0,054	1192,674	0,000
x_1	-1,027	-0,5136	0,054	-9,525	0,000
x_2	-1,286	-0,6432	0,054	-11,929	0,000
x_3	2,557	1,2787	0,054	23,716	0,000
x_1x_2	-1,711	-0,8554	0,054	-15,865	0,000
x_1x_3	2,133	1,0665	0,054	19,780	0,000
x_2x_3	3,430	1,7148	0,054	31,804	0,000
$x_1x_2x_3$	-1,899	-0,9493	0,054	-17,606	0,000

6.4.6 Performance analysis of recovery angle assembly in high CO_2 concentration

Recovery angle is a proposal for high velocities applications to offset the beam drift effect in ultrasonic pulse packets [1], [2]. In this context, recovery angle is analyzed in order to evaluate its performance in reduction of ultrasonic flow metering fault operating in high carbon dioxide concentration. Thus, recovery angle technique is implemented in both upstream and downstream transducers of Channel 1. Channel 2 transducers remains at reference position, facing the inner wall of the tube.

The implemented recovery angle is inspired in the work of Matson, Sui and Nguyen [2], where is presented the equation to estimate the beam drift angle. In that work, authors implemented a 6º recovery angle only in downstream transducers, however it is not presented experimental evaluation of flow metering performance after recovery angle assembly.

For the present work, instead does installation of special angled connections, as transducer holders in wind tunnel tube, the assembly in recovery angle is performed through the installation of an inclined sealing gasket between transducer flange and spool neck flange. It is implemented at 5.4º in both upstream and downstream transducer of Channel 1. The scheme of such assembly is shown in Figure 57.

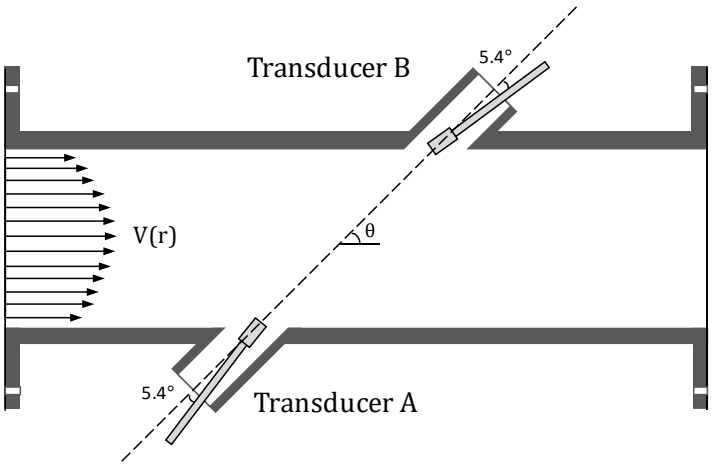

Figure 57 - Scheme of installation of ultrasonic transducers with recovery angle

The experimental methodology and data analysis follows the same procedure applied in previous sections 6.4.4 and 6.4.5 considering high carbon dioxide concentration tests, as well. Recovery angle is examined at three flow rate levels, as described in Table 18. Analysis by failure criteria types *A*, *B* and *C* are also applied.

Readings at three flow rate levels are presented in Figure 58. By analysis, failure criterion type *A* is applied comparing reference flow rate by Pitot tube and ultrasonic flow rate.

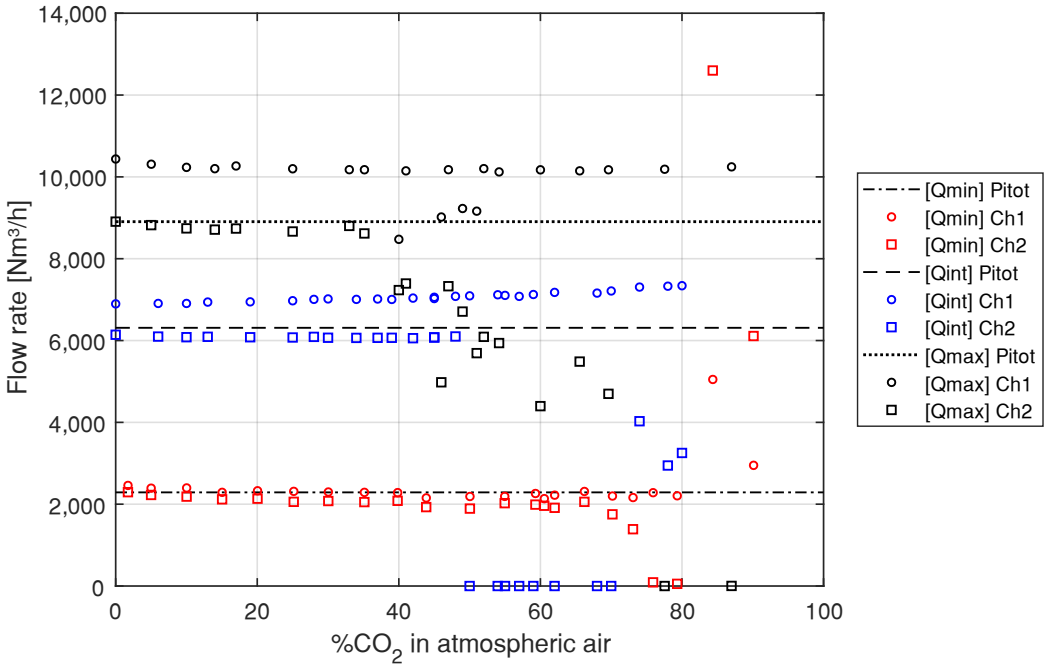

Figure 58 - Carbon dioxide effect on flow rate measurement considering assembly in recovery angle on transducers from Channel 1

At lowest flow rate under evaluation (Q_{min} = 2,300 Nm³/h), there are indication of failure type *A* for CO_2 concentrations higher than 84% in Channel 1. Comparing to readings from experiment at reference position, in which fault type *A* come up above 74% of CO_2, it is concluded that recovery angle assembly increases 10% maximum CO_2 concentration without failure type *A*. Still, at lowest flow rate, in Channel 2 all flow rate readings above 74% are in fault. This analysis agrees with previously experiments, indicating repeatability.

At intermediate flow rate (Q_{int} = 6,300 Nm³/h), there is no indication of failure type *A* in Channel 1, up to 80% of CO_2, which is the maximum carbon dioxide concentration achieved in this test. However, above 78% of CO_2, Signal Strength is below acceptable limit, according to technical specification. Besides, sound speed is out of acceptable range, thus indicating that flow rate measured froze above 78% of CO_2. In Channel 2, where transducers are kept in reference position, 100% of readings above 48% fails by criterion *A*.

At the highest flow rate under test (Q_{max} = 9,000 Nm³/h), there is no indication of failure type *A* in Channel 1 up to 87% of CO_2, which is the maximum achieved in this test. Meanwhile, as occurred at low flow rate and intermediate flow rate, sound speed is out of acceptable range, indicating that flow rate measured froze. In Channel 2, where transducers are kept in reference position, failure criterion *A* is detected above 41% of CO_2.

Failure criterion type *B* evaluates the measured sound speed, comparing it with estimated thermodynamic speed of sound by AGA 10 [72]. The acceptable speed of

sound limit remains between 250 m/s and 400 m/s (as described in Section 6.4.4). Readings are shown in Figure 59.

At Q_{min} = 2,300 Nm³/h, failure type *B* occurrence is simultaneously as failure type *A*. So, flow readings above 84% of CO_2 are fault by speed of sound out of acceptable range. However, there are punctual failure type *B* at 20% of CO_2, where 40% of readings are faulty although flow rate and Signal Strength are as expected. At this carbon dioxide concentration, there are also failure events in Channel 2, where 50% of readings are failures. In Channel 2, all sound speed readings above 74% of CO_2 are faulty.

At Q_{int} = 6,300 Nm³/h, there are occurrence of failure type *B* above 78% of CO_2 in Channel 1, which presents recovery angle. In Channel 2, which is in reference position, all sound speed readings above 74% of CO_2 are fault. In both transducers' pairs, there is isolate indication of failure type B at 25% of CO_2.

At Q_{max} = 9,000 Nm³/h, in Channel1 failure by sound speed out of limits is detected for carbon dioxide concentrations above 54%. In Channel 2, failure type B is only detected at 51% of CO_2 and at 60% of CO_2.

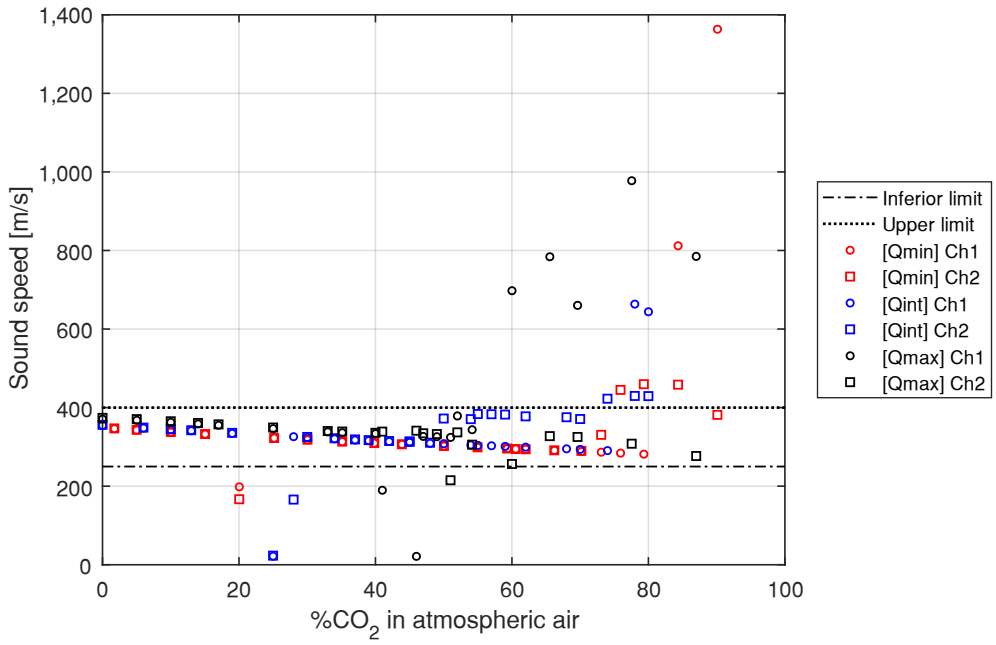

Figure 59 - Carbon dioxide effect on sound speed measurement with installation of recovery angle on transducers from Channel 1

Failure criterion type *C* analyze the performance parameter of the ultrasonic flow meter. According to manufacturer's recommendation, Signal Strength must be above 50. Figure 60 present results with application of recovery angle on Channel 1.

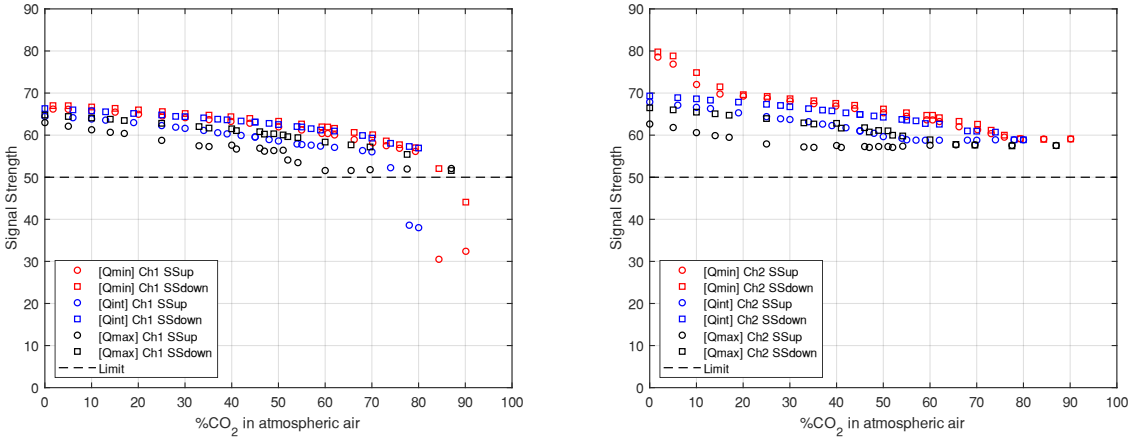

a) Channel 1 b) Channel 2

Figure 60 - Carbon dioxide effect on Signal Strength with application of recovery angle on transducers from Channel 1

At Q_{min} = 2,300 Nm³/h, failure by low Signal Strength are identified above 84% of CO_2 in Channel 1, which presents recovery angle in upstream and downstream transducer. In the same transducers, At Q_{int} = 6,300 Nm³/h failure type C occurs above 78% of CO_2. There is no indication of failure by low Signal Strength at Q_{max} = 9,000 Nm³/h in Channel 1.

Results indicate the effectivity of recovery angle application especially at Q_{max}, in which CO_2 limit without failure by low Signal Strengths is 45% with transducers in reference position and increased to 87% with the installation of recovery angle.

In Channel 2, which acoustical path length remains unchanged, there is no indication of failure by low Signal Strength in any of the three flow rates under test.

From experiments performed with high carbon dioxide concentration, flow rate variability can be analyzed to examine the effect of recovery angle on flow rate variability. Thus, Equation (6.22) is used in results from Channel 1. This analysis only considers readings in which any failure criterion is detected. At Q_{min} = 2,300 Nm³/h, flow rate variability lies between 1.17% and 3.97%. At Q_{int} = 6,300 Nm³/h, minimum flow rate variability is 0.14% and maximum ΔQ_{int} is 0.83%. At Q_{max} = 9,000 Nm³/h, flow rate variability is between 0.23% and 1.51%.

Table 26 summarize failure index after application of failure criteria A, B and C. The critical carbon dioxide concentration in which all readings are fault is also shown.

Table 26 - Summary of failure index of flow metering process with recovery angle installation on Channel 1 transducers

%CO_2	**Channel 1**			**Channel 2**		
	Q_{min}	Q_{int}	Q_{max}	Q_{min}	Q_{int}	Q_{max}
0 – 25	2.7%	10.9%	0.0%	3.4%	10.8%	0.0%
25 – 50	0.0%	0.0%	12.6%	0.0%	8.4%	10.5%
50 – 75	0.0%	0.0%	22.4%	9.6%	100.0%	100.0%
75 – 100	57.6%	100.0%	100.0%	100.0%	100.0%	100.0%
%CO_2 failure limit	79.3	74.0	54.1	73.1	50.0	49.0

6.5 CONCLUDING REMARKS

This chapter summarizes ultrasonic flow meter performance in wind tunnel considering the proposed methodology. First, isolated effect of flow rate is evaluated. Then, ultrasonic flow meter is examined at several flow rate levels and high carbon dioxide concentration.

Considering only atmospheric air flow, ultrasonic flow meter under test is considered validated for flow rate between 1.000 Nm³/h and 11.000 Nm³/h. Results shows that even wind tunnel assembly in open loop circuit, average flow rate as well as uncertainty level from Channel 1 and Channel 2 are different. Considering uncertainty at 95% confidence level, these flow rates overlap especially at lower flow rates.

At the sound speed analysis, despite sound speed is a thermodynamic property that is a function of temperature, pressure and gas composition, sound speed measured by ultrasonic flow meter varied with changes in flow rate level. Uncertainty also increased with flow rate level.

Path length reduction is first examined through induced variability of flow velocity, due to transducers obstruction. Results shown that up to 40% reduction in transducers distance, there is no significant increase in flow rate variability, as demonstrated in section 6.4.2. It is also noticed that transducers approximation also increases signal voltage of received signal. Besides, signal voltage decreases as flow rate increased.

Temperature do not affect flow metering performance, as shown by Signal Strength analysis (section 6.4.3). However, relative deviation of measured sound speed from estimated thermodynamic sound speed increases due to heating process, reaching a maximum deviation of 2.4%. Even so, results are considered validated, since other parameters remains as expected and the ultrasonic flow meter is not calibrated to measure sound speed.

Considering mixtures of atmospheric air flow and carbon dioxide, flow metering performance is analyzed up 100% of CO_2 for three distinct configurations: i) Transducers in reference position; ii) Transducers approximation procedure (path

length reduction) and iii) Installation in recovery angle assembly. After application of failure criteria, CO_2 limit without flow metering fail is quantified, as summarized in Table 27.

Table 27 - Summary of CO_2 concentration limit without failure (considering criteria *A*, *B* and *C*)

Configuration	**2,500 Nm³/h**	**6,300 Nm³/h**	**9,300 Nm³/h**
Reference position	74%	100%	45%
Path length reduction	100%	100%	100%
Recovery angle	79%	74%	54%

Analysis indicate that CO_2 deteriorates ultrasonic flow metering performance in wind tunnel, as concluded in dry calibration experiment in Chapter 4. Moreover, velocity profiles affect ultrasonic signal propagation, as shown by decrease of Signal Strength during experiments with transducer in reference position (section 6.4.1).

Transducers approximation is effective in reducing flow metering failures at selected three flow rate levels. This is in accordance with Lambert Beer law and also converges to dry calibration analysis. Recovery angle assembly also increases flow metering performance (section 6.4.6), but is not so effective as path length reduction (section 6.4.5).

Flow rate variability is analyzed with high carbon dioxide concentration in wind tunnel. Maximum flow rate variability is summarized in Table 28 for each configuration, considering CO_2 limit at Table 27.

Table 28 - Summary of maximum flow rate variability in experiments with carbon dioxide with no reading failure

Configuration	**2,500 Nm³/h**	**6,300 Nm³/h**	**9,300 Nm³/h**
Reference position	3.8%	1.1%	1.1%
Path length reduction	2.9%	1.3%	1.3%
Recovery angle	4.0%	0.8%	1.5%

7 CONCLUSION

7.1 FINAL REMARKS

Transit time ultrasonic flow meter is the preferred technology in offshore flare gas applications due to typical critical conditions of flare flow. Although ultrasonic flow meters have been used since the end of 1980's decade, flare gas flow metering remains as a technology challenge.

The main objective of this study is to define methodologies to evaluate flare gas ultrasonic flow meter performance in flow applications with high carbon dioxide concentration. In this context, one can define two major challenges.

First, flare gas flow presents large turndown ratio. At high velocities application, sound pressure is blown away by velocity profile, which may cause weakening of received signal and, in critical cases, may induce complete signal loss culminating failure in flow metering process. The second challenge is operation in attenuating media. Carbon dioxide is the natural gas component, which most reduces wave propagation in operational transducers frequency, due to molecular thermal relaxation phenomenon.

In this context, this work presents an experimental evaluation of ultrasonic flow metering performance in critical operating conditions. The strategies adopted involve to analyze these the effect of high velocity and attenuation first separated and then combined. Consequently, the methodology allows understanding, separately, its influence on flow metering performance. Then, alternatives to improve flow metering performance are examined in wind tunnel at high flow rate and high carbon dioxide concentration.

The best operation of ultrasonic flow meters occurs under no flow conditions, and operating in atmospheric air. Thus, initially the flow meter under test is mounted in dry calibration arrangement, in zero-flow condition, in order to stablish a reference state to further analysis. Dry calibration presents several advantages, such as: low cost, reproducible easily even in offshore field and do not change operational installation of the flow meter.

Flow meter validation experiment, in 7 hours test in atmospheric air, differences between measured sound speed a reference sound speed of a perfect gas remains constant. The ultrasonic flow meter is capable to operate up to 100% of CO_2 in no flow condition, with sound speed measured coherent with AGA 10 [72] reference sound speed and signal strength acceptable (section 4.4.2).

Transducers approximation procedure is first examined in dry calibration. It shown to be effective in reduction of sound speed deviation and increasing signal strength as well, as voltage of received signal. Using signal voltage, experimental

attenuation coefficient is estimated and compared to analytical values which results consistent at CO_2 concentrations higher than 50% (section 4.4.4).

To accomplish the objective of analyze ultrasonic flow metering performance at high flow rate and high carbon dioxide concentration, a wind tunnel is especially designed and built. The wind tunnel construction allows operation in closed circuit assembly, which flow is recirculated, and open circuit assembly, preferred to achieve a turbulent and fully developed velocity profile. Wind tunnel validation is performed through experimental velocity profile analysis mapped using LDA technique. Law of the wall analysis show that the velocity profile at three Reynolds number is not turbulent fully developed yet, but the profile factors present maximum deviation from analytical k-factor according to AGA 9 [6] of 0.51%. Besides, turbulent intensity and operation characterization are well defined (section 5.4).

Ultrasonic flow metering performance is evaluated in wind tunnel. Initial tests aim to validate flow metering performance in open circuit wind tunnel. Uncertainty level are also examined with 95% confidence level. Path length reduction is first examined in atmospheric air. Analysis indicate that transducers approximation increases flow rate variability with path length reduction above 50%.

For wind tunnel closed circuit assembly, temperatures up to 90ºC do not affect significantly neither technical performance parameters nor sound speed measurement of the ultrasonic flow meter. So, ultrasonic flow meter tests are firstly performed with transducers in reference position at high carbon dioxide concentration, which is facing the inner wall of the tube, at three flow rate levels. After applying failure criteria, it is identified carbon dioxide concentrations in fault begin in 70% of CO_2 at Q_{min} = 2,500 Nm³/h and 45% of CO_2 at Q_{max} = 9,300 Nm³/h.

Then, transducers approximation is examined in wind tunnel in high carbon dioxide concentrations. Transducers distance chosen for this analysis equivales to approximately 50% reduction of reference path length. Analysis conclude that this strategy is effective in failure reduction. Punctual intermittent failures are identified, but there are no permanent failures up to 100% of CO_2 even at maximum flow rate level.

The last experiment is the evaluation of recovery angle procedure. This strategy is interesting because transducers remains non-intrusive to core flow. In some cases, recovery angle can be implemented without changing original piping through installation of inclined sealing gasket between transducer flange and spool neck's flange, as implemented in current work.

Results shows that recovery angle is effective for failure events reduction in ultrasonic flow meter operation at high carbon dioxide level and flow rate: Q_{min} = 2,000 Nm³/h and Q_{max} = 9,000 Nm³/h, but it is not so effective as the strategy of transducers approximation. Anyway, at minimum flow rate under test CO_2 limit, without failure, increased from 74% for transducers in reference position to 84% considering installation of recovery angle. At maximum flow rate under evaluation, CO_2 limit without failure increased from 45% keeping transducers in reference position to 54% for

transducers approximated. At intermediate flow rate, analysis of assembly in recovery angle shows to be less effective than results with transducers in reference position. Thus, this case must be further investigated.

7.2 PROPOSAL FOR FUTURE WORK

Literature review and results presented in this thesis provide some proposal to further investigation.

- Detailed analysis about uncertainty of ultrasonic flow metering, considering uncertainty due to profile factor, transit times and covariance terms.
- Perform experiments at wind tunnel with high carbon dioxide concentration in low velocity range, from 0.3 m/s to 10 m/s.
- Analysis of an intermediate transducers distance as alternative to improve flow metering performance keeping acceptable turbulent intensity.
- Experimental evaluation of flow metering performance with installation of recovery angle and transducers approximated.
- Analysis of signal attenuation and flow metering performance of USFM in wet gas applications.
- Monitoring received signal of the ultrasonic flow meter using an oscilloscope in real-time during experiments with high carbon dioxide in the wind tunnel.
- Proposing methodologies for failure criterion by flow rate with is independent of reference flow meter, thus being field applicable.
- Field test of the proposed methodology.
- Characterization of velocity profile using LDV technique in open loop assembly.

8 REFERENCES

[1] K. S. Mylvaganam, “High-rangeability ultrasonic gas flowmeter for monitoring flare gas,” *IEEE Trans. Ultrason. Ferroelectr. Freq. Control*, vol. 36, no. 2, pp. 144–149, Mar. 1989.

[2] J. Matson, L. Sui, and T. Nguyen, “Ultrasonic Flare Gas Flow Meter Techniques for Extremes of High and Low Velocity Measurement and Experience with High CO2 Concentration,” *North Sea Flow Meas. Work.*, pp. 1–23, 2010.

[3] ANP/INMETRO, *Resolução Conjunta Anp/Inmetro Nº 1*. 2013, pp. 1–34.

[4] S. G. Ejakov, S. Phillips, Y. Dain, R. M. Lueptow, and J. H. Visser, “Acoustic attenuation in gas mixtures with nitrogen: Experimental data and calculations,” *J. Acoust. Soc. Am.*, vol. 113, no. 4, pp. 1871–1879, 2003.

[5] K. van Helden, D. A. Ehrlich, T. Dietz, and P. Tan, “Examination of Ultrasonic Flow Meter in CO 2 -rich Applications,” in *South East Asia Flow Measurement Workshop*, 2009, no. March, pp. 1–14.

[6] American Gas Association, “AGA Report No. 9: Measurment of Gas by Multipath Ultrasonic Meters,” Washington, DC, U.S.A, 2007.

[7] J. Matson, L. Sui, and T. H. Nguyen, “New and Old Challenges of High Velocity and High CO2 Concentration for Flare Gas Flow Measurement are met with Improved Ultrasonic Flow Meter Capability,” in *The Americas Workshop*, 2010, no. April, pp. 1–14.

[8] W. F. Barros, “Análise da variabilidade induzida pela concentração de CO2 nas leituras de medidores de vazão ultrassônicos para gás de queima,” Universidade Federal do Espírito Santo, 2016.

[9] W. Barros and R. Ramos, “Analysis of the Induced Variability By Co2 in Readings of Ultrasonic Flow Meters for Flare Gas,” in *16th Brazilian Congress of Thermal Sciences and Engineering*, 2016, pp. 1–10.

[10] D. Ensminger and L. J. Bond, *Ultrasonics: Fundamentals, Technologies, and Applications*, 3rd Edition. CRC Press, 2011.

[11] S. Kocis and Z. Figura, *Ultrasonic Measurements and Technologies*, 1st ed. London, UK: Chapman & Hall, 1996.

[12] L. E. Kinsler, A. R. Frey, A. B. Coppens, and J. V. Sanders, *Fundamentals of Acoustics*, 4th Edition. John Wiley & Sons, Inc., 2000.

[13] J. D. N. Cheeke, *Fundamentals and Applications of Ultrasonic Waves*, 2nd Edition. Boca Raton, Florida: CRC Press, 2012.

[14] F. P. Mechel, *Formulas of Acoustics*. Berlin, Heidelberg: Springer Berlin Heidelberg, 2004.

[15] F. Buiochi, “Análise dos métodos de medição de densidade de líquidos por ultra-som,” Universidade de São Paulo, 1994.

[16] T. Gudra, “Ultrasounds in gas media: generation, transmission, applications,” *Arch. Acoust.*, vol. 33, no. 4, pp. 581–592, 2008.

[17] F. Massa, “Ultrasonic Transducer for Use in Air,” *Proc. IEEE*, vol. 53, no. 10, pp. 1363–1371, 1965.

[18] R. B. Mathias, “Influência do perfil de velocidade do escoamento sobre a medição ultrassônica de vazão por tempo de trânsito,” Universidade Federal do Espírito Santo, 2010.

[19] M. Bruneau, *Fundamentals of Acoustics*, 1st Edition. London, UK: ISTE Ltd, 2006.

[20] J. D. Lambert, “Vibrational and rotational relaxation in gases,” Clarendon Press, Oxford, 1977.

[21] H. H. Rogers, “Absorption of Supersonic Waves in Mixtures of Air and Carbon Dioxide at Different Relative Humidities,” *Phys. Rev.*, vol. 45, no. 3, pp. 208–211, 1934.

[22] C. Kittel, “Ultrasonics research and the properties of matter,” *Reports Prog. Phys.*, vol. 11, no. 1, p. 308, Jan. 1947.

[23] M. Vermeulen, J. Drenthen, H. Den Hollander, P. Lanoux, and C. Groningen, “Practical Solution for Ultrasonic Flow Measurement in High CO2 Natural Gas Applications,” in *AGA Operations Conferance*, 2013, pp. 1–16.

[24] Y. Dain and R. M. Lueptow, “Acoustic attenuation in three-component gas mixtures—Theory,” *J. Acoust. Soc. Am.*, vol. 109, no. 5, pp. 1955–1964, 2001.

[25] A. Cottet, Y. Neumeier, D. Scarborough, O. Bibik, and T. Lieuwen, “Acoustic absorption measurements for characterization of gas mixing,” *J. Acoust. Soc. Am.*, vol. 116, no. 4, pp. 2081–2088, 2004.

[26] S. Yan, S. Wang, and Z. Dou, “A signal processing method applied to direct simulation Monte Carlo for predicting acoustic attenuation in gas mixtures,” *Meas. Sci. Technol.*, vol. 18, no. 5, pp. 1278–1286, May 2007.

[27] T. Liu, S. Wang, and M. Zhu, “Predicting acoustic relaxation absorption in gas mixtures for extraction of composition relaxation contributions,” *Proc. R. Soc. A Math. Phys. Eng. Sci.*, vol. 473, no. 2208, 2017.

[28] K. S. Zhang, S. Wang, M. Zhu, Y. Ding, and Y. Hu, “Decoupling multimode vibrational relaxations in multi-component gas mixtures: Analysis of sound relaxational absorption spectra,” *Chinese Phys. B*, vol. 22, no. 1, 2013.

[29] P. Laugier, “Diffraction correction for focused transducers in attenuation measurements invivo,” *Ultrason. Imaging*, vol. 9, no. 4, pp. 248–259, Oct. 1987.

[30] L. B. Evans, H. E. Bass, and L. C. Sutherland, “Atmospheric Absorption of Sound: Theoretical Predictions,” *J. Acoust. Soc. Am.*, vol. 51, no. 5B, pp. 1565–1575, 1972.

[31] A. American National Standards Institute, Committee S1, “ANSI S1.26-1995: Method for Calculation of the Absorption of Sound by the Atmosphere.” American National Standards Institute, New York, 1995.

[32] L. J. Bond, C. Chiang, and C. M. Fortunko, “Absorption of ultrasonic waves in air at high frequencies (10–20 MHz),” *J. Acoust. Soc. Am.*, vol. 92, no. 4, pp. 2006–2015, 1992.

[33] H. E. Bass, L. C. Sutherland, A. J. Zuckerwar, D. T. Blackstock, and D. M. Hester, “Atmospheric absorption of sound: Further developments,” *J. Acoust. Soc. Am.*, vol. 97, no. 1, pp. 680–683, Jan. 1995.

[34] T. P. Abello, “Absorption of Ultrasonic Waves by Various Gases,” *Phys. Rev.*, vol. 31, no. 6, pp. 1083–1091, Jun. 1928.

[35] R. W. Curtis, “An Experimental Determination of Ultrasonic Absorption and Reflection Coefficients in Air and in Carbon Dioxide,” *Phys. Rev.*, vol. 46, no. 9, pp. 811–815, Nov. 1934.

[36] A. Ehrlich, S. Ag, T. Dietz, and P. Tan, “Examination of ultrasonic flow meter in CO2 rich applications,” in *8th South East Asia Hydrocarbon Flow Measurement Workshop*, 2009, no. March.

[37] A. Petculescu, B. Hall, R. Fraenzle, S. Phillips, and R. M. Lueptow, “A prototype acoustic gas sensor based on attenuation,” *J. Acoust. Soc. Am.*, vol. 120, no. 4, pp. 1779–1782, 2006.

[38] X. M. Tang, M. N. Toksöz, P. Tarif, and R. H. Wilkens, “A method for measuring acoustic wave attenuation in the laboratory,” *J. Acoust. Soc. Am.*, vol. 83, no. 2, pp. 453–462, Feb. 1988.

[39] J. M. M. Pinkerton, “On the pulse method of measuring ultrasonic absorption in liquids,” *Proc. Phys. Soc. Sect. B*, vol. 62, no. 5, pp. 286–299, 1949.

[40] W. Xu and J. J. Kaufman, “Diffraction correction methods for insertion ultrasound attenuation estimation,” *IEEE Trans. Biomed. Eng.*, vol. 40, no. 6, pp. 563–570, Jun. 1993.

[41] R. C. Chivers, L. Bosselaar, and P. R. Filmore, “Effective area to be used in diffraction corrections,” *J. Acoust. Soc. Am.*, vol. 68, no. 1, pp. 80–84, Jul. 1980.

[42] J. Gibson, “TUV NEL Report 2013/286: Summary report of review of flare and vent gas emissions monitoring and reporting methods,” Glasgow, Scotland, 2013.

[43] M. Davoudi, M. R. Rahimpour, S. M. Jokar, F. Nikbakht, and H. Abbasfard, “The major sources of gas flaring and air contamination in the natural gas processing plants: A case study,” *J. Nat. Gas Sci. Eng.*, vol. 13, pp. 7–19, Jul. 2013.

[44] O. S. Ismail and G. E. Umukoro, “Global Impact of Gas Flaring,” *Energy Power Eng.*, vol. 04, no. 04, pp. 290–302, 2012.

[45] S. N. Barcellos, “Influência da composição do gás na medição de vazão de gás de tocha por tecnologia ultrassônica,” Universidade Federal do Espírito Santo, 2017.

[46] T. Folkestad and K. S. Mylvaganam, “Chirp excitation of ultrasonic probes and algorithm for filtering transit times in high-rangeability gas flow metering,” *IEEE Trans. Ultrason. Ferroelectr. Freq. Control*, vol. 40, no. 3, pp. 193–215, May 1993.

[47] L. C. Lynnworth and Y. Liu, “Ultrasonic flowmeters: Half-century progress report, 1955–2005,” *Ultrasonics*, vol. 44, pp. e1371–e1378, Dec. 2006.

[48] C. Carlander and J. Delsing, “Installation effects on an ultrasonic flow meter with

implications for self diagnostics," *Flow Meas. Instrum.*, vol. 11, no. 2, pp. 109–122, Jun. 2000.

[49] E. Thompson, "Fundamentals of multipath ultrasonic flow meters for gas measurement," in *Proceedings of the American School of Gas Measurement Technology*, 2011, p. 23.

[50] W. Manthey, N. Kroemer, and V. Magori, "Ultrasonic transducers and transducer arrays for applications in air," *Meas. Sci. Technol.*, vol. 3, no. 3, pp. 249–261, 1992.

[51] B. looss, C. Lhuillier, and H. Jeanneau, "Numerical simulation of transit-time ultrasonic flowmeters: Uncertainties due to flow profile and fluid turbulence," *Ultrasonics*, vol. 40, no. 9. pp. 1009–1015, 2002.

[52] R. S. Martins, J. R. Andrade, and R. Ramos, "On the effect of the mounting angle on single-path transit-time ultrasonic flow measurement of flare gas: a numerical analysis," *J. Brazilian Soc. Mech. Sci. Eng.*, vol. 42, no. 1, p. 13, Jan. 2020.

[53] T. T. Yeh and G. E. Mattingly, "Computer simulations of ultrasonic flow meter performance in ideal and non-ideal pipeflows," in *ASME Fluids Engineering Division Summer Meeting (FEDSM'97)*, 1997, p. 6.

[54] R. Ramos, "Desenvolvimento De Medidor De Vazão De Gás Por Ultra-Som: Modelagem, Protótipo E Testes," Universidade Federal do Espírito Santo, 2006.

[55] P. Lunde, K. E. Frøysa, R. A. Kippersund, and M. Vestrheim, "Transient Diffraction Effects in Ultrasonic Meters for Volumetric, Mass and Energy Flow Measurement of Natural gas," *21st Int. North sea flow Meas. Work.*, 2003.

[56] Jae Cheon Jung and Poong Hyun Seong, "Estimation of the flow profile correction factor of a transit-time ultrasonic flow meter for the feedwater flow measurement in a nuclear power plant," *IEEE Trans. Nucl. Sci.*, vol. 52, no. 3, pp. 714–718, Jun. 2005.

[57] P. I. Moore, G. J. Brown, and B. P. Stimpson, "Ultrasonic transit-time flowmeters modelled with theoretical velocity profiles: methodology," *Meas. Sci. Technol.*, vol. 11, no. 12, pp. 1802–1811, Dec. 2000.

[58] J. de Boer, G.; Lansing, "Dry calibration method for ultrasonic flow meters," in *North Sea Flow Measurement Workshop*, 1997, p. 17.

[59] M. Mori, K. Tezuka, and Y. Takeda, "Effects of Inner Surface Roughness and Asymmetric Pipe Flow on Accuracy of Profile Factor for Ultrasonic Flow Meter," in *Volume 2: Thermal Hydraulics*, 2006, vol. 2006, pp. 761–767.

[60] S. Franchini, A. Sanz-Andrés, and A. Cuerva, "Measurement of velocity in rotational flows using ultrasonic anemometry: the flowmeter," *Exp. Fluids*, vol. 42, no. 6, pp. 903–911, Jun. 2007.

[61] K. Tawackolian, O. Büker, J. Hogendoorn, and T. Lederer, "Calibration of an ultrasonic flow meter for hot water," *Flow Measurement and Instrumentation*, vol. 30. pp. 166–173, 2013.

[62] GE Sensing, "DigitalFlow™ XGF868i Programming Manual." GE Sensing, p. 146, 2015.

[63] Fluenta, “Complete User Manual for FGM160 with TFS.” Fluenta, p. 188, 2011.

[64] J. Nikuradse, *Laws of turbulent flow in smooth pipes*. Washington, U.S.A.: NASA TT F-10, 359, 1966.

[65] GE Sensing, “XGF868i Flare Gas Mass Flow Ultrasonic Transmitter,” no. April. p. 76, 2013.

[66] R. S. Martins, “Numerical simulations of installation effects caused by upstream elbows on single-path transit-time ultrasonic flare flow meters,” Universiade Federal do Espírito Santo (UFES), 2012.

[67] B. Mickan, G. Wendt, R. Kramer, and D. Dopheide, “Systematic investigation of flow profiles in pipes and their effects on gas meter behaviour,” *Measurement*, vol. 22, no. 1–2, pp. 1–14, Sep. 1997.

[68] C. Ruppel and F. Peters, “Effects of upstream installations on the reading of an ultrasonic flowmeter,” *Flow Meas. Instrum.*, vol. 15, no. 3, pp. 167–177, Jun. 2004.

[69] D. Zheng, P. Zhang, T. Zhang, and D. Zhao, “A method based on a novel flow pattern model for the flow adaptability study of ultrasonic flowmeter,” *Flow Meas. Instrum.*, vol. 29, pp. 25–31, 2013.

[70] J. G. Drenthen and G. De Boer, “The manufacturing of ultrasonic gas flow meters,” *Flow Meas. Instrum.*, vol. 12, pp. 89–99, 2014.

[71] K. Warner, Kevin; Zanker, “Noise reduction in ultrasonic gas flow measurement,” in *4th International Symposium on Fluid Flow Measurement*, 1999, p. 9.

[72] American Gas Association, “AGA Report No. 10: Speed of Sound in Natural Gas and Other Related Hydrocarbon Gases,” Washington, DC, U.S.A, 2002.

[73] American Petroleum Institute (API), “Manual of Petroleum Measurement Standards Chapter 14 - Natural gas fluids measurement,” Washington, D.C, 2007.

[74] Associação Brasileira de Normas Técnicas (ABNT), “NBR 16777: Medidores de vazão de gás de tocha (flare) e de gás ventilado para a atmosfera,” São Paulo, 2019.

[75] P. Lunde, K. E. Frøysa, and Neumann, *Handbook of uncertainty calculations - ultrasonic fiscal oil metering stations*, no. December. 2007.

[76] British Standards Institution, “BS 7965:2013 - Guide to the selection, installation, operation and calibration of diagonal path transit time ultrasonic flowmeters for industrial gas applications,” 2013.

[77] U. R. Nilsson and J. Delsing, “In situ detection of inaccurate gas flow meters using a fingerprint technique,” *Flow Meas. Instrum.*, vol. 9, no. 3, pp. 143–152, 1998.

[78] SOLV Flow Measurement, “FlowSolv V5.” 2018.

[79] GE Sensing, “Panaview.” 2017.

[80] Testo Instruments, “easyEmission version 2.8.” 2010.

[81] B. S. Finn, “Laplace and the Speed of Sound,” *Isis*, vol. 55, no. 1, pp. 7–19, 1964.

[82] X. M. Tang, M. N. Toksöz, P. Tarif, and R. H. Wilkens, “A method for measuring acoustic wave attenuation in the laboratory,” *J. Acoust. Soc. Am.*, vol. 83, no. 2, pp. 453–462, Feb. 1988.

[83] A. R. R. Salgado, “Perfect gas approach validation aiming esimation of thermophysical properties in flare flows considering operaional data,” in *Proceedings of the 20th International Congress of Mechanical Engineering – COBEM 2009*, 2009, p. 8.

[84] F. C. da Silva, “Analise comparativa de medidor de vazão em flare por tecnologia ótica e pitometria utilizando túnel de vento,” Universidade Federal do Espírito Santo, 2012.

[85] J. Hill, A. Weber, and J. Weber, “Qualification of Ultrasonic Flow Meters for Custody Transfer of Natural Gas Using Atmospheric Air Calibration Facilities,” in *North Sea Flow Measurement Workshop*, 2002, p. 12.

[86] National Instruments, “LabVIEW™ myRIO 2014.” 2013.

[87] American Conference of Governmental Industrial Hygienists, “Industrial Ventilation: A Manual of Recommended Practice.” 23th Edition, 1998.

[88] ISO/FDIS 3966:2008, “Measurement of fluids flow in closed conduits - Velocity area method using Pitot static tubes,” vol. 2009. ISO, Geneva, p. 54, 2008.

[89] Kimo, “Technical Datasheet Pitot tube L type.” .

[90] F. M. White, *Viscous Fluid Flow*, 2nd Edition. McGraw-Hill, 1991.

[91] T. A. Davidson, “Simple and accurate method for calculating viscosity of gaseous mixtures,” 1993.

[92] Z. Zhang, *LDA Application Methods*. 2010.

[93] TSI, “FlowSizer 64.” 2015.

[94] L. J. De Chant, “The venerable 1/7th power law turbulent velocity profile: a classical nonlinear boundary value problem solution and its relationship to stochastic processes,” *Appl. Math. Comput.*, vol. 161, no. 2, pp. 463–474, Feb. 2005.

[95] H. Schlichting, *Boundary-layer theory*, 6th Edition. New York: McGraw-Hill, 1968.

[96] J. O. Hinze, *Turbulence: An introduction to its mechanism and theory*, 1st Edition. McGraw-Hill, 1958.

[97] L. G. Franco, R. Ramos, and G. da F. Alves, “Establishment of a Reference State for Evaluation of Attenuating Effects in Gas Flow Measurement by Ultrasonic Technology,” in *25tb International Congress of Mechanical Engineering*, 2019, p. 9.

[98] D. C. Montgomery and G. C. Runger, *Applied Statistics and Probability for Engineers*, 6th Edition. Hoboken, NJ: John Wiley & Sons, Inc., 2014.

[99] F. C. de Almeida, E. C. de Oliveira, and C. R. H. Barbosa, “Design of experiments to analyze the influence of water content and meter factor on the

uncertainty of oil flow measurement with ultrasonic meters," *Flow Meas. Instrum.*, vol. 70, p. 101627, Dec. 2019.

[100] J.C.G.M., "Evaluation of measurement data — Guide to the expression of uncertainty in measurement," *Int. Organ. Stand. Geneva ISBN*, vol. 50, no. September, p. 134, 2008.

[101] The MathWorks Inc., "MATLAB." Natick, Massachusetts, 2018.